Technische Universität München

Fakultät für Chemie

Electrospinning of Lithium and Magnesium Ion Conductors

Patrick Walke, M.Sc.

Vollständiger Abdruck der von der Fakultät für Chemie der Technischen Universität München zur Erlangung des akademischen Grades eines

Doktors der Naturwissenschaften (Dr. rer. nat.)

genehmigten Dissertation.

Vorsitzender:	Prof. Dr. Thomas F. Fässler
Prüfende/-r:	1. Prof. Dr. Tom Nilges
	2. Prof. Dr. Hubert A. Gasteiger
	3. Prof. Dr. Richard Weihrich

Die Dissertation wurde am 23.03.2022 bei der Technischen Universität München eingereicht und durch die Fakultät für Chemie am 07.06.2022 angenommen.

Danksagung

Ich bedanke mich bei allen Personen, die mich in den letzen Jahren bei meiner persönlichen und akademischen Entwicklung begleitet haben. Besonders hervozuheben sind dabei:

- **Prof. Dr. Tom Nilges**, für die Aufnahme in die Arbeitsgruppe, das interessante Thema und die Möglichkeit dieses Arbeit durchzuführen, das Vertrauen bei allen wissenschaftlichen und organisatorischen Aufgaben, für die zeitintensiven Diskussionen und all die Dinge die eine gute Betreuung ausmachen.
- **Lucia Weissenborn**, für Ihre Unterstützung bei allen bürokratischen Hürden und die Organisation in der Arbeitsgruppe.
- **Fabian Schatz**, für die freundliche Aufnahme in die TUMint.Energy Research GmbH und die Möglichkeit diese Arbeit in meine Arbeitsalltag zu integrieren.
- **Dr.Katharina Freitag**, die Electrospinning als Technik in dre Arbeitsgruppe etabliert hat und mir wahrend meiner Masterarbeit vieles beigebracht hat, was die Durchfürung dieser Arbeit ermöglicht hat.
- **Die Arbeitsgruppe von Prof. Dr. Hubert Gasteiger**, in der ich meine ersten Erfahrung mit der Elektrochemie sammeln durfte und die mir bis heute mit Rat und Tat zur Seite standen.
- **Wei Jun Chua**, der mit seiner Bachelorarbeit einen Beitrag zu dieser Arbeit geleistet hat.
- **Alfred Rabenbauer**, der mit seinem Forschungspraktikum zu dieser Arbeit beigetragen hat und seine Masterarbeit bei mir absolviert hat.
- **Anna Kirchberger**, die während ihrer Masterarbeit und der ersten Zeit ihrer Promotion mich mit ihrem Fleiß und Ehrgeiz unterstützt hat und für viel Spaß im Büro und Labor gesorgt hat.
- **Felix Reiter**, für die gute Zeit zusammen im Labor, die SEM Aufnahmen und die Hilfe beim Bilder bearbeiten.
- **Kathrin Vosseler**, für die SEM Aufnahmen.
- **Anna Vogel**, für die gute Zusammenarbeit im Labor und machnmal mehr oder weniger notwendigen Kaffepausen seit dem ersten Praktikum im Studium.
- **Allen** aktuellen und ehemaligen Mitarbeiter im AK Nilges für die schöne Zeit in der Universität und bei allen gemeinsamen Unternemungen.

- **Meiner Familie**, die mich immer bedingungslos unterstützt.
- **Nora Walke**, meiner Frau, die seit meiner Schulzeit immer für mich da ist und mich unterstützt wo immer sie kann.

Contents

Abstract

Polymer electrolytes based on poly(ethylene oxide) (PEO) are prepared *via* electrospinning and for comparison *via* solution casting and hot pressing. For lithium ion conducting polymer membranes two different conducting salts LiX [X= $(CF_3SO_2)_2N^-$ ($TFSI^-$), BF_4^-] are used. By varying the conducting salt concentration the additive-free solid polymer electrolytes (SPEs) with the highest ionic conductivity are identified. For both systems the highest process-able salt concentration, PEO:LiX 18:1, show the highest ionic conductivities of 5×10^{-7} S/cm for $LiBF_4$ and 9.8×10^{-6} S/cm for LiTFSI, both at 293 K. To increase the ionic conductivity without losing the fibrous structure of the electrospun membranes, admixing of organic and inorganic additives is tried. The PEO:LiTFSI system is optimized to show an ionic conductivity of 1.9×10^{-5} S/cm at 293 K by adding succinonitrile (SN) to result in a molar composition of PEO:SN:LiTFSI 36:8:1. Use of SN and nanostructured Al_2O_3 leads to an increased ionic conductivity of 5.5×10^{-5} S/cm at 293 K for a PEO:SN:$LiBF_4$ 18:3:1 +2wt% Al_2O_3.
With the change to applying $Mg(TFSI)_2$ the concept of electrospun polymer electrolytes is transfered to magnesium ion batteries (MIBs). The highest ionic conductivity up on different concentrations of conducting salt and plasticizer (SN) is achieved with a PEO:$Mg(TFSI)_2$ 36:1 composition and determined to be 1.2×10^{-5} S/cm at 293 K and thus drastically higher compared to solution casted membranes with the same composition.
All prepared membranes are conducted to structural and electrochemical analysis. Crystallinity is investigated by powder X-ray diffraction (P-XRD). Fiber morphology is observed by scanning electron microscopy (SEM) and thermal properties are determined by differential scanning calorimetry (DSC). The ionic conductivities are calculated from impedance spectroscopy and ion transport is investigated with cyclic voltammetry.

Kurzzusammenfasssung

Polymerelectrolyte basierend auf Polyethylenoxid (PEO) werden mittels Elektrospinning und für Vergleichsmessungen mittels Heißpressen und Lösungsgießen hergestellt. Um Lithium-Ionen-leitende Membranen zu erhalten, werden zwei verschiedene LiX [X = $(CF_3SO_2)_2N^-$ ($TFSI^-$), BF_4^-] verwendet. Durch Varriation der Leitsalzkonzentration und ohne den Einsatz weiterer Additive werden die Festkörper-Polymer-Elektrolyte (engl. Solid Polymer Electrolytes, SPEs) mit der höchsten ionischen Leitfähigkeit identifiziert. Diese wurde bei in beiden System mit der höchsten im Prozess einsetzbaren Konzentration, PEO:LiX in einem molaren Verhältniss von 18:1 erziehlt und liegen bei 5×10^{-7} S/cm für $LiBF_4$ und $9,8 \times 10^{-6}$ S/cm für LiTFSI, jeweils bei 293 K. Im Weiteren wird versucht die ionische Leitfähigkeit durch den Einsatz von organischen oder anorganischen Additiven zu erhöhen, ohne dabei die Faserstruktur der Membran zu verlieren. Das System PEO:LiTFSI kann durch den Einsatz von Succinonitril (SN) optimiert werden. Die Leitfähigkeit des so erhaltene Polymerelektrolyten mit einer molaren Zusammensetzung von PEO:SN:LiTFSI 36:8:1 liegt bei 1.9×10^{-5} S/cm bei 293 K.
Die Verwendung von Succinonitril und nanostrukturiertem Al_2O_3 im Polymerelektrolyten PEO:$LiBF_4$ führt bei einer finalen Zusammensetzung von PEO:SN:$LiBF_4$ 18:3:1 + 2wt% zu einer erhöten ionischen Leitfähigkeit von 5.5×10^{-5} S/cm bei 293 K. Mit dem Wechsel zu $Mg(TFSI)_2$ wird das Konzept elektrogesponnener Polymerelektrolyte auf Magnesium Ionen Batterien (MIBs) übertragen. Durch variation von Leistsalzkonzentration und Weichmacher (SN) wird die höchste Leitfähigkeit bei einer molaren Zusammensetzung von PEO:$Mg(TFSI)_2$ 36:1 zu 1.2×10^{-5} S/cm bei 293 K bestimmt. Die Leitfähigkeiten der elektrogesponnen Membranen liegen dabei bei gleichbleibender Zusammensetzung, zum Teil um mehrere Größenordnungen, über jenen, die an durch Lösungsgußhergestellten Membranen gemessen werden.
An allen hergestellten Membranen wird eine strukturelle und electrochemische Analyse durchgeführt. Die Kristallinität wird mittels Pulverdiffraktometrie (P-XRD) untersucht. Die Morphologie der Fasern wird mit Rasterelektronenmikroskopie (engl. scanning electron microscopy, SEM) abgebildet und die thermischen Eigenschaften werden mit Diffenrentitalthermoanalyse (engl. differential scanning calorimetry, DSC) untersucht. Die ionischen Leitfähigkeiten werden aus impedanzspektroskopische Daten berechnet und die Zyklisierbarkeit mittes Cyclovoltammetry untersucht.

List of Abbreviations

AN	acetonitrile
ASSB	all-solid-state battery
BOB	bis(oxalato)borate, $B(C_2O_4)_2^-$
CPE	composite polymer electrolyte
DSC	differential scanning calorimetry
GPE	gel polymer electrolyte
LIB	lithium ion battery
MIB	magnesium ion battery
PAN	polyacrylonitrile
PEIS	potentiostatic electrochemical impedance spectroscopy
PEO	poly(ethylene oxide)
PVDF	poly(vinylidene fluoride)
PVDF-HFP	poly(vinylidene fluoride-*co*-hexafluoropropylene)
SN	succinonitrile
SPE	solid polymer electrolyte
TFSI	bis(trifluoromethane)sulfonimide, $(CF_3SO_2)_2N^-$

1 Introduction

On the way to an environmental-friendly future and the associated move from fossil to sustainable energy sources, lithium ion batteries (LIBs) pushed through as energy carrier. They are widely used for portable devices and electrical vehicles and potential candidates for storage of peak energy in the grid.[1] The main components in commercial LIBs haven't changed drastically during the last decades. On one side they consist of a lithium transition metal oxide active material in a composite cathode. As an active species on the anode side graphite is widely used. Electrodes are separated by a porous polymer membrane soaked with an organic lithium-ion conducting electrolyte. This organic electrolyte brings some challenges. The used components are deleterious and flammable and therefore a potential risk of leakage or thermal runaway occurs.[2] Also, the dissolution of transition metals from the cathode active material, therefore the degradation of it associated to capacity fading remains a drawback of some liquid electrolytes.[3] Another challenge is the desire to enhance the potential window and thus, the power for new generation lithium-based batteries, as LIBs are getting close to their physicochemical limit.[4] Besides finding cathode materials with higher reduction/oxidation potential, the change from composite to lithium metal anodes would increase the operation window. As lithium metal reacts with organic liquids, the combination of conventional electrolytes and lithium metal anodes leads to more hazardous batteries with fast degradation.[5, 6] A potential approach to address these challenges are all solid state batteries (ASSBs), where the liquid electrolytes are substituted by solid electrolytes. These solid electrolytes are either an inorganic ion conducting phase or a polymer based composite.[1, 7] Another approach, and also part of the post lithium-ion technology, is the change to non-lithium-based batteries, like magnesium ion batteries. Switching to a 2+ charged ion as the mobile species brings some new benefits and challenges.[8]

1.1 All-Solid-State-Batteries

The possibility of higher energy densities and faster charging leads to an increasing interest in all-solid-state batteries.[6] The plus in energy density and safety by replacing liquid electrolytes with a solid electrolyte (SE) has to be guided by a new understanding for cell stacking, cell chemistry and ionic transport mechanisms.[9] While conventional

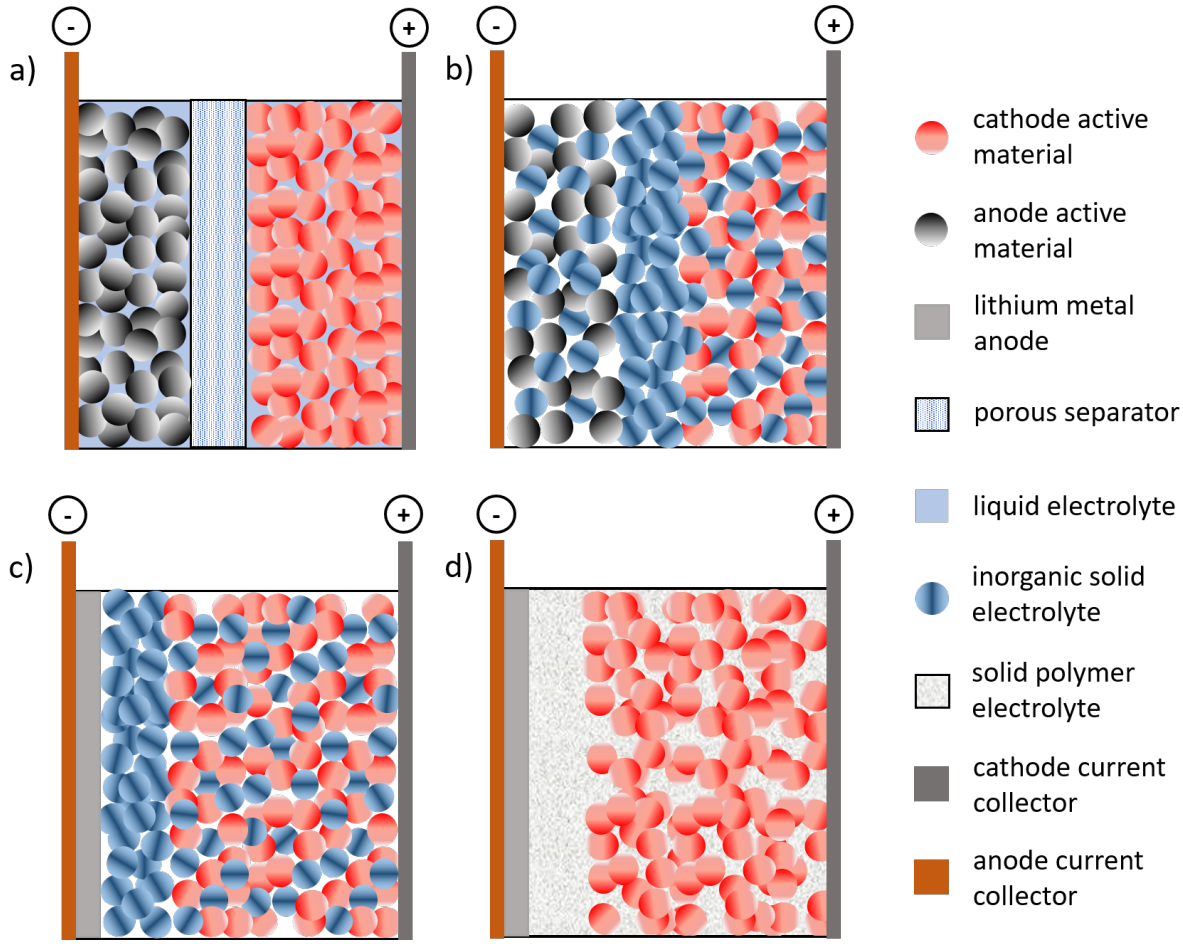

Figure 1: *Schematic structure of a) a conventional lithium ion battery with a porous separator membrane and liquid electrolyte, b) an all solid state battery with inorganic solid electrolyte and a mixture of solid electrolyte and active material mixed as cathode and anode, c) an all solid state battery with lithium metal anode, solid electrolyte and mixed solid electrolyte and active material cathode and d) an all solid state battery with lithium metal anode and solid polymer electrolyte. The need of conductive carbon is neglected in all schemes.*[6, 10, 11]

LIBs have their porous electrodes and separators filled with liquid electrolyte, Figure 1a, for ASSBS there are different ways of incorporating a solid electrolyte to ionically connect anode and cathode while electrically separating them. One approach is to build composite anodes and cathodes where the active material is mixed with an inorganic solid electrolyte and an electrically conductive carbon. These two electrodes are separated by a layer of inorganic electrolyte, Figure 1b. The use of lithium metal

anodes instead of composite anodes could increase the operating voltage and power of an ASSB further. One possibility is to use a composite cathode and an inorganic solid electrolyte as described before, Figure 1c. The inorganic solid electrolyte could also be substituted by a solid polymer electrolyte, Figure 1d. The SPE is used to fill all pores of the cathode and as an electrolyte layer to separate the lithium metal anode and the cathode active material.

1.2 Solid Electrolytes

As described for the different cell stacking options for ASSBs, solid electrolytes are either based on crystalline or glassy inorganic ion conductors or on polymers mixed with conducting salts, inorganic fillers or organic, plasticizing additives.[7, 12] In this section an overview over the different electrolyte systems is given. Regardless of the chosen approach the used electrolyte system has to fulfill certain requirements. The ionic conductivity at room temperature should be about 10^{-4} S/cm or above. The electrolytes should have a wide electrochemical operation window and low electrical conductivity. The lithium ion transference number should be high, ideally the electrolytes are single ion conductors.[13] Preferably, the ionic conductivity shows a low temperature dependency (low activation energy) and large temperature range for operation.[14]

1.2.1 Inorganic Solid Electrolytes

By exhibiting moderate to high ionic conductivity a lot of different crystalline or amorphous inorganic systems are qualified as inorganic solid electrolytes. To give a systematic overview, the different systems could be sorted by differentiating between oxides or sulfides.[15] A further classification is given by sorting the inorganic solid electrolytes by their structure. Here they are divided into LISICON-like, Argyrodite, Garnet, NASICON-like, Li-Nitride, Li-Hydride, Perovskite and Li-Halide.[13, 16]
LISICON is used as an abbreviation for lithium super ion conductor, the term describes solid solutions which are isostructual with γ-Li_3PO_4.[17, 18] A known example is $Li_{10}GeP_2S_{12}$, which exhibits an ionic conductivity of 10^{-2} S/cm at room temperature with a transference number of $t_{Li^+} = 0.99$.[9, 19]
The Argyrodite structure type goes back on the crystal structure of Ag_8GeS_6.[20] A Li ion conducting representative of this structure is Li_6PS_5Br operating with an ionic conductivity in the order of 10^{-3} S/cm.[21, 22]
The first lithium metal oxides with a garnet-type structure were $Li_5La_3Nb_2O_{12}$ and $Li_5La_3Ta_2O_{12}$. Their overall ionic conductivity was determined to be 10^{-6} S/cm at room temperature.[23] Later Ta or Nb were substituted by Zr, so a $Li_5La_3Zr_2O_{12}$ (LLZO) garnet type solid electrolyte was reported with an increased overall lithium ion con-

ductivity of 10^{-4} S/cm at room temperature.[24]
NASICON-like structures are based on an $A_xB_2(PO_4)_3$ composition. The structure is built up by PO_4 tetrahedra connected to the corners of BO_6 octrahedra. The resulting channels are filled with A^+ ions. A basic example is the $LiTi_2(PO_4)_3$.[13, 25] The aluminum-doped version of this structure $Li_{1.3}Al_{0.3}Ti_{1.7}(PO_4)_3$ shows Li ion mobility up to 7×10^{-4} S/cm.[26]
Lithium nitrides and lithium phosphorus nitrides, Li_3N and $LiPN_2$, respectively show a conductivity of up to 10^{-4} S/cm at elevated temperatures.[27, 28]
As an example for lithium hydrides, $LiBH_4$ was reported to show fast Li mobility at conductivities of 10^{-7} S/cm.[29] This material is suitable for potential application with a lithium metal anode and $LiCoO_2$ cathode.[30]
The Pervoskite structure is based on a ABO_3 composition. The BO_3^- corner linked octrahedra built up a cage for the A^+, which is thereby surrounded by 12 oxygen atoms.[31] One example for a solid electrolyte with this structure is $Li_{0.34}La_{0.51}TiO_{2.94}$. The material shows an overall room temperature conductivity of 10^{-4} S/cm.[16, 32]
The most prominent Li-Halides are spinel-type chlorides Li_2MCl_4 with M = Mg, Mn, Fe, Cd. Those are Li-ion conductors with a conductivity in the range of 10^{-4} S/cm.[33, 34]

1.2.2 Polymer Electrolytes

In 1973 P.V.Wright first demonstrated the solubility of alkali metal salts in poly(ethylene oxide).[35] It was only two years later when he presented their ionic conductivity.[36] The good electrochemical and physical properties of PEO mixed with LiX [X = BF_4^-, ClO_4^-, $(CF_3SO_2)_2N^-$ ($TFSI^-$), $B(C_2O_4)_2^-$ (BOB^-)...] salts makes the polymer still a main component in many SPEs.[37, 38] Polymer electrolytes are either classified as solid polymer electrolytes (SPEs), gel polymer electrolytes (GPEs) or composite polymer electrolytes (CPEs). SPEs consist of a polymer matrix, a conducting salt and small amounts of plasitcizers or organic liquids. GPEs are based on the same components as SPEs but with a higher fraction of (ionic) liquids. CPEs are SPEs or GPEs with inorganic particles used as additives.[39, 40] For some systems in literature it is not completely clear, whether they should be classified as SPEs, GPEs or CPEs. Nevertheless, this classification will be used here to structure the overview on different polymer electrolytes.

Solid Polymer Electrolytes

Poly(ethylene oxide) is still present as a polymer host in the majority of the solid polymer electrolytes. This is due to its high dielectric constant and the excellent ability to dissolve cations with the ether groups[37, 41] It is suitable for combination with a huge variety of conducting salts and other fillers.[42] Besides ethers also polysulides and polyamines are possible candidates to coordinate ions with the electrons of the

heteroatoms.[43] The ionic conductivity of the SPE with PEO as a host is strongly dependent on the used conducting salt. Large and soft anion containing LiX are used preferably as these are easily dissolved and the anion acts as plasticizer.[44, 45]
If $LiPF_6$, a common conducting salt in liquid electrolytes for LIBs, is admixed to PEO at 15wt% reaches an ionic conductivity of 10^{-4} S/cm at 318 K. The conductivity rises with conducting salt concentration and reaches a plateau at 15wt%, further increase to 20w% conducting salt content does not increase the ionic conductivity at these temperatures.[46]
For the system PEO_n:$LiBF_4$ a maximum conductivity of about 10^{-6} S/cm at 293 K is reported if n = 3. The conductivity again depends on the conducting salt concentration.[47]
Early reports from 1986, where $Li(CF_3SO_3)$ is used in molar ratio of PEO:$Li(CF_3SO_3)$ of 10:1 of about 10^{-7} S/cm at 293 K is calculated from AC impedance methods.[48, 49]
A solid polymer electrolyte utilizing LiTFSI as a conducting species at the same molar composition of PEO:LiTFSI 10:1 ionic conductivity of 4×10^{-5} S/cm are achieved.[50]
The use of plasticizers is a common way to enhance the Li^+ mobility in polymer electrolytes. For some solid lubricants it is not clear whether they should be sorted as SPEs or GPEs. A few examples with succinonitrile (SN) as organic additive should be named here. In the system PEO:LiTFSI with a molar ratio of 11:1 the ionic conductivity is raised from near 5×10^{-6} S/cm for a SN-free SPE to 5×10^{-5} S/cm when 15% SN are added. The maximum conductivity is reached for a PEO-free SN:LiTFSI system. The latter shows poor mechanical stability and due to the absence of polymer can not be categorized as SPE anymore.[51]
When PEO:$LiBF_4$ SPEs are activated by a high amount of SN the ionic conductivity is drastically increased. A PEO:SN:$LiBF_4$ with a molar composition of 9:30:1 is reported to show 1.1×10^{-3} S/cm at 300 K.[52]
As examples, other then PEO, polyacrylonitrile (PAN), poly (vinylidene diflouride) (PVDF), poly(methyl methacrylate) (PMMA) and poly(vinyl alcohol) (PVA) should be named.[42, 53, 54] Another concept for SPEs with lithium transference numbers as high as $t_{Li^+} = 1$ are single-ion conducting polymer electrolytes. Here the anion is fixed to or part of the host polymer to make the Li^+ the only mobile species. The interested reader is referred to a review of Zhou *et al.*.[42, 55]

Gel Polymer Electrolytes

In the field of GPEs a variety of organic solvents and ionic liquids are used as liquid part. Only few examples should be named here.
Poly(ethylene glykol) (PEG) with low molecular mass of 600g/mol can be used to substitute PEO in a PEO:$Li(CF_3SO_3)$ 9:1 system. The initial (0% PEG) electrolyte performed with an ionic conductivity of 1.3×10^{-5} S/cm at 298 K. This conductivity

was increased with increasing amount of PEO being substituted by PEG. The maximum was reached at a PEO:PEG:PEO:Li(CF_3SO_3) composition of 4.5:4.5:1 with an ionic conductivity of 1.7×10^{-3} S/cm at 298 K.[56]
Besides PEG a mixture of the organic solvents ethylene carbonate (EC) and propylene carbonate (PC) is used to gel polymer electrolytes. PAN-based GPEs with different LiX (X = ClO_4^-, AsF_6^-, $CF_3SO_3^-$) reached ionic conductivities in the range of 10^{-3} S/cm at 298 K, and thus as high as liquid electrolyte $LiClO_4$ in EC/PC.[57, 58]
Low viscosity or room temperature ionic liquids as 1-butyl-3-methylimidazolium bis-(trifluoromethylsulfonyl)imide (BmImTFSI) are another option to gel polymer electrolytes. The advantage of liquid electrolytes is the high boiling point compared to organic solvents, what brings a plus in safety. When combined with a mixed PMMA/PVC:LiTFSI 70 wt%:30 wt% (PVC, poly(vinyl chloride) an ionic conductivity of 1.6×10^{-4} S/cm at 298 K is reached if 60 wt% of the GPE is BmImTFSI. In comparison 1.1×10^{-6} S/cm at 298 K are reached in this system if no ionic liquid is used.[58, 59]

Composite Polymer Electrolytes

To form CPEs different kinds of inorganic particle are used in a polymer matrix. Besides the ionic conductivity, the mechanical strength should be increased by the addition of these particles.[40] One option are the inorganic solid electrolytes named in the section before. Another option are non lithium containing solids, mostly oxides like TiO_2, $BaTiO_3$, ZnO or Al_2O_3.[60]
So the addition of 10 wt% TiO_2 to a polymer electrolyte system PEO:$LiClO_4$ with a molar composition of 8:1 showed increased ionic conductivity of 10^{-5} S/cm at 303 K. In comparison the ionic conductivity of SPE PEO:$LiClO_4$ SPE with a molar composition of 8:1 without any further additives is at 10^{-8} S/cm at 303 K.[61]
One example to demonstrate the use of barium titanate in CPEs is the addition of 1.4 wt% $BaTiO_3$ to a PEO:$LiClO_4$ polymer electrolyte with a molar composition of 8:1. The small amount of inorganic additive resulted in an increase of ionic conductivity by one order of magnitude to result in 1.1×10^{-3} S/cm at 343 K.[62]
Addition of 5% ZnO to the same PEO:$LiClO_4$ 8:1 electrolyte leads to an 100-fold increase in ionic conductivity at about 300 K resulting in 10^{-7} S/cm. At around 360 K the ionic conductivities of the ZnO containing and the additive free system are both determined to be at 10^{-4} S/cm.[63]
The system PEO:$LiClO_4$ 10:1 is reported to have increased ion transport properties if 25wt% Al_2O_3 is added during membrane preparation. The room temperature conductivity raised from 9.1×10^{-7} S/cm to 1.1×10^{-3} S/cm to 4.8×10^{-6} S/cm.[64] Nano-porous Al_2O_3 with different surface modifications are tested to investigate, if not only equally

sized particles and homogeneous distribution of these particles is crucial for increased conductivities. Therefore, 10wt% nano-structured Al_{23} with acidic, basic, neutral or weakly acidic surface are used on a PEO:LiTFSI polymer electrolyte with a molar composition of 9:1. The conductivity increased from 1.98×10^{-5} S/cm for a weakly acidic surface to 5.61×10^{-5} S/cm for a acidic surface. Al_2O_3-free PEO:LiTFSI 9:1 SPEs show 7.03×10^{-6} S/cm in this study. All conductivities were measured at 298 K.[65]
The number of different possible polymer hosts, conducting salts, inorganic and organic additives leads to countless combinations for polymer electrolytes.[40, 66, 67]

1.3 Magnesium Ion Batteries

To drastically increase the volumetric capacity in ASSBs the use of a Li-metal anode is crucial, compare Figure 1. Besides the increased power this also brings the hazards of short circuits due to dendrite growth and high reactivity with the atmosphere, moisture and other cell components. An alternative to Li metal anodes is the switch to Magnesium Ion Batteries (MIBs). The redox potential of magnesium is just about 600 mV higher than for lithium, -2.4 V vs. SHE for Mg/Mg^{2+} compared to -3.0 V vs. SHE for Li/Li^{+}.[8] Although the specific capacity is also lower for magnesium, the volumetric capacity is higher, 2062 mAh/cm^3 for lithium compared to 3833 mAh/cm^3.[68] Further advantages of magnesium are the facts that magnesium metal anodes are considered dendrite-free and that the metal is one thousand times more abundant than lithium.[69] But the activation of magnesium metal anodes is still challenging, as it builds up a passivating electrode-electrolyte interface with most of the known electrolyte systems used in LIBs.[70]

The first MIBs were presented in 2000 by Aurbach *et al.*. There a Mg-metal foil anode, a $Mg_xMo_3S_4$ (x = 0−1) Chevrel phase cathode active material and $Mg(AlCl_{3-x}R_xR')_2$ in hexane as an electrolyte were used.[70] The research in Mg-ion cathode materials concentrated either on the optimization of the Chevrel phase[71] or on systems more familiar with LIB cathode materials like $MgMn_2O_4$ or MgS batteries.[72, 73, 74] Besides finding a stable, high potential cathode with fast Mg^{2+} diffusion, the design of electrolyte system suitable for efficient operation with Mg metal anodes is an ongoing challenge.[74, 75]

The first solution showing electrochemically induced stripping and plating of Mg ions on a Mg metal surface were based on *Grignard* reactions.[76] Besides these, magnesium organoborates were reported in 1990 by Gregory et al.[77], they, together with *Grignard*-type electrolytes, failed in practical application.[70, 78]

Another starting point is based on early reports of plating Mg from organic solvents like dimethylacteamide or dimethylformaide using $Mg(CF_3SO_3)_2$ as a conducting salt.[79] In more recent studies $Mg(TFSI)_2$ in ether solvents like diemthylether,[80] glyme and diglyme with ionic conductivities of 5×10^{-3} S/cm[81, 82] is used as suitable electrolyte for application.

Gel polymer electrolytes (GPEs) are suggested based on the concepts known from LIBs and liquid electrolytes. Some of them work with a PEO polymer-host Mg conducting salt, *e.g.* $Mg(TFSI)_2$, $Mg(ClO_4)_2$ or $Mg(CF_3SO_3)_2$, together with poly(ethylene glycol) diglycidyl ether (PEGDE) as liquid component. The GPE, where the $TFSI^-$ anion is used, shows an ionic conductivity in the range of 10^{-3} S/cm at room temperature.[83] As it is desirable to have liquid-free batteries, like the ASSB approaches for LIBs, numerous inorganic solid electrolytes[84] and solid polymer electrolytes are reported for

MIBs. Comparable to those polymers used with lithium and sodium conducting salts, poly(ethylene oxide) or poly(propylene) oxide are used as matrix for Mg^{2+} ion conducting SPEs.[85, 86] In some of them additionally inorganic additives like Al_2O_3 or MgO are used to enhance the conductivity, the mechanical stability, or both. As conducting salt a variety of different MgX_2 salts is used.[87] As an example, again $Mg(TFSI)_2$ is admixed at a low concentration of PEO:$Mg(TFSI)_2$ 9:1 or PEO:$Mg(TFSI)_2$ 40:1. The resulting SPEs showed an ionic conductivity of 10^{-6} S/cm and 10^{-7} S/cm at room temperature.[88] Polymers other than PEO which are used for Mg-ion conducting SPEs are polyvinyl alcohol (PVA), polyacrylonitrile (PAN) or polyvinylidene difluoride (PVDF).[87] The latter shows a conductivity of 6×10^{-8} S/cm when $Mg(NO_3)_2$ is used at a PVDF:$Mg(NO_3)_2$ composition of 7:3. This conductivity is increased by the addition of 3w% MgO to 10^{-4} S/cm at 303 K.[87, 89]

1.4 Electrospinning

In 1934 a process to prepare polymer threads in an electrical field was introduced by A. Formhals.[90] Based on this finding electrospinning was developed. A process, where polymer fibers can be obtained from a polymer melt or a polymer solution.[91, 92] The polymer solution (or melt) is, with a constant feed rate, pressed through a cannular. To this metal cannular a high voltage supply is connected, in order to apply voltages in the kV range to the polymer solution. The cannular is fixed with a known, but changeable distance to a grounded collector. [93] At the tip of the cannular a liquid drop is formed. By increasing the applied potential, a charge is build up at the surface of this tip. If the potential is high enough, the liquid drop at the tip becomes conical and a *Taylor Cone*[94] is formed as illustrated in Figure 2.[91, 95] The polymer chains

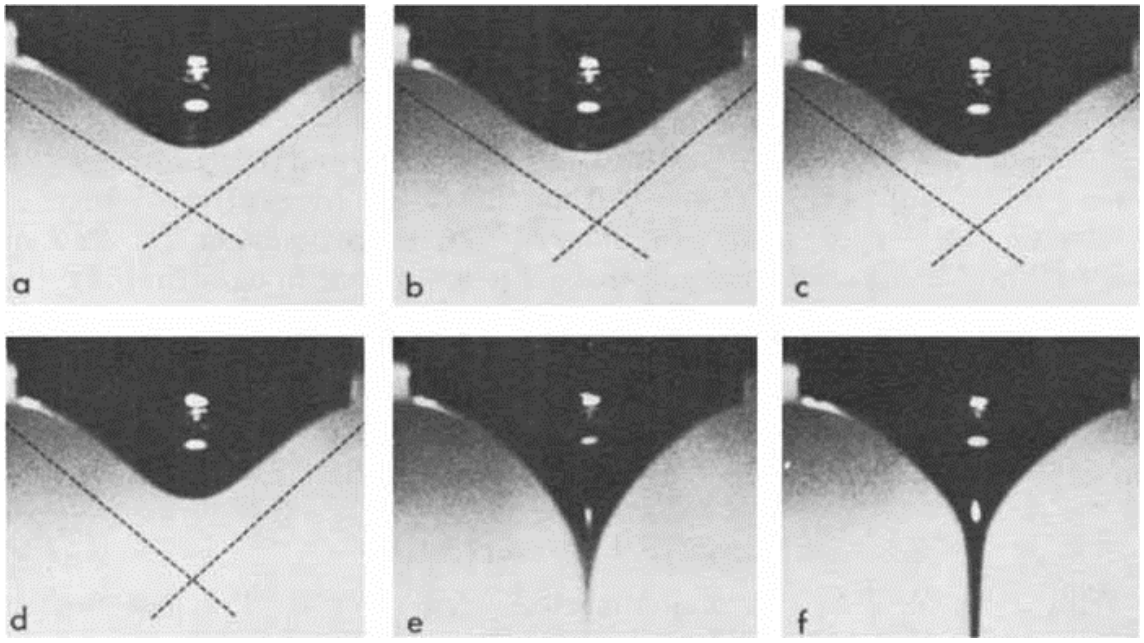

Figure 2: *Images showing the development of polymer solution from a drop to a jet with increasing voltage from a) to f). The conical form is called Taylor Cone. Figure reprinted with permission of John Wiley and Sons, from "Electrostatic Fiber Spinning from Polymer Melts. I. Experimental Observations on Fiber Formation and Properties; L. Larrondo and R. St. John Manley; Journal of Polymer Science: Polymer Physics Edition; Vol.19:909-920;* ***1981****. Permission conveyed through Copyright Clearance Center, Inc.*

in the solution stabilize the jet. The solvent evaporates constantly on the way to the collector, thereby the diameter of the jet shrinks. This leads to an increase of charge per area. When the repulsive force between the charges exceed the surface tension of the liquid jet, it splits into more and more jets with smaller diameter.[96] With this, polymer fibers in the sub-micrometer rang are obtained. Successful fiber fabrication and the morphology of the obtained fibers depend on various internal and external factors listed

in Table 1. Internal factors are properties of the used educts, like the molecular weight of the polymer and the dielectric effect of the solvent, or the overall polymer solution, like the surface tension of the solution. External factors are properties of the used electrospinning setup, like voltage, distance between the cannular and the collector or the type of collector used.[93, 95, 97]

Table 1: *List of internal and external factors influencing the formation of polymer fibers during the electrospinning process.*

internal factors	external factors
molecular weight of the polymer	voltage
solution viscosity	feed rate
surface tension	temperature
solution conductivity	effect of collector
dielectric effect of solvent	diameter of cannular
	collector-cannular distance
	atmosphere
	type of collector

1.5 Electrospun Polymer Electrolytes

Polymer membranes produced *via* electrospinning are already used in applications from medical use to electronics.[98] In the field of batteries electrospun products have been tested in every component of the cell. The first step into the direction of electrospun polymer electrolytes, is the use of electrospun polymer membranes soaked with a liquid electrolyte. Doing this, inert polymers with a large temperature window for application are used, *e.g.* PVDF or PAN. Besides this, a variety of electrospun GPE is known, most of them based on PVDF or poly(vinylidene fluoride-*co*-hexafluoropropylene) (PVDF-HFP).[99] There are only few reports on membranes prepared *via* electrospinning where no additional liquid electrolyte is used.[100] With a electrospun PEO:PC:$LiClO_4$ 5×10^{-6} S/cm at r.t. are reported for a molar composition of 17:4.7:1.[101] The same group reported electrospun polymer electrolytes based on a molar compostion of PEO:EC:$LiClO_4$ 17:5.4:1, where SiO_2 or Al_2O_3 nanoparticles are added. For silicon dioxide the highest ionic conductivity is reported for the addition of 0.07wt% SiO_2 to reach 8×10^{-6} S/cm at r.t., while for the addition of aluminum oxide the maximum ionic conductivity is reported at 0.21wt% Al_2O_3 to be 6×10^{-6} S/cm at the same temperature.[102] In a comparative study of different LiX (X= Cl, TFSI, ClO_4) an electrospun membrane with a molar composition of PEO:EC:$LiClO_4$ 11.3:7.2:1 was determined to have an ionic conductivity of 3×10^{-4} S/cm at room temperature if acetonitrile is used as solvent.[103] Our group reported on electrospun PEO:SN:$A$$BF_4$ (A=

Li, Na) solid electrolytes in the recent years. For lithium conducting membranes the highest ionic conductivity is determined to be 2×10^{-4} S/cm at room temperature for a molar composition of PEO:SN:$LiBF_4$ 36:8:1.[104] For sodium conducting membranes the ionic conductivity also is at 10^{-4} S/cm at room temperature at the same molar composition of EO:SN:$NaBF_4$ 36:8:1.[105]

2 Experimental Methods

2.1 List of Chemicals

Table 2: *List of used chemicals with the respective manufacturer and purity.*

Chemical	Manufacturer	Grade
Al_2O_3	AEROXIDE®, Evonik	-
acetonitrile	VWR	>99.8%, H_2O < 30 ppm
acetonitrile	Sigma Aldrich	purified
$LiBF_4$	Sigma Aldrich	> 99,99%
LiTFSI	Sigma Aldrich	⩾ 98%
$Mg(TFSI)_2$	Sigma Aldrich	⩾ 98%
Poly(ethylene oxide) ($M_w = 300.000$)	Sigma Aldrich	-
succinonitrile	Sigma Aldrich	99%

Nanostructured Al_2O_3 is dried at 473 K and < 10^{-2} mbar in vacuum glass oven (*Büchi*) for three days. Poly(ethylene oxide) is dried at 313 K and < 10^{-2} mbar for 24 h. To purify succinonitrile, it is sublimated at 313 K and < 10^{-2} mbar in a dried *Schlenk*-flask. After purification and drying, all chemicals are stored in a glovebox (*MBraun*). The solvent and conducting salts are used as provided and also stored under inert gas conditions.

2.2 Solvent-based Membrane Preparation

Two different solvent-based preparation methods are used to obtain homogeneous polymer membranes. Electrospinning produces membranes of thin polymer fibers, while solution casting results in dense, non-porous polymer films. Both techniques can be run with the same polymer-based solutions and are therefore suitable to investigate the influence of the preparation method on the resulting solid polymer electrolyte membranes.

2.2.1 Poly(ethylene oxide)-based Polymer Solutions

To prepare PEO-based solutions for usage in SPE preparation, all steps have to be carried out under inert atmosphere and dry conditions.
In a first step a 50 mL *Schlenk* flask with magnetic stirrer is dried at an argon *Schlenk-Line*. Therefore, a vacuum of 10^{-2} mbar is applied while the flask is heated with a *Heat-Gun* (Typ 3522, *STEINEL*). After the flask is cooled down to r.t., it is flushed with argon. This sequence is repeated three times before the flask is transferred to a *Glove Box*. The required amount of acetonitrile is added to the pre-dried PEO. The

mixture is continuously stirred. When the PEO is fully dissolved (approx. 1 h), the conductive salt of choice is added to the solution. After one hour of homogenization, SN is added if needed. The solution is stirred overnight prior to the solution casting or electrospinning process.
If nanostructured Al_2O_3 has to be added to the polymer solution, it is dispersed in acetonitrile using Ultra-Turrax mixing (T18 digital ULTRA TURRAX®, *IKA*) for 2×2 min at 10000 rpm before dissolving the polymer.

The ratio of PEO to succinonitrile and conducting salt is denoted in molar ratios. To calculate the moles of the polymer, the molar mass of the repeating unit is used.

2.2.2 Electrospinning

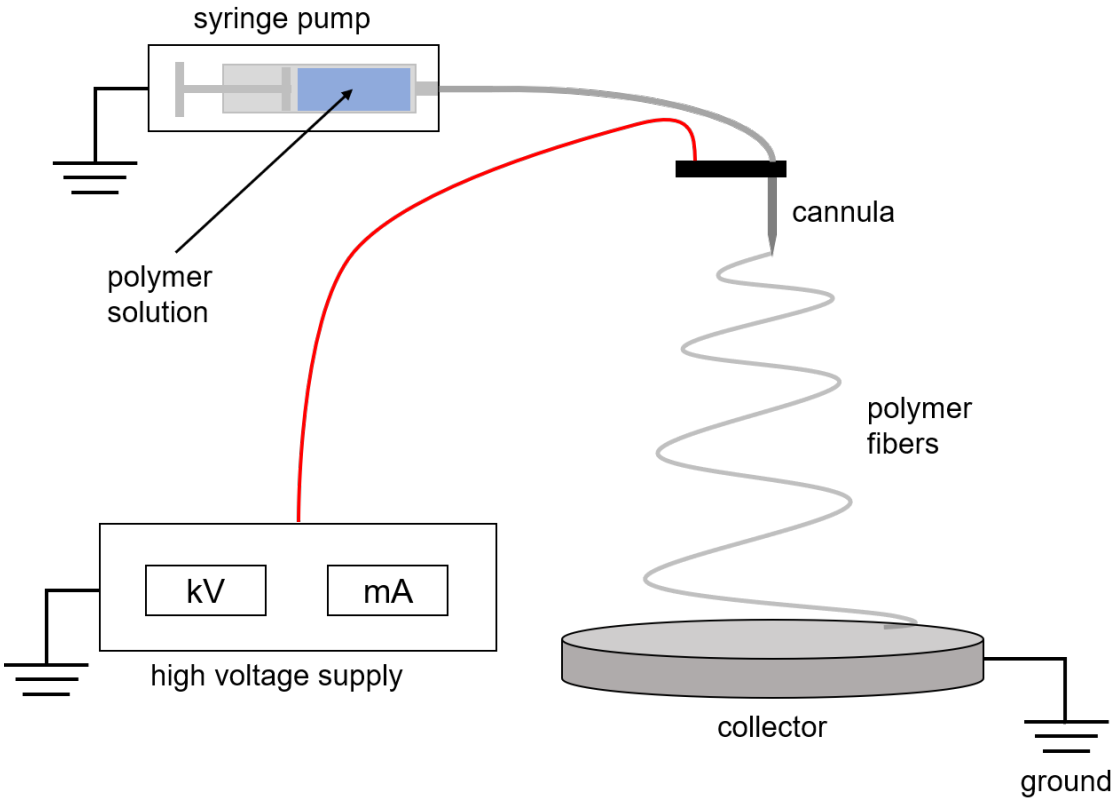

Figure 3: *Scheme of the electrospinning setup used for the fabrication of fibrous polymer membranes.*

Prepared polymer solutions are taken with a 10 mL syringe (*NORM-JECT* ®). The syringe is mounted to a syringe pump (Modell 540060, *TSE-Systemprogammable Syring Pump*). The cannula tip is cut to result in a straight opening, and connected to the syringe using a Teflon-tube (60° Shore, inner diameter 2 mm). The cannula is attached over a grounded collector and connected to a high voltage supply (LNC 30000-2pas,

Heinzinger). A scheme of the setup is given in Figure 3. The distance between the tip of the cannula and the grounded collector is adjustable between 5 cm and 25 cm. The applied voltage is between 5 kV and 30 kV. An aluminum ring with 10 cm diameter is prepared with a cross of Teflon tape and used as collector, compare Figure 4.
To start the electrospinning process, the solution is pumped through the cannula until a drop is formed at the tip. The high voltage is switched on and the syringe pump set to a constant feed rate to supply sufficient polymer solution at the tip of the cannula to allow continuous formation of polymer fibers at the collector. Feed rate, voltage and collector distance have to be adjusted to the properties of the used solution.
The electrospinning process proceeds under ambient conditions. The obtained membranes are dried in vacuum at r.t. for 24 h and stored under inert atmosphere.

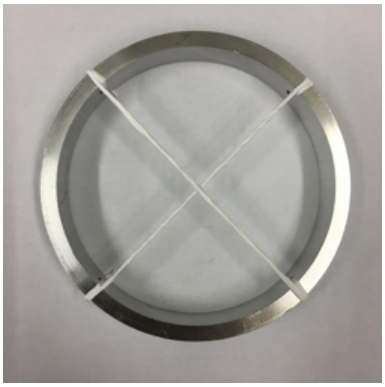

Figure 4: *Aluminum ring, prepared with a Teflon tape cross, used as collector in the electrospinning process.*

2.2.3 Solution Casting

To aim for nonporous polymer membranes, the prepared polymer solutions are dropped onto a glass plate. The solution is dried at room temperature at 1 atm to prevent the formation of bubbles in the membrane. After 2 h the polymer films are transferred to a vacuum chamber and dried under vacuum at r.t. for 24 h. The dried products are stored under inert gas conditions until conducted to analysis.

2.3 Solvent-free Membrane Preparation

In contrast to the solvent-based preparation techniques, hot pressing is used as a solvent-free possibility to aim for self-standing and homogeneous polymer membranes. Hot pressing is suitable for all particle-free SPE combinations. If inorganic particles are used, hot pressing does not fulfill adequate mixing of all educts and hence leads to inhomogeneous products.

2.3.1 Hot Pressing

To aim for hot pressed SPEs, all educts are mixed in a mortar and ground to obtain a homogeneous mixture of solids. The mixture is then transferred to a pressing tool (Figure 5), which was made by the workshop of the TUM Chemistry department. To prevent the polymer membrane from sticking to the pressing tool, a heat and chemical resistant MYLAR® foil is used. The filled pressing tool is placed between the heating plates (4000 Series™, High Stability Temperature Controller, *Specac*) of a hydraulic press (Atlas™Manual 15 TON Hydraulic Press, *Specac*). The membranes are pressed with 5 t for 2 h at 363 K. After the pressing tool is cooled to r.t., it is opened and the SPEs are stored under inert gas conditions until applied to characterization methods.

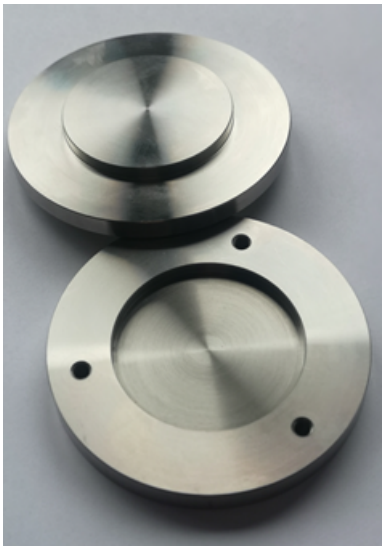

Figure 5: *Pressing tool for hot pressing polymer membranes.*

2.4 Analytical Methods

2.4.1 Powder X-Ray Diffraction

The crystallinity of the produced polymer membranes is checked *via* X-ray powder diffraction. Small discs of the sample (diameter = 10 mm) are fixed between two stripes of tape (Magic Tape®, *Fa. Scotch*, *3M*) before mounted in a flat-bed sample holder. Measurements were conducted using a *STOE* STADI P-diffractometer with a Ge(111)-monochromator for Cu K_α (λ = 1.54056 Å) and a *Dectris* MYTHEN DCS 1K solid state detector. Diffraction patterns are collected in a 2θ-range from 5° to 80° with 1° step size and 10 s/step., resulting in a total measurement time of 16 min. All measurements are carried out at r.t.

2.4.2 Differential Scanning Calorimetry

The thermal properties of the products are investigated by differential scanning calorimetry. Aluminum crucibles are filled and closed by cold pressing in inert atmosphere (Ar). The measurements are conducted in a *Netzsch* Maia DSC 200 F3 under constant nitrogen flow. The sample is measured for two cycles between 123 K and 523 K with a heating and cooling rate of 10 K/min. For electrospun samples only the first cycle is taken for discussion, as the unique fiber structure is destroyed once the sample is molten.

2.4.3 Scanning Electron Microscopy

To observe the fibrous structure of the prepared membranes, small samples of the dried SPEs are fixed to a conductive carbon tape and attached to the sample holder of the scanning electron microscope (SEM). Two different devices are used depending on the need to do energy-dispersive X-Ray spectroscopy (EDX) in combination with the SEM imaging.
If EDX is required, the sample holder is transferred to the vacuum chamber of a JOEL JCM-6000 NeoScop™, which is operated with a JEOL JED-2200 EDS. For SEM imaging an acceleration of 15 kV is applied.
If no EDX is required, the sample is imaged with a EVO MA10 SEM (*ZEIS*), which is operated at lower acceleration voltage of 5 kV.

2.4.4 Electrochemical Properties

Ionic Conductivity *via* Electrochemical Impedance Spectroscopy

Determination of ionic conductivity is done by electrochemical impedance spectroscopy. For potentiostatic frequency dependent measurements, a TSC battery cell (*rhd instruments*) with nickel-coated stainless-steel electrodes (diameter = 8 mm) is used in combination with a potentiostat (*Metrohm Autolab B. V.*). The integrated temperature element and the impedance measurements are controlled by the same software (*NOVA 2.1*, *Autolab B.V.*, Version 2.1). The fitting function of the software is used to interpret the obtained impedance data by defining a suitable equivalent circuit. Before every measurement, the required temperature is applied to the sample and maintained for 1200 s to ensure equal temperature distribution across the sample thickness. During the measurement, a sinus wave with an amplitude of 20 mV vs. OCV is used in a frequency range from 10^7 to 10^{-1} Hz. In every frequency decade at least six points are recorded. After the measurement the samples temperature is changed again. Samples are measured in a temperature range according to their thermal properties (upper temperature limit < melting point of SPE).

From the fitted resistances r [Ω], the ionic conductivity σ [S/cm] is calculated by using equation 1, where d [cm] is the thickness and A [cm^2] is the contact area in the cell. The thickness of SPEs is determined after the temperature dependent measurements with a micrometer screw (*Holex*, 0-25 mm, 0.001 mm accuracy).

$$\sigma = \frac{1}{r} \times \frac{d}{A} \tag{1}$$

Activation Energy

The activation energy E_A [kJ/mol] is determined by using an *Arrhenius*-Type plot, where $\ln(\sigma)$ of the temperature dependent measurements is plotted over the inverse temperature 1/T, following equations 2-3:

$$\sigma = A \times e^{-\frac{E_A}{RT}} \tag{2}$$

$$ln(\sigma) = ln(A) - \frac{1}{T}\frac{E_A}{R} \tag{3}$$

where σ [S/cm] is the total ionic conductivity, A the pre-exponential factor, R [J/(mol*K)] the universal gas constant and T [K] the temperature. Using a linear fit, equation 4,

the activation energy is calculated from the slope m by using equation 5.

$$y = mx + t \tag{4}$$

$$E_{\mathrm{A}} = -m \times R \tag{5}$$

Cyclic Voltammetry

To check the transport properties of the SPEs, symmetrical metal vs. metal electrochemical cells are applied. As electrode material, a metal suiting the SPE is chosen. The electrode material (Li-metal, Mg-metal) is chosen to suit the conducting species in the tested membranes. Coin cell configuration (*Hohsen*) is used with 1-1.5 mm solid state spacers to fill the cell bodies and apply sufficient pressure for the electrochmical cycling. (Figure 6) After the cells are closed under argon atmosphere, they are transferred to a climate chamber (*Binder*) set to 298 K and connected to a VMP3 potentiostat (*Biologic*) to apply the cyclic voltammetry (CV). After an initial EIS measurement and an initial 10 min OCV period, the potential is varied with a constant rate between an an equidistant positive/negative voltage limit according to the determined OCV.

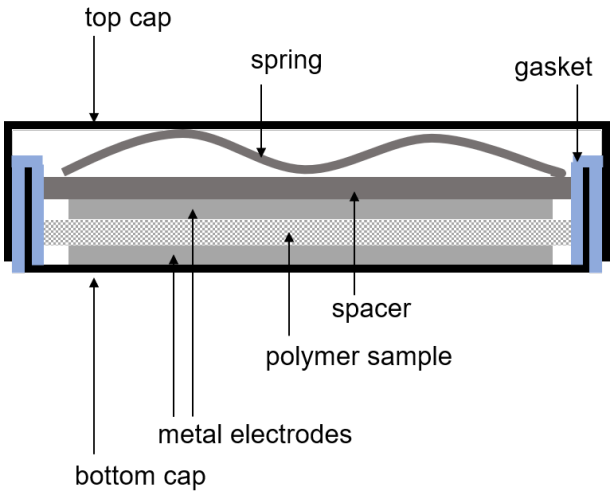

Figure 6: *Coin cell configuration used for cyclic voltammetry of solid polymer electrolytes between two metal electrodes.*

2.4.5 Dynamic Light Scattering

The particle size distribution of nanostructured particles was determined *via* dynamic light scattering (DLS). Therefore, the particles were dispersed in acetonitrile and filled in single use disposable poly(styrene) cuvettes. These were placed in a *Malvem Zetasizer ZS* and measured with a wavelength of 633 nm at 298 K. Particle sizes between 0.4 nm and 10,000 nm were detected.

2.4.6 Nuclear Magnetic Resonance Spectroscopy

All solid state nuclear magnetic resonance experiments were performed on *Advanced III* spectrometer (*BRUKER*) with a 7 T magnet with resonance frequencies of 75.4 MHz for ^{13}C, 116.5 MHz for ^{7}Li and 282.4 MHz for ^{19}F. A *BRUKER* 4 mm triple resonance MAS NMR probe was used during all measurements. To get information on the dynamics of the ions of the conducting salts, temperature dependent static measurements were performed for ^{7}Li and ^{19}F. For more insights into the polymer matrix ^{13}C-MAS NMR experiments were conducted. As references for all measurements LiCl(aq) for ^{7}Li, TMS for ^{13}C and $CFCl_3$ for ^{19}F were used.[106]

3 Results

3.1 Electrospun Li(TFSI)@Polyethylene Oxide Membranes as Solid Electrolytes

Patrick Walke[a], Katharina M. Freitag[a], Holger Kirchhain[b], Matthias Kaiser[b], Leo van Wüllen[b] and Tom Nilges[a]

[a] Technical University Munich, Department for Chemistry, Lichtenbergstraße 4, 85748 Garching bei München

[b] Augsburg University, Institute of Physics, Universitätsstraße 1, 86159 Augsburg

Z. Anorg. Allg. Chem. **2018**, 644, 1863-1874
First published online: November 27th 2018
DOI:10.1002/zaac.201800370

In the search for safer electrolytes, one possible solution are solid polymer electrolytes.[107] Poly(ethylene oxide) (PEO)is a prominent candidate to be used as polymer matrix, as it is known for its excellent ability to solve alkali metal salts.[35] In earlier works, our group showed that electrospinning is a suitable technique to fabricate dense networks of micrometer fibers consisting of PEO and $LiBF_4$ or BF_4. Those networks could be applied as solid polymer electrolytes (SPEs).[104, 105] In this project, we investigated the possibility to produce lithium bis(trifluoromethansulfonyl)imide (LiTFSI) containing electrospun PEO-based SPEs and their electrochemical properties. Therefore, PEO:LiTFSI and plasticizer-containing PEO:SN:LiTFSI membranes with different molar compositions are prepared *via* electrospinning. For the plasticizer-free PEO:LiTFSI SPEs molar compositions of 36:1 and 18:1 are successfully prepared. Those ratios are maintained for the addition of succinonitrile leading to membranes with molar ratios of PEO:SN:LiTFSI 36:8:1 and 18:3:1, which can be successfully prepared. For all compositions dense networks of 1-3 μm fibers are obtained. With XRD no longe range ordering other than of pure PEO is observed. Further analysis with solid state NMR showed an amorphous PEO_{11}LiTFSI and a crystalline PEO_6LiTFSI phase. From DSC the melting points are determined to 323 K and 325 K for PEO:LiTFSI 36:1 and 18:1. Adding SN slightly decreased the melting points to 322 K and 313 K for PEO:SN:LiTFSI 36:8:1 and 18:3:1 compositions. The from impedance spectroscopy calculated ionic conductivity for plasticizer-free membrane with the lowest conducting salt content, PEO:LiTFSI 36:1 is determined to be 4.4×10^{-6} S/cm at 298 K which increases to 1.1×10^{-4} S/cm

at 328 K. For membranes with double the amount of conductive salt, PEO:LiTFSI 18:1 the ionic conductivity raises to 9.8×10^{-6} S/cm at 298 K and 2.8×10^{-4} S/cm at 328 K. The activation energy of these membranes is about 72 kJ/mol, independent of the conducting salt concentration. The addition of plasticizer has no pronounced positive effect. For the PEO:SN:LiTFSI 18:3:1 membrane the ionic conductivity at 293 K is determined to 8.6×10^{-6}, if the SN content is increased to a PEO:SN:LiTFSI 36:8:1 composition the ionic conductivity raises to 1.9×10^{-5} at 293 K even though the conducting salt concentration is lower. The activation barriers are determined to 77 kJ/mol (18:3:1) and 57 kJ/mol (36:8:1). Although the activation energy is lower for the latter, the ionic conductivity is only increased by a small value. Samples of all compositions are tested in symmetrical Li vs. Li coin cells. After few initial formation cycle all membranes can be cycled for at least 14 cycles, when cycled between -1 V and 1 V vs. Li/Li^+ whit a constant scanning rate.

Author contributions: P.W. and K.M.F. prepared the polymer membranes, determined the ionic conductivity from electrochemical impedance measurements, examined the phase analysis via X-ray powder diffraction and the thermal properties from differential scanning calorimetry, made the scanning electron microscopy pictures and tested the cycle ability in symmetrical Li vs. Li coin cells with cyclic voltammetry measurements. H.K. and M.K. carried out the solid state NMR measurements and interpreted the resulted data. P.W., K.M.F., H.K., L.v.W. and T.N. were involved in writing the manuscript. P.W., H.K., L.v.W. and T.N. discussed the results and revised the manuscript.

Journal of Inorganic and General Chemistry
ZAAC
Zeitschrift für anorganische und allgemeine Chemie

DOI: 10.1002/zaac.201800370

ARTICLE

Electrospun Li(TFSI)@Polyethylene Oxide Membranes as Solid Electrolytes

Patrick Walke,[a] Katharina M. Freitag,[a] Holger Kirchhain,[b] Matthias Kaiser,[b] Leo van Wüllen,*[b] and Tom Nilges*[a]

Dedicated to Prof. Dr. W. Bensch on the Occasion of his 65th Birthday

Abstract. Thin membranes of lithium-bis(trifluoromethan)sulfonimide@poly (ethylene oxide) (or Li(TFSI)@PEO) were fabricated by electrospinning from acetonitrile solutions of the starting materials at room temperature. Membranes were tested with and without succinonitrile (SN), acting as a plasticizer to enhance the ion mobility in the systems. Our experiments substantiate, that SN does influence the electrochemical performance and physical properties of the membranes. Homogeneous amorphous membranes were only realized for SN-containing samples, while phase segregation and crystallization occurred for SN-free representatives. Membranes of different compositions were tested and the optimum molar mixture of PEO:SN:Li(TFSI), in terms of membrane conductivity, was identified as 36:8:1. Conductivities up to up to 2.8×10^{-4} S·cm^{-1} were determined by impedance spectroscopy for this membrane. Used as solid electrolytes without the aid of any additional electrolyte in symmetric Li vs. Li cells, a reasonable stability upon Li cycling could be observed. Here we illustrate that electrospun plasticizer-modified Li(TFSI)@PEO membranes show high conductivities at very low conductive salt concentrations, compared with solution casted or hot pressed representatives. This feature renders these materials as potential candidates for separators in all solid-state batteries or related energy storage applications.

Introduction

Battery science focuses more and more on all-solid state solutions for electrodes, electrolytes and separators, where no liquid phase is necessary.[1–3] A solution, out of many others, to address this issue is the usage of polymer electrolytes and conductive salt additives[4] without the aid of additional liquid phases. Ideally, the conductive salt additive fully dissociates in the polymer matrix, the mobile ion species can attract as many as possible coordination sites in the polymer to allow enhanced ion mobility/transport, and the salt@polymer membrane is stable against reactive electrodes, like for instance bare Li or Na metal.[5] The scientific work on such a multi parameter problem began more than 40 years ago with the discovery that polyethylene oxide (PEO) can effectively be used as a matrix and can act as a proper host for conductive salts, inducing fast ion transport.[6]

Many blends or pseudo binary and ternary systems exist today, varying the polymer host, the conductive salt and the additive.[7] Such additive or plasticizer in conductive salt@polymer membrane tends to accelerate the ion mobility or improves the mechanical properties of the system. Solution casting, dip coating, or hot pressing are common methods to realize ion conducting thin membranes. Recently, an alternative process to access thin membranes of conductive salts in polyethylene oxide (PEO), like $LiBF_4$@PEO [8] and $NaBF_4$@PEO ,[9] has been reported. In this process, electrospinning was used to fabricate thin-film membranes, which showed high conductivities up to 9×10^{-4} S·cm^{-1} and reasonable stability against lithium and sodium metal. In the case of $LiBF_4$@PEO membranes, a conductivity increase of two orders of magnitude, compared with solution casted systems at room temperature, illustrates the potential of these materials. While the lithium systems were optimized by succinonitrile (SN), acting as a plasticizer additive, the $NaBF_4$@PEO showed almost the same electrochemical performance without such a modification. Those positive results motivated us to evaluate the influence of anion exchange on the electrochemical properties and the cation mobility in related materials. We decided to investigate lithium-bis(trifluoromethan)sulfonimide [Li(TFSI)] as a conductive salt additive, due the well-known and beneficial properties of this compound in battery applications. It is a well-established conductive additive in polymer electrolytes[10] and plays a crucial role in modern ionic liquid-optimized battery electrolytes,[11] just to name some. Another important point is the good dissociation tendency in many solvents and the overall excellent electrochemical stability.

* Prof. Dr. T. Nilges
E-Mail: tom.nilges@lrz.tum.de
* Prof. Dr. L. van Wüllen
E-Mail: leo.van.wuellen @physik.uni-augsburg.de
[a] Synthesis and Characterization of Innovative Materials Group
Department of Chemistry
Technical University of Munich
Lichtenbergstrasse 4
85748 Garching b. München, Germany
[b] Institute of Physics
Augsburg University
Universitätsstrasse 1
86159 Augsburg, Germany
Supporting information for this article is available on the WWW under **http://dx.doi.org/10.1002/zaac.201800370** or from the author.

Without any doubt, alternative solid ion conductors are of interest, which unify properties like high ion conductivity, electrochemical stability, low toxicity and low price. Our general purpose is to verify if electrospinning of conductive salt@polymer membranes is an alternative route to classically fabricated ones. Herein, we report on the synthesis and characterization of electrospun Li(TFSI)@PEO membranes, which might become an interesting solid ion conductor alternative to present solution casted or hot pressed representatives.

Experimental Section

Synthesis of Membranes: The solution for electrospinning composed of different starting materials was prepared by dissolving PEO (7.95 mmol, 0.350 g) in 7.5 mL acetonitrile (VWR, >99.8, H_2O <30 ppm) until the PEO is completely dissolved. Li(TFSI) was added in the right amount to this solution (see Table 1) and stirred until everything is dissolved. In the final step, the plasticizer was added and the whole solution was stirred overnight for full homogenization. The whole process was performed in a flask in an argon atmosphere.

Table 1. Compositions of Li(TFSI)@polyethylene membranes including the amount of plasticizer SN (if necessary).

PEO:SN:Li(TFSI)	PEO / mol%	SN /mol% (g, mmol)	Li(TFSI) /mol% (g, mmol)
36:0:1	97.3	–	2.7 (0.0633, 0.22)
18:0:1	94.7	–	5.3 (0.1266, 0.44)
18:3:1	82.0	13.5 (0.1057, 1.32)	4.5 (0.1266, 0.44)
36:8:1	80.0	17.8 (0.1414, 1.76)	2.2 (0.0633, 0.22)
36:14:1	70.5	27.5 (0.2475, 3.10)	2.0 (0.0207, 0.22)

Membranes were fabricated by electrospinning in a home-made electrospinning apparatus as described previously in literature.[8] All fibers were fabricated with a 0.9 mm injector, at a flow rate of 3 mL·min^{-1}, and an acceleration voltage of 17 kV. The fibers were collected on a flat bed collector and dried at a vacuum of $p < 7 \times 10^{-2}$ mbar for 3 d. Each membrane was stored in a glove box under inert gas atmosphere (argon, H_2O, and O_2 < 1 ppm) prior to usage.

X-ray Powder Diffraction Phases Analysis: Powder XRD measurements of selected membranes were executed with a STOE STADI P diffractometer (Cu-$K_{\alpha 1}$ radiation, λ = 1.54051 Å, Ge monochromator) with a flat-bed sample holder. α-Si (a = 5.43096 Å) was used as internal standard. The sample membranes were punched out from the ready-prepared and dried membranes and measured directly in transmission geometry.

Differential Scanning Calorimetry (DSC): DSC measurement of all Li(TFSI)@polyethylene oxide membranes were performed in aluminum crucibles with a NETZSCH DSC 200 F3 Maja. A standard heating and cooling rate of 10 K·min^{-1} was used during the measurements. All measurements were performed in a continuous nitrogen stream.

Scanning Electron Microscopy (SEM): SEM pictures of the entire membranes were taken with an EVO MA10 Scanning Electron microscope (Zeiss) using an acceleration voltage of 2–5 kV. Such a low voltage was applied to avoid charging effects of the membranes during the measurements.

Electrochemical Characterization: Total conductivities were measured with a Metrohm Autolab B. V. potentiostat and an integrated FRA 32 *M* module. Membranes of 1 cm in diameter were punched out from a large area membrane and placed between nickel-coated stainless-steel electrodes in rdh Instruments TSC battery cell unit. The thicknesses of the membranes were determined by a Holex micrometer screw up to an accuracy of ± 0.1 µm. Impedance spectra were recorded in a frequency range of 1 MHz to 0.01 Hz and a temperature range of 278 to 328 K in steps of 5 K.

Cyclovoltammetry was conducted with a VMP3 Potentiostat from Biologic in a symmetric cell setup with Li metal electrodes of 1.3 cm diameter and 0,6 cm thickness on both sides of the membrane. The symmetrical cell was mounted in a glove box in an argon atmosphere (O_2 and H_2O concentration < 1 ppm) and placed inside a coin cell without the usage of any additional conductive additive or electrolyte. A voltage window of ± 1 V was applied to the coin cells and a scanning rate of 0.1 mV·s^{-1} was chosen at 298 K. The thickness of the membranes was 100 µm.

Nuclear Magnetic Resonance Spectroscopy: Solid state nuclear magnetic resonance experiments were performed with a BRUKER Avance III spectrometer equipped with a 7 T magnet at resonance frequencies of 75.4 MHz, 116.5 MHz, and 282,4 MHz for ^{13}C, ^{7}Li and ^{19}F, respectively. A 4 mm triple resonance MAS NMR probe from Bruker was used for all measurements. Temperature dependent ^{7}Li and ^{19}F NMR measurements were performed under static conditions to obtain information about the dynamics of the Li cation and TFSI anion within the membranes. Additional ^{13}C-MAS NMR experiments were performed to characterize the PEO membrane. The signals were referenced as usual to LiCl(aq) for ^{7}Li, $CFCl_3$(aq) for ^{19}F and TMS for ^{13}C employing adamantane as external reference. Temperature calibration was performed employing the chemical shift of the ^{207}Pb NMR signal of $Pb(NO_3)_2$ as a chemical shift thermometer.[12]

Typically, relaxation delays between 5 s and 120 s were used for ^{7}Li and ^{19}F; for ^{13}C, relaxation delays of 10 s to 60 s were used for the single pulse excitation spectra, whereas 5s were used for the $^{13}C\{^{1}H\}$-cross polarization (CP)-MAS spectra with high power proton decoupling. For quantitative ^{13}C spectra, recorded after single pulse excitation under high power proton decoupling, relaxation delays of up to 300 s were used to ascertain full relaxation of possible crystalline constituents (crystalline PEO or PEOxLiTFSI).

Supporting Information (see footnote on the first page of this article): The supplement contains Nyqvist-Plots of represantative impedance measurements and additional Solid State NMR spectra.

Results and Discussion

State-of-the-art Solid Electrolyte Systems Based on PEO:Li(TFSI)

Li(TFSI)@PEO materials and membranes have been prepared by solution casting and has been intensively examined in the past as solid electrolytes.[13–15] A reasonable high ion conductivity up to 2.9×10^{-3} S·cm^{-1} was observed for certain compositions, which render such systems as potential candidates for applications as solid state ion conductors. The binary

phase field (Figure 1) of the two compounds shows several more or less defined crystalline compounds (see Figure 1) and it is dependent on the molar mass of PEO. Data for Figure 1A and B were adapted from the literature [M(PEO) = 4.5×10^3 g·mol^{-1}],[13–15] and weight fractions and mol fractions are denoted for clarity. In Figure 1C [16] we denote the originally reported Li(TFSI)-PEO phase diagram for M(PEO) = 4×10^6 g·mol^{-1}, whereas Figure 1D represents a M(PEO) = 5×10^6 g·mol^{-1} one.[17] Finally, Figure 1E shows the phase diagram for M(PEO) = 4.5×10^3 g·mol^{-1}.[14] In our study we used PEO with a molar mass of 3×10^5 g·mol^{-1} for best electrospinning performance. Our melting points determined for the different LiTFSI-PEO membranes are consistent with the ones reported for the low molar mass PEO phase diagram in Figure 1E. We therefore use this phase diagram for further discussions and interpretations.

In the Li(TFSI)-PEO phase diagram for M(PEO) = 4.5×10^3 g·mol^{-1} [14] three crystalline complexes with PEO:LiTFSI = 2:1, 3:1, and 6:1 exist in this system. Of special interest is the compositional range with 6:1 to 12:1, for which a crystallinity gap was postulated, consequently entailing the prospect of high ionic conductivity.

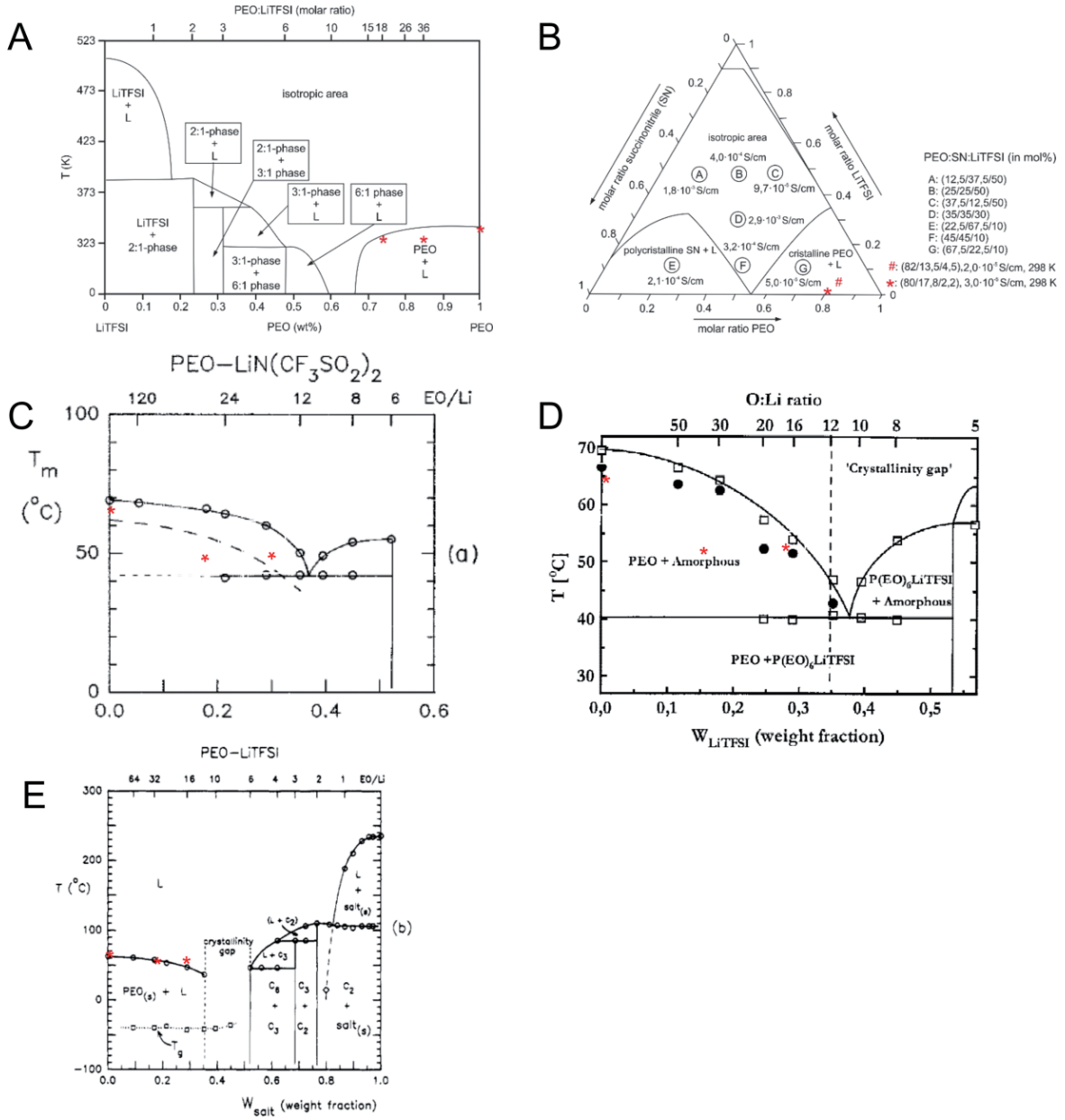

Figure 1. Binary Li(TFSI)-PEO and ternary Li(TFSI)-PEO phase diagrams adapted from data given in the literature (Vallee 1992,[13] Lascaud 1994,[14] and Echeverri 2012,[15] (left). (C) Li(TFSI)-PEO phase diagram [M(PEO) 4×10^6 g·mol^{-1}].[16] (D) Li(TFSI)-PEO phase diagram [M(PEO) 5×10^6 g·mol^{-1}].[17] (E) Li(TFSI)-PEO phase diagram [M(PEO) 3.9–4.5×10^3 g·mol^{-1}].[14] Stars * and # mark the melting points and sample compositions of the electrospun membranes, investigated in this study for M(PEO) = 3×10^5 g·mol^{-1} samples. (A) and (B) reprinted from reference[18], (C) – (E) reprinted with permission from…(to be filled in the case of acceptance.

However, subsequent studies have shown that this crystallinity gap is only accessible when employing PEO of low molecular weight. For high molecular weight PEO, the material was shown to consist of a mixture of pure PEO, crystalline $(PEO)_6$LiTFSI, and an amorphous eutectic with PEO:LiTFSI ≈ 11:1.[16,19] *Marzantowicz* et al. have monitored the crystallization of (PEO)*n*LiTFSI for $M(PEO) = 5 \times 10^6$ g·mol^{-1} within the crystallinity gap by conductivity measurements with simultaneous polarizing-microscopy and X-ray diffraction.[20] According to these authors an effective phase segregation occurs for compositions close to the eutectic. Once crystalline PEO or $(PEO)_6$LiTFSI has started to precipitate, salt is rejected to or drained from the remaining amorphous phase, so its composition is shifted towards the competing crystalline phase whose crystallization becomes thus favorable.

With an increasing amount of PEO, the well-defined crystalline compounds are vanishing and a much more complex phase behavior is present. In a NMR study[21] using high molecular weight PEO [$M(PEO) = 5 \times 10^6$ g·mol^{-1}] an ensemble of three different phases are found, pristine PEO, crystalline 6:1 PEO:LiTFSI, and amorphous 11:1 PEO:LiTFSI. Here, the amorphous phase plays a crucial role for the ionic mobility in the systems.

The pseudo-binary title membranes with the compositions of PEO:LiTFSI = 18:1 and 36:1 are located in the latter mentioned phase field and are marked with red stars in Figure 1, which represents and economic amount of conductive salt in the systems. *Prud'Homme* et al. has shown that a certain amount of ether functionalities is necessary in the compound to provide a substantial ion transport and conductivity through the membranes. It became obvious, that crystallization of the above-mentioned 6:1, 3:1 and 2:1 phases should be avoided, in order to provide an effective and high ion transport through the membranes. Crystallization hinders the fast and effective ion transport and traps the ions in defined environments. The transfer of ions on a short scale happens by coordination via the ether functionalities and long-range ion mobility occurs by local hops of the ions to oxygen pockets between the same or neighbored PEO chains. Two systems with a composition of 6:1 and 50:1 were subject to a conductivity study and 5×10^{-8} S·cm^{-1} and 2×10^{-7} S·cm^{-1} were determined as room temperature conductivities.[20] If the two systems are heated above the melting point this conductivity difference vanishes. In the non-crystalline and isotropic regime, enough ether functionalities are present for an effective ion transport. *Marzantowicz* et al.[19] investigated solution casted PEO:LiTFSI samples with 8:1, 10:1, 12:1, und 16:1 composition and they found fractions of the crystalline 6:1 compound, as well as partial crystalline PEO in their samples. The amount of crystalline 6:1 phase decreases with an increasing PEO content. A conductivity of 1×10^{-6} S·cm^{-1} was observed for the 16:1 sample at 293 K, which increases to 3×10^{-4} S·cm^{-1} at 328 K.

In our experiments we intended to get as close as possible to this composition but due to experimental reasons the maximal composition we could realize by electrospinning was 18:1 and we were only able to use PEO with an molar mass of $M(PEO) = 3 \times 10^5$ g·mol^{-1}. In terms of resource efficiency, this 18:1 composition is even better because it does contain less conductive salt than the previously mentioned ones.

Plasticizers like ethylene carbonate (EC) [22] or succinonitrile (SN) are applied to the PEO:Li(TFSI) systems in order to accelerate the chain motilities of the PEO matrix, to enhance the ion mobility in the compounds, and to reduce aging effects, which occur upon storage.[23] We selected SN for our studies due to the melting point of ca. 330 K, instead of EC, which melts at 309 K.[23] SN fits better to the expected range of application of the Li(TFSI)@PEO membranes, which is limited by the melting point of PEO (see Figure 4). A quasi-ternary phase field containing solution-casted Li(TFSI), PEO and SN materials were reported by *Echeverri* et al.[15] In Figure 1, the entire phase field is denoted, based on the reported data. The phase field can be separated in three different regions, an area with a high fraction of crystalline PEO, a second one with significant amounts of crystalline SN, and an isotropic region, where only amorphous phases are present. Conductivities in the different regions of the phase field are also given in this figure. An obvious trend can be observed which clearly shows, that high Li(TFSI) and SN contents, no phase separation, and a suppression of crystalline phases are important for an enhanced conductivity (this is valid in the isotropic region). This observation is in good accordance with the findings for the plasticizer-free membranes, where the highest conductivities are also found in isotropic and amorphous regions. The lowest conductivities in the quasi-ternary phase field are found in the PEO-rich region, where the SN and Li(TFSI) content is low and PEO is crystallized. Recently, a Density Functional Theory (DFT) and ab initio Molecular Dynamics (MD) simulation study examined the mechanisms and diffusion pathways in amorphous and crystalline PEO:Li(TFSI) 3:1 phases. Activation barriers for the Li ion hopping were determined (0.53 eV in the amorphous vs. 1.2 eV in the crystalline stage) and only half the activation energy is needed to move ions in the amorphous stage.[24] This finding is in perfect agreement with the experimental observation.

Another study by *Fan* et al. investigated the influence of an increasing SN content [0 to 95 mol% SN and 5 mol% Li(TFSI)] in solution casted PEO:SN:Li(TFSI) samples.[25] They found an increase of the conductivity from the SN-free sample of 5×10^{-5} S·cm^{-1} to the PEO-free one of 2×10^{-3} S·cm^{-1} at 293 K. Unfortunately, they found a significantly reduced mechanical stability for the PEO-free material compared with the SN-free one. A good compromise was a 14:3:1 one, where they found reasonable mechanical stability and conductivities of 5×10^{-4} S·cm^{-1} at 293 K and 2×10^{-3} S·cm^{-1} at 328 K.

Due to the findings stated above we decided to prepare compounds in the PEO-rich phase field for our electrospun membranes [PEO:SN:Li(TFSI) = 18:3:1 and 36:8:1] to check if low concentrations of the conductive and expensive salt and electrospinning of the membranes can result in more positive results than for the solution casted samples. Again, our 18:3:1 membrane represents the maximum salt concentration, which we were able to use for an electrospun membrane. The other 36:8:1 membrane represents the sample with the highest spin-

able SN contend and a reduced conductive salt fraction as compared with the other sample.

Electrospun PEO:Li(TFSI) Membranes

In Figure 2, representative SEM pictures of the two electrospun membrane systems with 18:1 and 36:1 composition (molar ratio) are shown. In both cases, we were able to fabricate a dense and uniform membrane with fiber diameters of 1–3 µm. A little denser membrane was realized in the case of the plasticizer-free 18:1 membrane than for the 36:1 system.

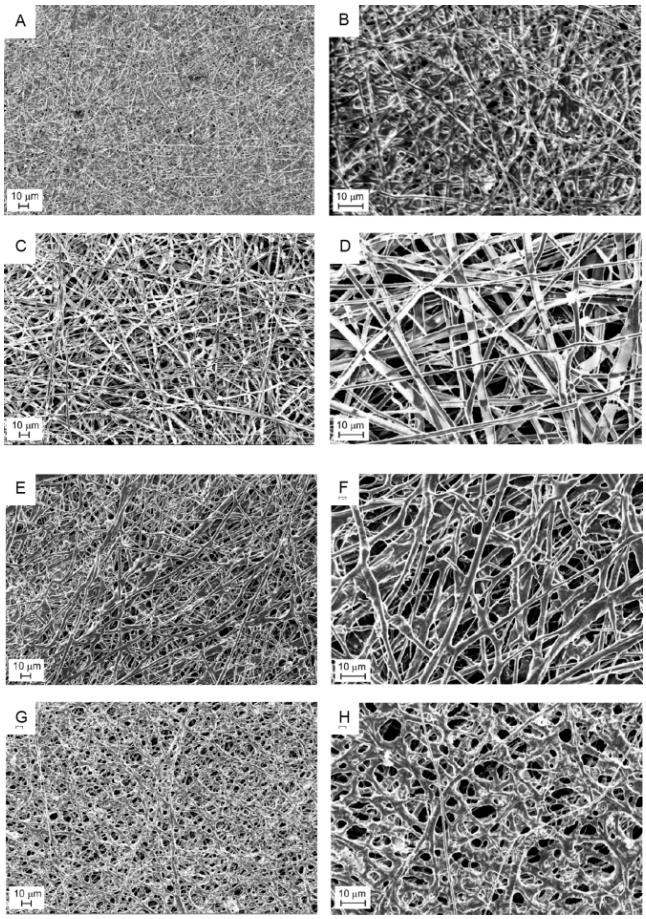

Figure 2. Representative SEM pictures of plasticizer-free Li(TFSI)@PEO with a molar PEO:LiTFSI ratio of 18:1 (A, B) and 36:1 (C, D), and plasticizer-containing (Li(TFSI),SN)@PEO membranes with a molar PEO:SN:Li(TFSI) ratio of 18:3:1 (E,F) and 36:8:1 (G,H).

Fortunately, and in contrast to the solution-casted samples reported in literature, we found no hints for the formation of crystalline 6:1 and other crystalline compounds in the XRD patterns. Very small particles or amorphous phases cannot be ruled out at this point (see later on in the NMR Section). At least, a hint of a lower crystallization tendency of PEO and an increased amount of an amorphous phase (broad signature around 20° 2θ) can be estimated (see Figure 3 top).

The melting points of the 18:1 and 36:1 membranes are slightly reduced from 336 to 325 and 323 K, respectively (Figure 4, top). In the case of the 18:1 a second thermal effect at

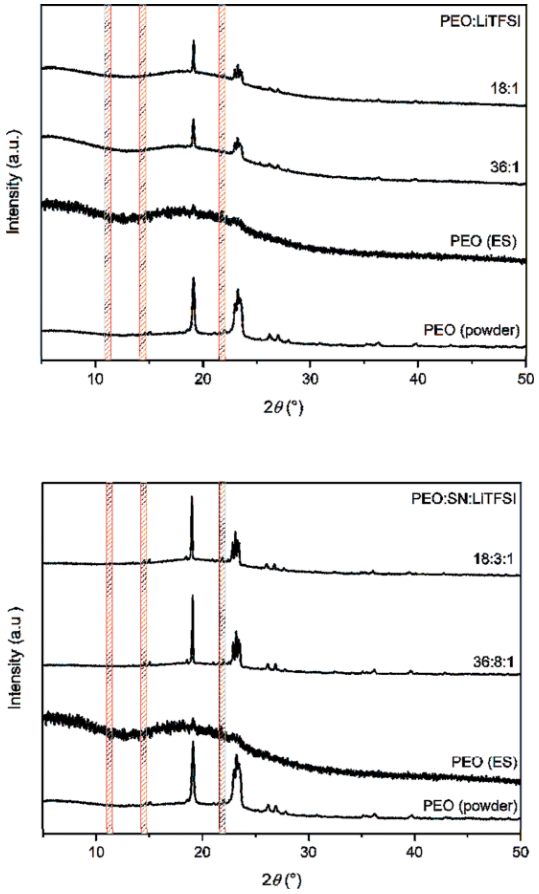

Figure 3. X-ray powder diffraction of plasticizer-free Li(TFSI)@PEO (top) and plasticizer-containing (Li(TFSI),SN)@PEO (bottom) membranes. The composition of each membrane is given in the figure. The red areas illustrate the regions were reflections of the crystalline $(PEO)_6Li(TFSI)$ might occur.[19,26]

308 K was found in the DSC experiment which one can assign to the solidification of the eutectic mixture according the phase diagram of high-molar mass PEO in Figure 1D.

Selected 18:0:1 and 36:0:1 membrane were investigated by impedance spectroscopy (IS) and cyclic voltammetry (CV) in order to verify the ion mobility, the ion transport properties, and the electrochemical stability against Li in battery half cells. The total ionic conductivity was determined from two different batches of dried membranes measured in two temperature windows of 278 to 303 K and 293 to 328 K. For the 36:0:1 membrane with the lowest Li(TFSI) content, we observed a conductivity of 4.4×10^{-6} S·cm^{-1} at 293 K which increased to 1.1×10^{-4} S·cm^{-1} at 328 K. Even this low conductive salt content results in higher room temperature conductivities as compared to the solution-casted 16:1 sample (1×10^{-6} S·cm^{-1} at 293 K) reported by *Marzantowicz* et al. in the literature.[19]

Upon doubling of the conductive salt component, the 293 K conductivity raised half an order of magnitude to 9.8×10^{-6} S·cm^{-1} which ended up at 328 K in a conductivity of 2.8×10^{-4} S·cm^{-1} (see Figure 5A).

Let's focus now on a comparison of electrospun systems directly. In a recent study, $LiBF_4$ was used as a conductive salt

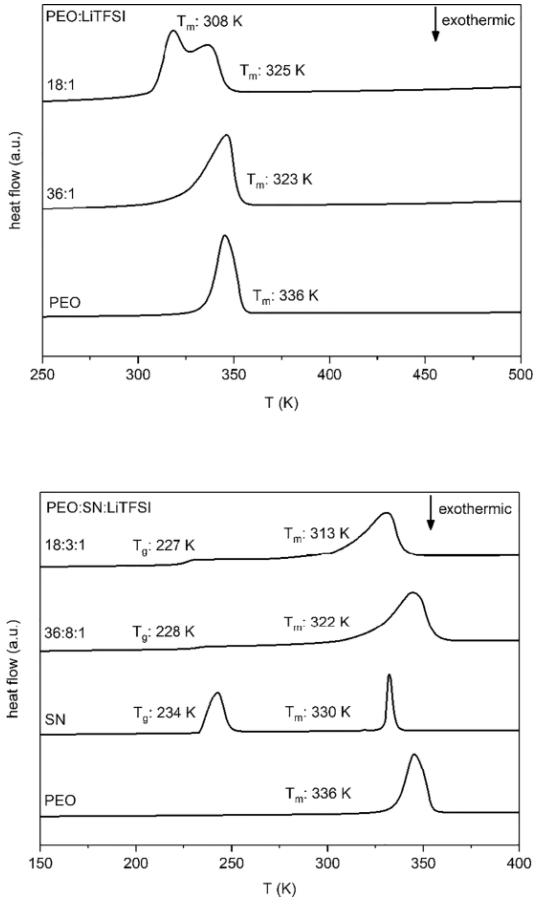

Figure 4. DSC curves of plasticizer-free Li(TFSI)@PEO and plasticizer-containing (Li(TFSI),SN)@PEO membranes, including the pure starting materials PEO and SN. The composition of each membrane in mol% is given in the figure.

additive and the same membrane compositions were examined concerning their electrochemical properties. For the 36:0:1 $LiBF_4$@PEO membrane a conductivity of 5.6×10^{-7} S·cm^{-1} at 293 K was found, which is one order of magnitude lower than for the Li(TFSI)@PEO membrane.[8] At 328 K the 36:0:1 $LiBF_4$@PEO membrane shows 1.5×10^{-5} S·cm^{-1}, which is again lower than the one of the Li(TFSI)@PEO membrane at the same temperature (1.1×10^{-4} S·cm^{-1}). The same tendency and increase in conductivity is present for the 18:0:1 membrane. Here, the $LiBF_4$@PEO membranes are again almost one order of magnitude lower in conductivity ($LiBF_4$@PEO membranes: 1.2×10^{-6} S·cm^{-1} at 293 K; 3.8×10^{-5} S·cm^{-1} at 328 K). Data are summarized in Figure 5E. It seems to be the case, that the type of the anion may cause a significant improvement of the total conductivity, which might be beneficial for applications. The question arose at this point, if the exchange does affect the activation energy for the ion hopping in the Li(TFSI) system.

We therefore conducted an Arrhenius plot and derived the activation barriers from the slope of the curves. Both membranes show Arrhenius-type behavior and an averaged activation barrier of 71(1) kJ·mol^{-1} (36:0:1 membrane) and 72(1) kJ·mol^{-1} (18:0:1 membrane). Data are summarized in Figure 5B. These activation barriers are almost the same than observed for $LiBF_4$@PEO membranes (75 kJ·mol^{-1}), featuring exactly the same conductive salt content. According to the activation barriers it seems that the exchange of $[BF_4]^-$ by $[TFSI]^-$ does not induce any changes. At least the coordination behavior of the Li ions in the PEO matrix seems to be not affected by the anion exchange, and the postulated mechanism of ion transport in PEO, where Li^+ is coordinated by oxygen of the PEO matrix and the Li ion transport is determined by an increased PEO chain mobility,[27–29] is still valid. For a detailed discussion of the underlying mechanism, the reader is referred to check the literature.[8,9] An investigation of the local ion mobility's is discussed in the NMR Section later on.

In order to evaluate the Li ion transport properties, we conducted CV measurements in a symmetric Li|Li(TFSI)@PEO|Li setup at room temperature. In Figure 6A and B we show the data for the 36:0:1 and the 18:0:1 membrane. Both membranes deliver a symmetric CV signal in a voltage range of ± 1 V, which is characteristic for a reversible Li transport under the given conditions. The 36:1 membrane shows a slight and continuous increase of the capacity up to the 14th cycle, whereas the 18:1 membrane seems to undergo a certain induction process in the first CV cycles, prior to the point when steady-state conditions are reached. This takes place at about 10 CV cycles. This finding is in contrast to $LiBF_4$@PEO membranes of the same composition,[18] where a steady loss of capacity was observed after the same amount of cycles. It became obvious, that Li(TFSI)@PEO membranes show an enhanced stability for the Li ion transport through the membrane compared with the $LiBF_4$ counterparts.

Electrospun PEO:SN:Li(TFSI) Membranes

In the case of $LiBF_4$@PEO electrospun membranes, the usage of SN as plasticizer was beneficial for the stability and overall electrochemical performance. Upon SN usage in those systems, the Li transport was reversible and a steady Li ion transport was realized and measured in CV experiments. The total conductivity raised almost two orders of magnitude, while the activation energy was more than halved. This results motivated us to verify the influence of SN to the Li(TFSI)@PEO membranes. We prepared membranes of the same composition than investigated before for the $LiBF_4$@PEO membranes, in order to make them as comparable as possible. Therefore, we prepared PEO:SN:Li(TFSI) = 36:8:1 and 18:3:1 membranes and conducted the same set of experiments than for the plasticizer free samples. We were able to spin comparable membranes in terms of fiber size, and density for the title membranes, as well as in the case of the previously examined and reported ($LiBF_4$,SN)@PEO ones (see Figure 1). In all cases, the fibers displayed a diameter of 1–3 µm, added up to a total membrane thickness of ca. 100 µm, and comparable fiber densities.

According to X-ray phase analysis it became obvious, that SN slightly increases the unwanted crystallization of PEO, as compared with the plasticizer-free membranes. Crystallization of PEO tends to reduce the ion mobility and increases the bonding interaction to Li ions in the matrix.[30,31] We observed

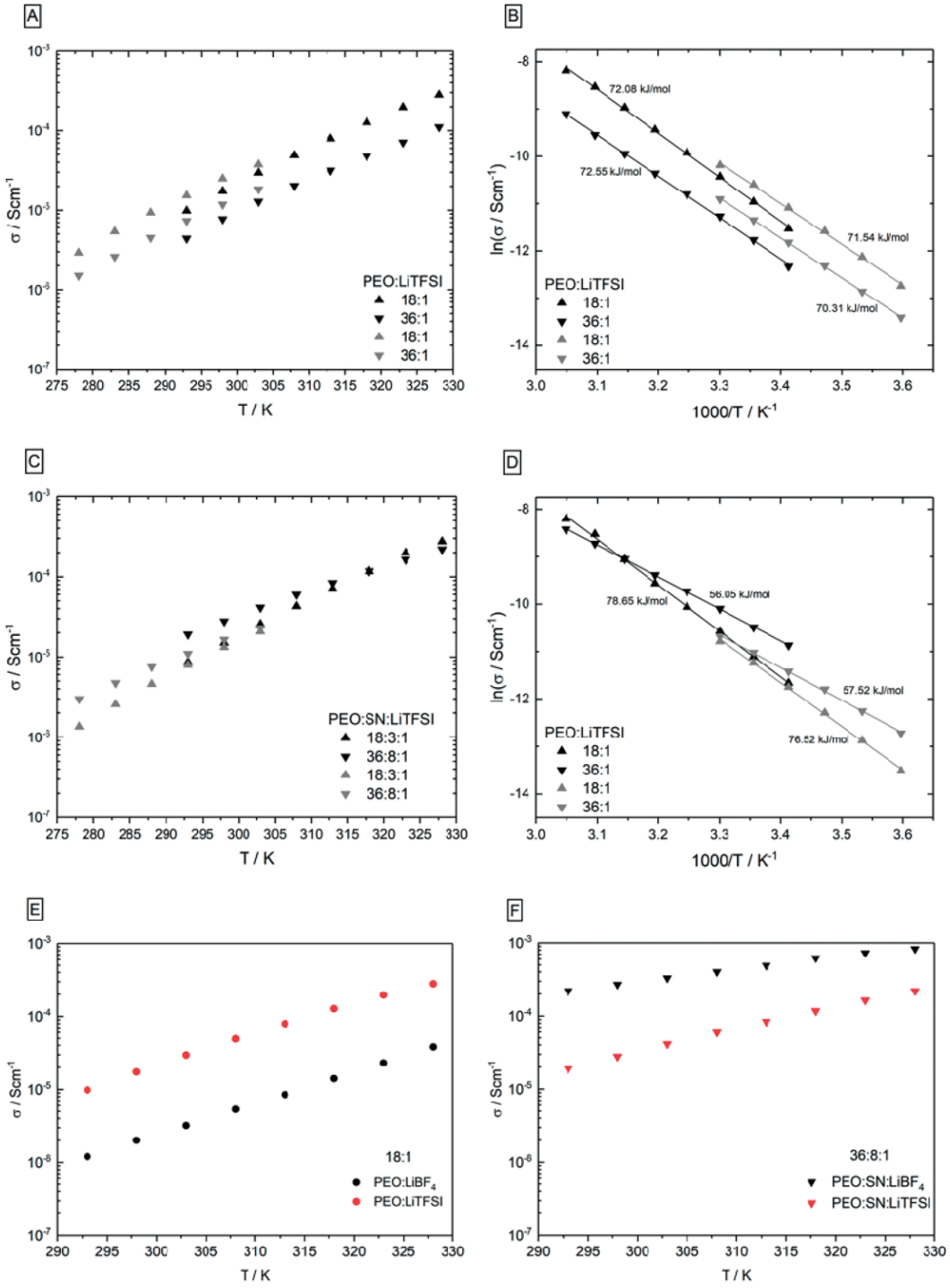

Figure 5. Total conductivities (A, C) of plasticizer-free Li(TFSI)@PEO and (Li(TFSI),SN)@PEO membranes, measured in two temperature ranges of 278 to 303 K (grey triangles), and 293 to 328 K (black triangles). On the right side (B, D) Arrhenius plots are denoted and activation energies are given. The composition (molar ratio) of the membranes is given for each set of experiments. (E, F) Conductivities of plasticizer-free and plasticizer-containing Li(TFSI)@PEO (red, 293 to 328 K data) and $LiBF_4$@PEO systems (black). Data for the $LiBF_4$@PEO systems are taken from reference[8].

a certain increased tendency for PEO to crystallize if SN is added as a component to the electrospinning solution, which manifest in more defined and stronger reflections in the XRD diffractograms (Figure 2). As observed for the plasticizer-free membranes, a shift in the melting points of the material can be observed. The additional SN reduces the melting points of 36:8:1 and 18:3:1 membranes, only a few Kelvin to values rather close to the values found for the SN-free ones. We deter-

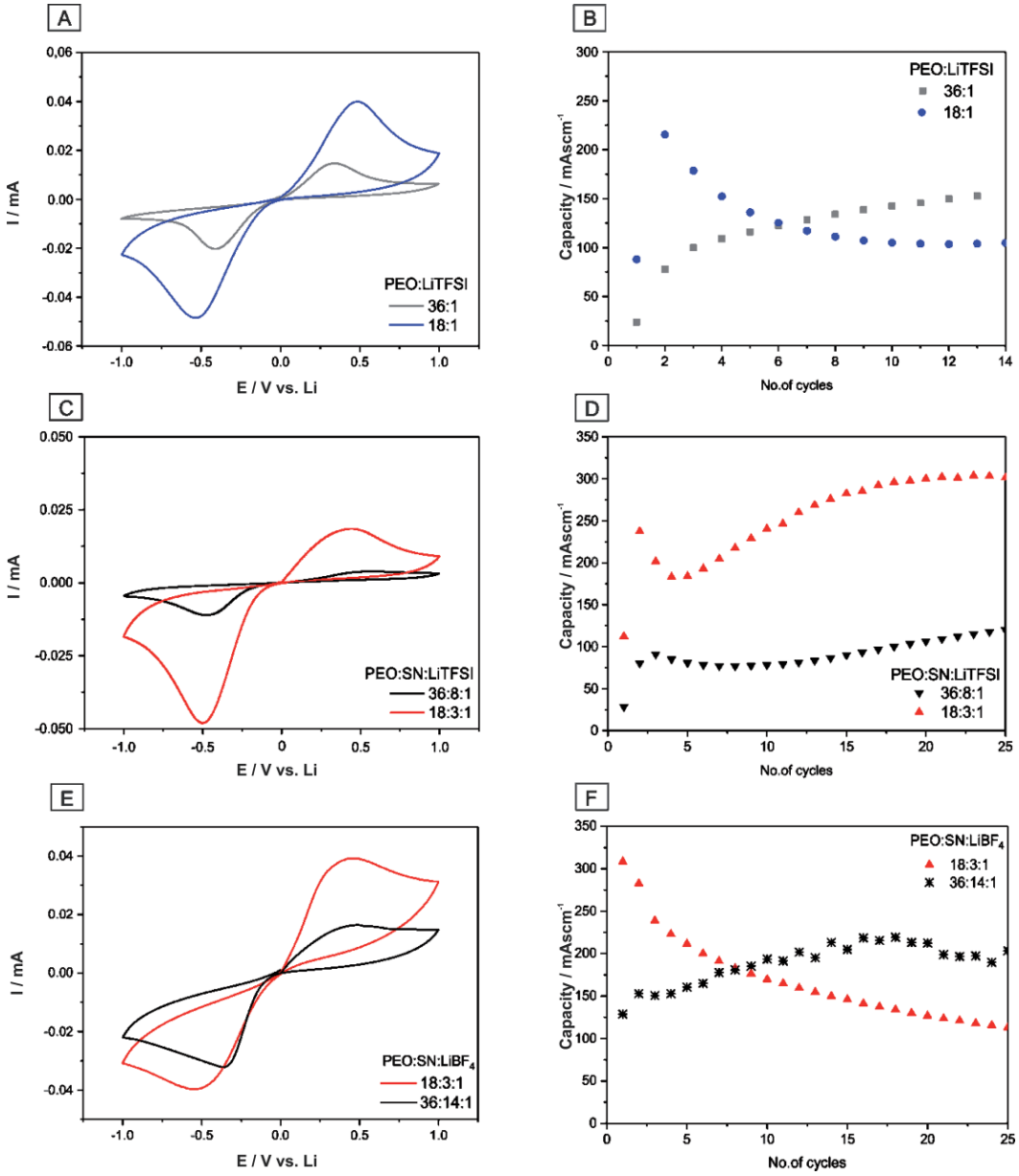

Figure 6. (A) CV's of symmetric Li|PEO:Li(TFSI) 36:1 membrane|Li and Li|PEO:Li(TFSI) 18:1 membrane|Li cells, and (B) capacity evolution after 14 consecutive CV cycles. (C) CV's of symmetric Li|PEO:SN:Li(TFSI) 36:8:1 membrane|Li and Li|PEO:SN:Li(TFSI) 18:3:1 membrane|Li cells. (D) Capacity evolution after 25 consecutive CV cycles. (E, F) CV data and capacities for $LiBF_4$:SN:PEO 18:3:1 and 36:14:1 membrane for comparison. The values for the 18:3:1 and 36:14:1 membrane are taken from reference[8].

mined onset values of 323 K and 313 K, respectively. As in the case of the plasticizer-free membranes, a certain lambda shape of the DSC signals is present, which might be due to a certain phase separation within the amorphous phase fractions. There is no segregation detectable leading to crystalline phases, as one might see in Figure 2.

Taking a look on the total conductivities of the SN-containing samples we see almost no difference to the SN-free ones (cf. Figure 5A and C). Upon SN increase only a tiny positive effect to the room temperature conductivity (8.6×10^{-6} S·cm^{-1} at 293 K for the 18:3:1 membrane vs. 1.9×10^{-5} S·cm^{-1} at the same temperature for the 36:8:1) can be found. Unfortunately, we were not able to successfully spin an 18:8:1 sample, which might be higher in conductivity than the 18:3:1 one. This feature illustrates the limit of the electrospinning process where not every wanted composition can be addressed.

The activation barrier seems to be unaffected by the plasticizer for the 18:3:1 membrane where 77(1) kJ·mol^{-1} was determined, a value, which is in the same range than observed for the plasticizer-free 18:0:1 case. If the SN content is increased up to the maximum which we were able to spin (36:8:1), the activation energy is reduced to 57(1) kJ·mol^{-1}. Unexpectedly, the conductivity is not changed in this case.

In order to explain this finding and to clarify the role of SN in the membranes we performed solid State NMR spectroscopy to shine more light onto this feature.

After the set of impedance measurements as summarized in Figure 5 we checked the morphology of a Li(TFSI),SN)@PEO (36:8:1) membrane. As shown in Figure 7 the fiber structure within the membrane is still present and no significant morphology change took place. This finding is important because the maintained fiber structure is important to preserve the improved properties. If significant pressure is applied to the membrane the morphology will be destroyed and the properties will be comparable with the solution casted samples.

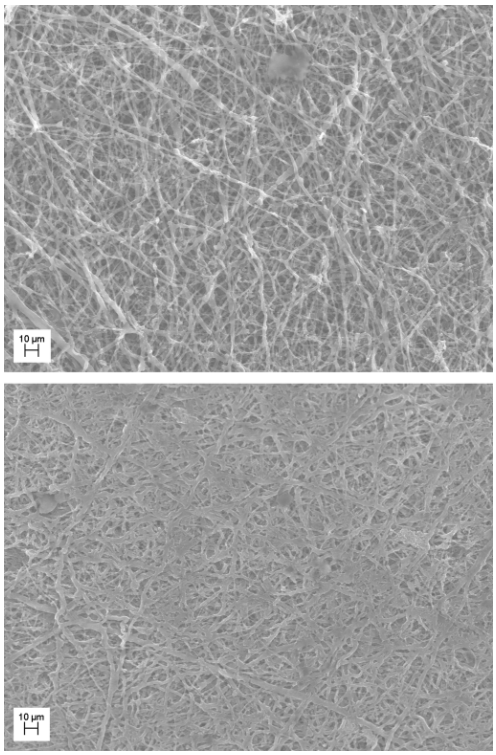

Figure 7. A [Li(TFSI),SN]@PEO (36:8:1) membrane before (top) and after (bottom) the impedance measurement cycle shown in Figure 5.

NMR Spectroscopic Investigations on Electrospun PEO:SN:Li(TFSI) Membranes

Solid state NMR experiments were performed to obtain more information about the structural details, the phase organization and dynamic processes present in the membranes. Figure 8 shows the temperature dependent evolution of the line widths of the ^{7}Li and ^{19}F signals in the investigated membranes. Room temperature ^{7}Li and ^{19}F-Spectra may be found in Figures S3 and S4 (Supporting Information). While the spectra for the plasticizer containing samples PEO:SN:LiTFSI 36:8:1 and 18:3:1 are characterized by a single narrow lorentzian line, the spectrum for the SN free 18:0:1-membrane exhibits a superposition of a narrow lorentzian line and a second much broader contribution, indicating dynamic heterogeneity.

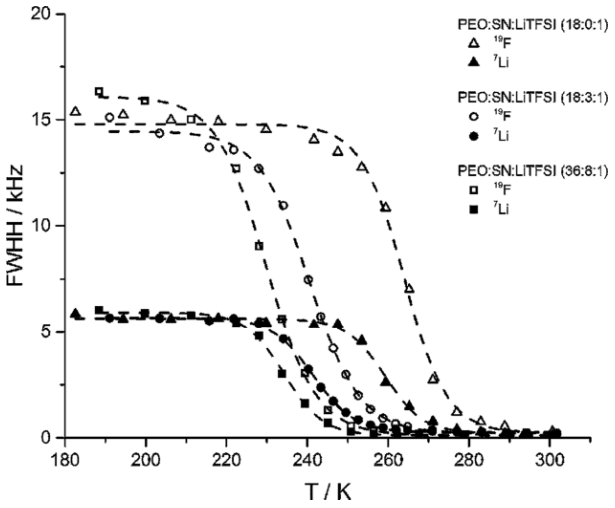

Figure 8. Evolution of the ^{7}Li and ^{19}F linewidth as a function of temperature for PEO:SN:LiTFSI 18:0:1, 18:3:1 and 36:8:1. Dashed lines are guides to the eye.

At low temperatures, at which no dynamic process is active in the membranes (rigid lattice regime), the lines are broadened by the orientation dependence of the internal interactions, which scale with the second Legendrian, $3\cos^2\beta$–1, with β denoting the angle between the direction of the magnetic field B_0 and the principal axis of the relevant internal interaction. Any motional process will therefore result in an at least partial averaging of the interactions and entail a narrowing of the NMR line width. Whereas for the ^{19}F nucleus the line width is governed by the chemical shift and dipole interactions, for I = 3/2 nucleus ^{7}Li the line width of the central m = ½ → m = –½ transition is dominated by the homonuclear dipole interaction. From the onset temperature of the motional narrowing, the activation energy for the relevant motional process may be calculated following the empirical Waugh-Fedin relation $E_A = 0.156 \times T_{onset}$ with T_{onset} denoting the onset temperature of the beginning of the line narrowing.[32] As the onset temperature the temperature, at which the linewidth reduces to $(\nu_{rigid\ lattice} - \nu_{mot\ narrowing})/2 + \nu_{mot\ narrowing}$ was taken.

From Figure 8 we learn that – as for the electrospun system PEO-SN-$LiBF_4$[8] – the activation energies for anion and cation dynamics in the plasticizer free membrane 18:0:1 are somewhat higher [40 kJ·mol^{-1} (T_{onset} = 259 K) and 41 kJ·mol^{-1} (T_{onset} = 264 K) for ^{7}Li and ^{19}F respectively] as compared to the plasticizer containing membranes PEO:SN:LiTFSI 36:8:1 and 18:3:1, which exhibit activation energies of 36 kJ·mol^{-1} and 38 kJ·mol^{-1}, respectively.

The ^{13}C NMR experiments were performed to obtain information about the dynamics of the polymer and its phase organization. Apart from amorphous and crystalline PEO phases such as an amorphous eutectic PEO_{11}LiTFSI phase and crystalline PEO_6LiTFSI have been observed in a recent study.[21] The ^{13}C MAS NMR spectra for the plasticizer-free sample 18:0:1 and one of the plasticizer containing samples 36:8:1, obtained under high power proton decoupling, are shown in Figure 9 and Figure 10. The dominant signal at δ = 70 ppm in the 36:8:1 sample can be assigned to ^{13}C nuclei of PEO in a

highly dynamic amorphous PEO:SN:LiTFSI phase. This assignment is supported by the ^{13}C MAS NMR spectrum, recorded without proton decoupling (cf. Figure 8, inset 1). Here, the signal splits into a triplet due to the ^{1}J(C-H) coupling to the methylene protons. The detection of this triplet signals the complete removal of the significant line broadening due to the ^{13}C–^{1}H dipolar coupling and hence indicates a remarkably high, almost liquid like PEO mobility. The signal at δ = 14 ppm, originating in the methylene carbons of the succinonitrile, also exhibits the splitting into a triplet (cf. Figure 8, inset 2), supporting the view of a highly mobile, plasticizer containing PEO-SN-LiTFSI phase. The signal for the SN nitrile group is found at δ = 118 ppm, together with a quartet stemming from the CF_3 groups of the TFSI anion.

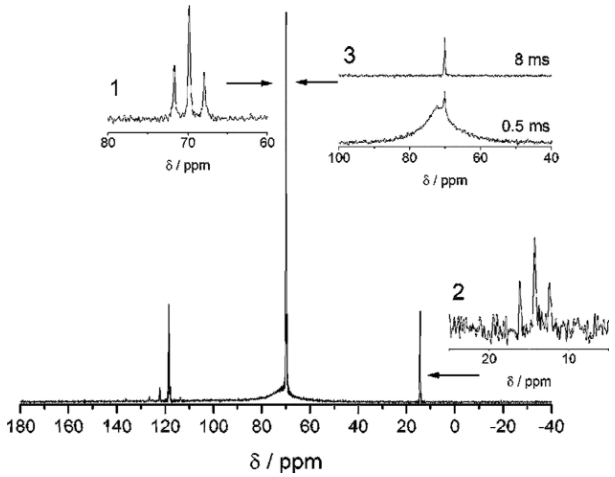

Figure 9. ^{13}C NMR spectrum of PEO:SN:LiTFSI 36:8:1 at room temperature acquired with high power proton decoupling. Inset 1 and 2: ^{13}C NMR spectra acquired without high power proton decoupling. Inset 3: ^{13}C-^{1}H-cross polarization measurements conducted with 0.5 and 8 ms contact time.

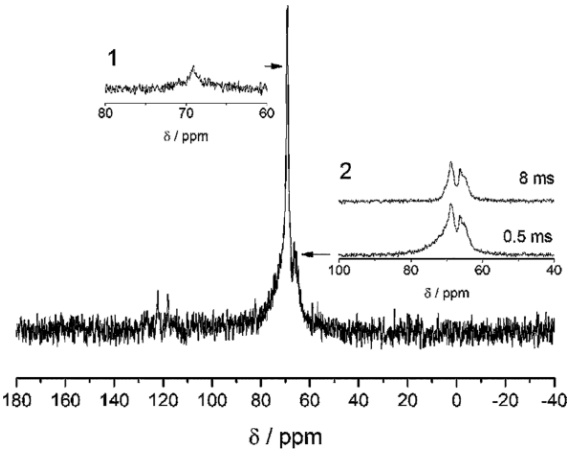

Figure 10. ^{13}C NMR spectrum of PEO:SN:LiTFSI 18:0:1 at room temperature acquired with high power proton decoupling. Inset 1: ^{13}C NMR spectrum acquired without high power proton decoupling. Inset 2: ^{13}C-^{1}H-cross polarization measurements conducted with 0.5 and 8 ms contact time.

For the 18:0:1 sample, the splitting of the 70 ppm signal into a triplet is barely visible (Figure 10, inset 1). This indicates that the segmental mobility of the PEO chains in the plasticizer free PEO:LiTFSI phase is significantly lower as compared to those of the ternary samples. These results support the finding from the static ^{7}Li and ^{19}F NMR experiments. In addition, for the 18:0:1 sample, two signals at δ = 66 ppm and 69 ppm are discernible in the CPMAS spectra (cf. Figure 9 inset 3). The chemical shift of these signals is identical to those of the crystalline PEO_6LiTFSI phase as observed by *Koester* et al.[21] In addition, the contact time behavior, i.e. the evolution of CP signal intensity with contact time, which can usually be taken as a fingerprint for a given structural environment, is found to be comparable to those of typical PEO_6Li*X* phases (as, for example, PEO_6LiBF_4 etc.[31]). The dependence of the signal intensity M on the contact time t_{CP} – in a simplified thermodynamic model of cross polarization – follows Equation (1):

$$M = \frac{1}{1-\frac{T_{IS}}{T_{1\rho}}}\left\{\exp\left(-\frac{t_{CP}}{T_{1\rho}}\right)-\exp\left(-\frac{t_{CP}}{T_{IS}}\right)\right\} \quad (1)$$

with $T_{1\rho}$ denoting the ^{1}H relaxation time in the rotating frame and $1/T_{IS}$ the cross polarization rate, which increases with the I-S heteronuclear dipolar coupling. Thus, the contact time dependence critically depends on the magnitude of the ^{13}C–^{1}H dipolar coupling[33,34] and on the $T_{1\rho}$ of the protons. The absence of the corresponding signals in the XRD might be readily explained by the small size of the crystalline PEO-LiX domains. Thus, in the plasticizer free 18:0:1 membrane, a fraction of the Li salt is trapped within an immobile PEO_6LiTFSi phase, which is in perfect agreement with the dynamic heterogeneity as observed in the static ^{7}Li and ^{19}F-NMR experiments. The presence of the PEO_6LiTFSI phase is also corroborated by the endothermic effect observed in the DSC curves at 308 K. According to the phase diagram as published e.g. by *Edman* et al. and *Labreche* et al.,[16,17] in this compositional regime proeutectic PEO should coexist with an eutectic phase composed of PEO_6LiTFSI and PEO. According to our results, the combined action of electrospinning and SN as plasticizer are necessary to circumvent the formation of this crystalline phase. A deconvolution of the ^{7}Li MAS-NMR spectrum of this sample (Figure S6, Supporting Information) reveals that only 20 % of the lithium cations reside in the highly dynamic amorphous PEO:LiTFSI-phase (linewidth 52 Hz), while 80 % of the lithium ions are trapped in the immobile crystalline PEO_6LiTFSI phase, characterized by a 524 Hz broad signal that is accompanied by quadrupolar satellites.

The broad signal at δ = 72 ppm in both spectra, which in the CPMAS spectra can only be observed at rather short contact times (cf. Figure 9, inset 3 and Figure 10 inset 2), then have to be assigned to ^{13}C nuclei in PEO of only limited mobility. Since the XRD of this sample exhibits clear reflexes of crystalline PEO, we tentatively assign this signal to pristine crystalline PEO. The considerable width of this line has been ascribed to an interference of the decoupling efficiency by the molecular motion, the peculiar contact time behavior by a very short proton $T_{1\rho}$.

A rather important aspect relates to the long term stability of the materials, which poses a mandatory prerequisite if these are to be used in battery applications. For the 18:3:1 sample,

the ^{13}C MAS NMR spectrum (cf. Figure S5, Supporting Information), recorded after two years after sample preparation, does not exhibit any traces of immobile PEO:LiTFSI phases, rendering this material suitable for battery application.

Conclusions

Li(TFSI) was successfully used as a conductive salt additive in PEO to synthesize electrospun fiber membranes. A combined phase analytic and spectroscopic investigation was needed to illustrate and understand the complex phase formation behavior for the electrospun membranes under consideration. Dependent on the composition and the usage of SN as a plasticizer, various ratios of crystalline and amorphous phases are formed, which contribute to the physical properties of the membranes.

Electrospinning of membranes represent a valuable new method for the synthesis of solid elelctrolytes compared with solution casted ones, featuring improved ion conductivity. Crystalline amounts of $[Li(TFSI)]_x$@PEO adducts are drastically reduced by this method optimizing the ion mobility and conductivity. Nevertheless, this study also shows that phase segregation is an unwanted issue and crystalline phases with immobile Li ions and even Li-free ones are formed. It became clear, that in some cases such crystalline phases are not detectable by X-ray phase analysis and only Solid State NMR spectroscopy helped to identify them non-doubtfully. The Li(TFSI) conductive salt additive reduces the melting point of the solid ion-conducting membranes only slightly, still offering an acceptable range for possible applications.

The usage of a plasticizer like SN, which was successfully applied to electrospun MBF$_4$@PEO membranes, capable to improve the segment mobility (and conductivity) of the PEO matrix, was also tested for the Li(TFSI)@PEO systems. In accordance with plasticizer- modified MBF$_4$@PEO membranes, the plasticizer has a significant influence on the electric properties of the Li(TFSI)@PEO systems. The best overall performance shows a homogeneous 36:8:1 membrane with conductivities of 2×10^{-6} S·cm^{-1} to 2.8×10^{-4} S·cm^{-1}, in a temperature interval of 278 K to 328 K. Values for the plasticizer-free membranes are only slightly lower but we found phase segregation and dynamic inhomogenities, which renders a usage non-favorable at the present stage. For the 18:0:1 phase only 20 % of the Li ions were localized in a beneficial amorphous phase while 80 % of the Li ions were immobile. Li(TFSI)@PEO membranes are characterized by a higher electrochemical stability against Li electrodes in CV experiments than comparable LiBF$_4$@PEO ones. Plasticizer-free and containing Li(TFSI)@PEO membranes show steady capacities after a short induction period of ca. 10 CV cycles. This behavior is better than for comparable LiBF$_4$@PEO systems, where a steady state is only realized with significantly larger SN and lower conductive salt additive amounts. To improve the electrochemical performance and conductivity of the Li(TFSI)@PEO membranes, smaller fiber sizes and an increased contact density of the electrospun fibers might be helpful.

Overall, electrospun Li(TFSI)@PEO membranes are an interesting alternative for state-of-the-art separators and as solid ion conducting material in battery applications.

Abbreviations
CV - Cyclovoltametry
DFT - Density Functional Theory
IS - Impedance Spectroscopy
MD - Molecular Dynamics
DSC - Differential Scanning Calorimetry
NMR - Nuclear Magnetic Resonance
PEO - Polyethylene oxide
SEM - Scanning Electron Microscopy
SN - Succinonitrile
TFSI - Bis(trifluoromethan)sulfonimide

Acknowledgements

The support by the TUM Graduate School for F.B. is gratefully acknowledged.

Keywords: Solid electrolyte; Solid ion conductors; Electrospinning; Lithium; Lithium-bis(trifluoromethan)sulfonimide

References

[1] Y. Hu, X. Sun, *J. Mater. Chem. A* **2014**, *2*, 10712–10738.
[2] J. B. Goodenough, P. Singh, *J. Electrochem. Soc.* **2015**, *162*, A2387–A2392.
[3] L. Fan, S. Wei, S. Li, Q. Li, Y. Lu, *Adv. Energy Mater.* **2018**, *8*, 1702657.
[4] E. Strauss, S. Menkin, D. Golodnitsky, *J. Solid State Electrochem.* **2017**, *21*, 1879–1905.
[5] L. Long, S. Wang, M. Xiao, Y. Meng, *J. Mater. Chem. A* **2016**, *4*, 10038–10069.
[6] D. E. Fenton, J. M. Parker, P. V. Wright, *Polymer* **1973**, *14*, 589.
[7] I. Osada, H. de Vries, B. Scrosati, S. Passerini, *Angew. Chem. Int. Ed.* **2016**, *55*, 500–513.
[8] K. M. Freitag, H. Kirchhain, L. van Wüllen, T. Nilges, *Inorg. Chem.* **2017**, *56*, 2100–2107.
[9] K. M. Freitag, P. Walke, T. Nilges, H. Kirchhain, R. J. Spranger, L. van Wüllen, *J. Power Sources* **2018**, *378*, 610–617.
[10] Y. Tominaga, *Polym. J.* **2017**, *49*, 291–299.
[11] D. R. MacFarlane, M. Forsyth, P. C. Howlett, M. Kar, S. Passerini, J. M. Pringle, H. Ohno, M. Watanabe, F. Yan, W. Zheng, S. Zhang, J. Zhang, *Nat. Rev. Mater.* **2016**, *1*, 15005.
[12] A. Bielecki, D. P. Burum, *J. Magn. Reson. Ser. A* **1995**, *116*, 215–220.
[13] A. Vallée, S. Besner, J. Prud′Homme, *Electrochim. Acta* **1992**, *37*, 1579–1583.
[14] S. Lascaud, M. Perrier, M. A. Vallee, S. Besner, J. Prud′homme, M. Armand, *Macromolecules* **1994**, *27*, 7469–7477.
[15] M. Echeverri, N. Kim, T. Kyu, *Macromolecules* **2012**, *45*, 6068–6077.
[16] C. Labreche, I. Levesque, J. Prud'homme, *Macromolecules* **1996**, *29*, 7795–7801.
[17] L. Edman, A. Ferry, M. M. Doeff, *J. Mater. Res.* **2000**, *15*, 1950–1954.
[18] K. M. Freitag, *Elektrogesponnene PEO-basierte Festkörperelektrolyte*, Dissertation TU München, **2017**, p. 31.
[19] M. Marzantowicz, J. R. Dygas, F. Krok, J. L. Nowiński, A. Tomaszewska, Z. Florjańczyk, E. Zygadło-Monikowska, *J. Power Sources* **2006**, *159*, 420–430.

[20] M. Marzantowicz, J. R. Dygas, F. Krok, A. Łasińska, Z. Florjańczyk, E. Zygadło-Monikowska, A. Affek, *Electrochim. Acta* **2005**, *50*, 3969–3977.
[21] T. K.-J. Köster, L. van Wüllen, *Solid State Ionics* **2008**, *178*, 1879–1889.
[22] Y.-T. Kim, E. S. Smotkin, *Solid State Ionics* **2002**, *149*, 29–37.
[23] V. M. Schmidt, *Elektrochemische Verfahrenstechnik*, Wiley-VCH GmbH & Co. KGaA, **2003**.
[24] S. Xue, Y. Liu, Y. Li, D. Teeters, D. W. Crunkleton, S. Wang, S. Xu, et al., *Electrochim. Acta* **2017**, *235*, 22–128.
[25] L.-Z. Fan, J. Maier, *J. Electrochem. Commun.* **2006**, *8*, 1753–1756.
[26] Y. G. Andreev, V. Seneviratne, M. Khan, W. A. Henderson, R. E. Frech, P. G. Bruce, *Chem. Mater.* **2005**, *17*, 767–772.
[27] W. H. Meyer, *Adv. Mater.* **1998**, *10*, 439–448.
[28] A. Maitra, A. Heuer, *Phys. Rev. Lett.* **2007**, *98*, 227802.
[29] A. Maitra, A. Heuer, *Macromol. Chem. Phys.* **2007**, *208*, 2215–2221.
[30] S. M. Zahurak, M. L. Kaplan, E. A. Rietman, D. W. Murphy, R. J. Cava, *Macromolecules* **1988**, *21*, 654–660.
[31] N. Voigt, L. van Wüllen, *Solid State Ionics* **2014**, *260*, 65–75.
[32] J. S. Waugh, E. I. Fedin, *Sov. Phys. Solid State* **1963**, *4*, 1633.
[33] W. Kolodziejski, J. Klinowski, *Chem. Rev.* **2002**, *102*, 613–628.
[34] W. Xiaoling, Z. Shanmin, W. Xuewen, *Phys. Rev. B* **1988**, *37*, 9827.

Received: August 28, 2018
Published online: November 27, 2018

Z. Anorg. Allg. Chem. **2018** · ISSN 0044–2313

SUPPORTING INFORMATION

Title: Electrospun Li(TFSI)@Polyethylene Oxide Membranes as Solid Electrolytes
Author(s): P. Walke, K. M. Freitag, H. Kirchhain, M. Kaiser, L. van Wüllen,* T. Nilges*
Ref. No.: z201800370

Supplement

Electrospun Li(TFSI)@Polyethylene Oxide Membranes as Solid Electrolytes

by

Patrick Walke[a)], Katharina M. Freitag [a)], Holger Kirchhain [b)], Matthias Kaiser [b)], Leo van Wüllen [b),*], Tom Nilges [a),*]

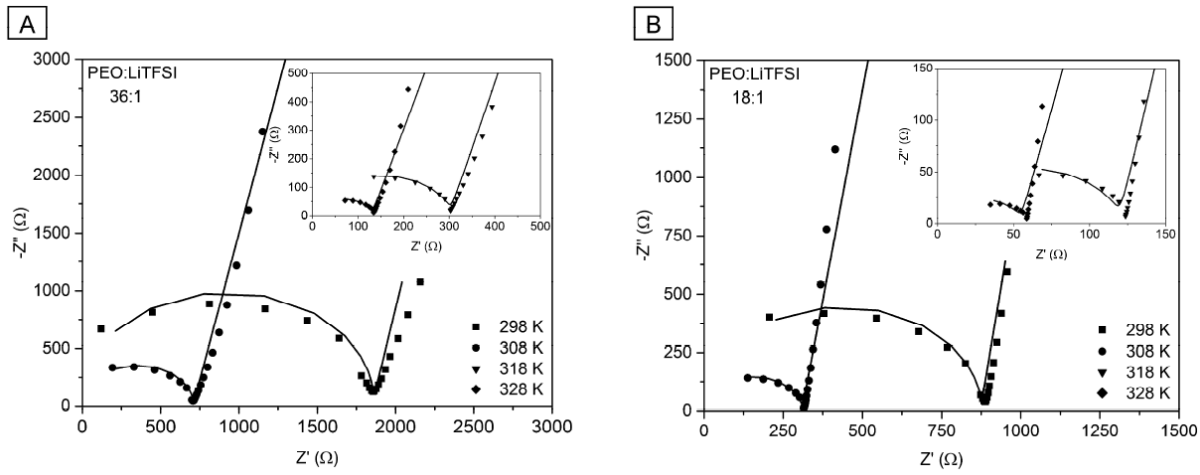

Figure S1. Nyquist plots and fitting curves (Ersatzschaltbild) of two LiTFSI@PEO membranes at four different temperatures in a frequency range of 1 MHz to 0.1 Hz (from left to right).

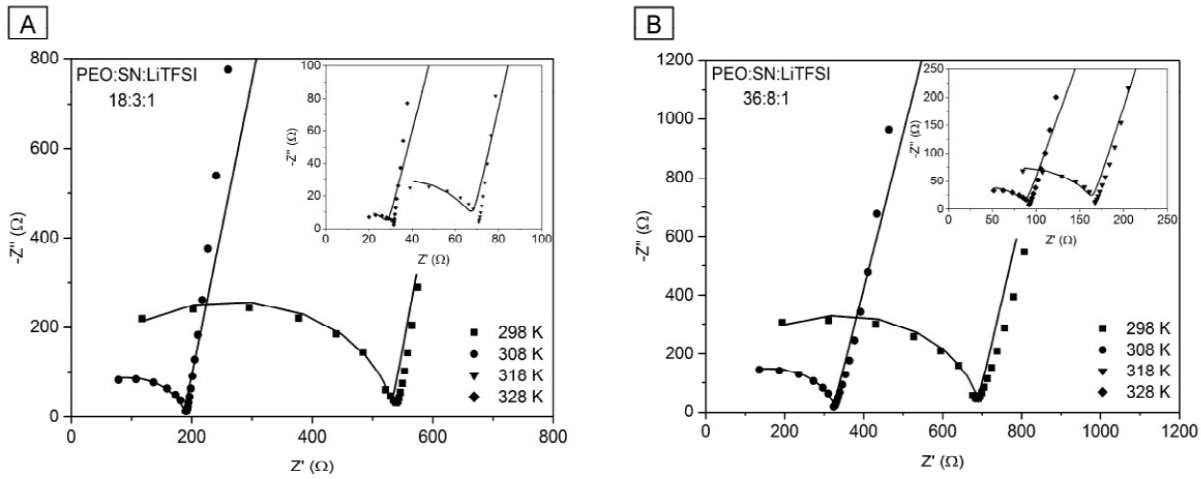

Figure S2. Nyquist plots and fitting curves (Ersatzschaltbild) of two (LiTFSI,SN)@PEO membranes at four different temperatures in a frequency range of 1 MHz to 0.1 Hz (from left to right).

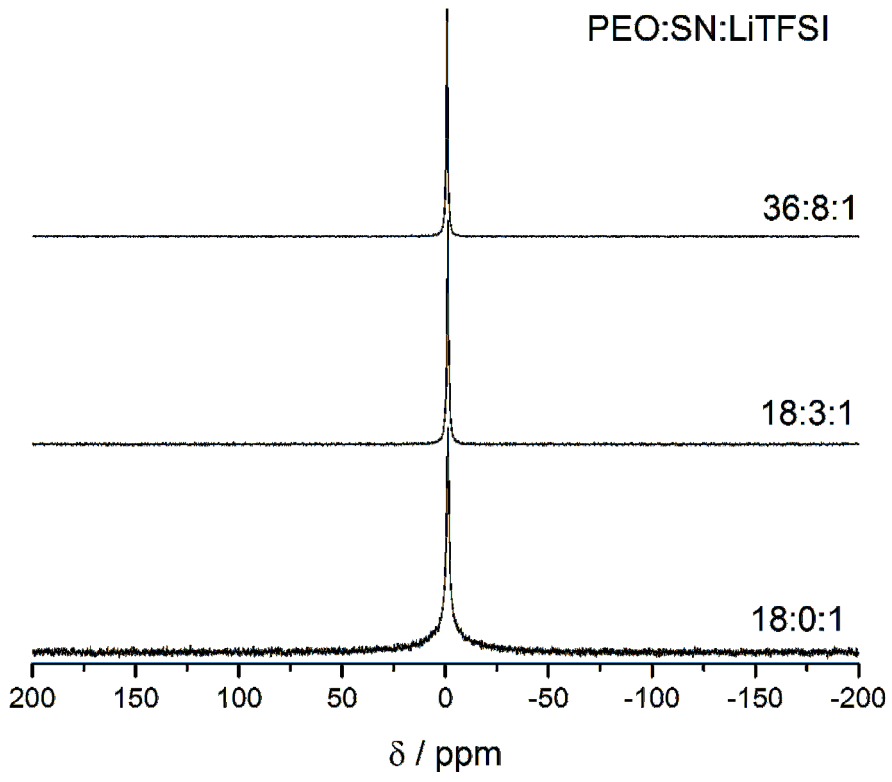

Figure S3. static ^{7}Li single pulse excitation spectra of PEO:SN:LiTFSI 18:0:1, 18:3:1 and 36:8:1 at room temperature.

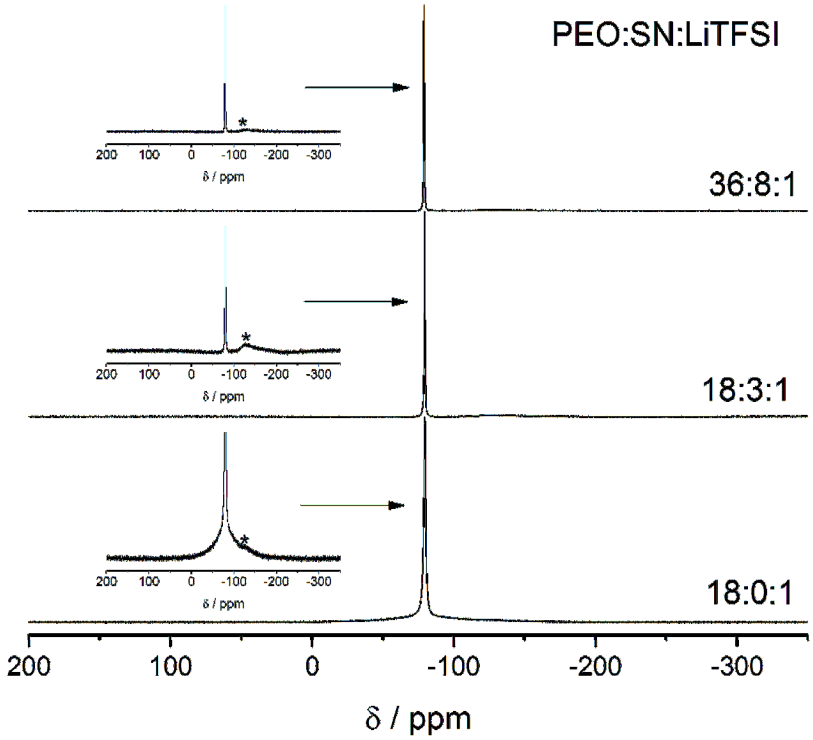

Figure S4. static ^{19}F single pulse excitation spectra of PEO:SN:LiTFSI 18:0:1, 18:3:1 and 36:8:1 at room temperature. The insets show a magnification of the signal's baseline. A small residual teflon background in the spectra is marked by a *.

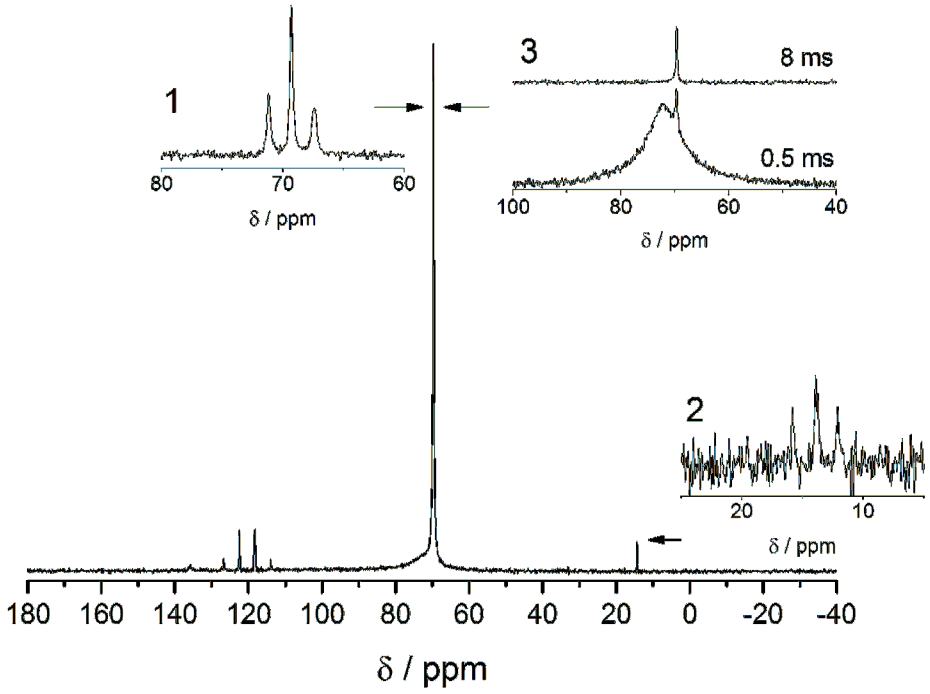

Figure S5. ^{13}C-spectrum of PEO:SN:LiTFSI 18:3:1 at room temperature acquired with high power proton decoupling. Inset 1 and 2: ^{13}C-spectra acquired without high power proton decoupling. Inset 3: ^{13}C-^{1}H-cross polarization measurements conducted with 0.5 and 8 ms contact time.

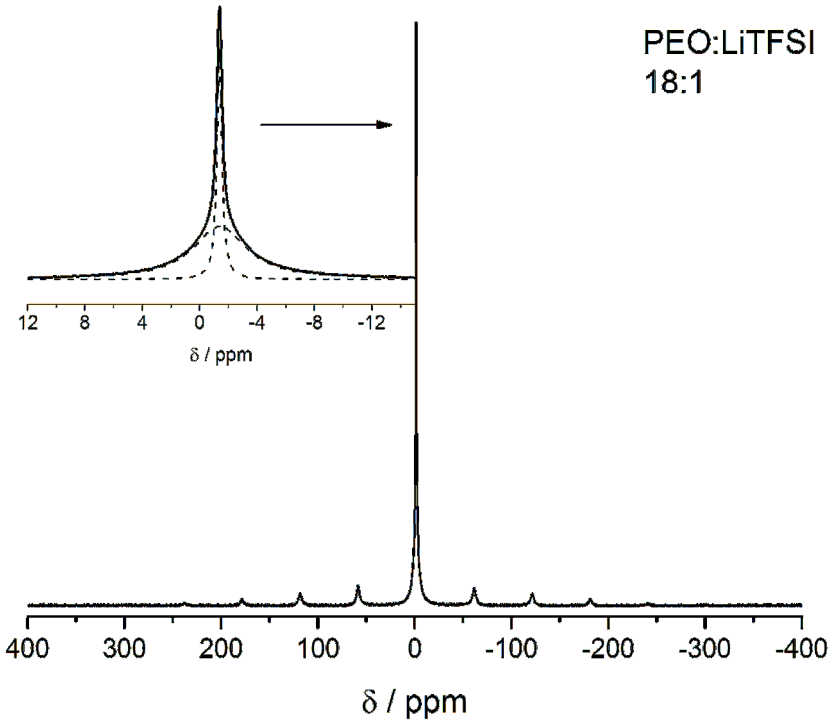

Figure S6. ^{7}Li-MAS spectrum of PEO:LiTFSI 18:1 recorded at room temperature. The Inset shows the deconvolution of the heterogeneous central transition.

3.2 Effect of nanostructured Al_2O_3 on poly(ethylene oxide)-based solid polymer electrolytes

Patrick Walke[a], Anna Kirchberger[a], Felix Reiter[a], Daniel Esken[b] and Tom Nilges[a]

[a] Technical University Munich, Department for Chemistry, Lichtenbergstraße 4, 85748 Garching bei München

[b]Evonik Operations GmbH, Rodenbacher Chaussee 4, 63457 Hanau-Wolfgang, Germany

Z. Naturforsch. **2020** (online)
First published online: September 20th 2020
DOI:10.1515/znb-2021-0091

Reaching for safer and more powerful batteries, one approach is to replace liquid electrolytes by solid polymer electrolytes (SPEs). Besides various combinations of polymers. conducting salts and plasticizers, the addition of inorganic fillers as Al_2O_3 are possible routes to enhance the properties of these membranes. The SPEs are prepared by electrospinning, solution casting and hotpressing. PEO is used in combination with $LiBF_4$ and succinnitrile (SN), as this combination already showed positive results.[104] In a first step different $LiBF_4$ concentrations in a PEO matrix are tested to show influence on the ionic conductivity. PEO:$LiBF_4$ SPEs with molar compositions of 36:1, 27:1 and 18:1 are prepared *via* electrospinning. The resulting membranes consist of amorphous fibers with melting points T_m between 331 K and 337 K. The glass transition temperature T_g for the samples with the lower $LiBF_4$ concentrations are 227 K (36:1) and 231 K (27:1) and thus quite similar to 223 K of pure electrospun PEO. For the PEO:$LiBF_4$ 18:1 SPE T_g dropped to 176 K. The ionic conductivity of rises with the lithium salt content from 1.5×10^{-7} S/cm for the PEO:$LiBF_4$ 36:1 membrane to 5.0×10^{-7} S/cm for the PEO:$LiBF_4$ 18:1 membrane, both at 293 K. Hence, a molar composition of PEO:$LiBF_4$ 18:1 is chosen for further testing. In the next step, electrospun, hot pressed and solution casted SPEs with the same molar composition are compared to evaluate the influence of the preparation method on the product. When solution casting or hat pressing PEO:$LiBF_4$ 18:1 membranes non porous crystalline membranes are obtained, in contrast to the amorphous fiber-based membranes from electrospinning. The ionic conductivity drops by an order of magnitude to 2.5×10^{-8} S/cm for hot pressed and 6.7×10^{-8} S/cm for solution casted membranes at 293 K. For all further

experiments only electrospinning and solution casting are applied as hot pressing is not a suitable method to homogeneously spread inorganic particle across the membranes.

Author contributions: P.W. and A.K. contributed equally to this study. They carried out all membrane preparations, the impedance spectroscopy, powder x-ray diffraction and differential scanning calorimetry. A.K. determined the particle size distribution *via* dynamic light scattering. F.R. conducted the scanning electron microscopy and energy dispersive X-ray spectroscopy. P.W., A.K. and T.N. have written the manuscript. P.W., A.K., T.N. and D.E. discussed the data and revised the manuscript.

Patrick Walke, Anna Kirchberger, Felix Reiter, Daniel Esken and Tom Nilges*

Effect of nanostructured Al_2O_3 on poly(ethylene oxide)-based solid polymer electrolytes

https://doi.org/10.1515/znb-2021-0091
Received July 8, 2021; accepted July 31, 2021;
published online September 20, 2021

Abstract: In this study, we investigated the effect of nanostructured Al_2O_3 particles on Li ion conducting, poly(ethylene oxide) (PEO)-based membranes prepared by electrospinning, solution casting and hot pressing. Pure PEO:$LiBF_4$ solid polymer electrolytes (SPEs) and also plasticizer containing membranes were investigated with various amounts of Al_2O_3. In a first step, the best-performing composition of pure PEO:$LiBF_4$ concerning the resulting ionic conductivity was identified and used as a standard for further experiments. In the following, the influence of the preparation method, the nature of the Al_2O_3, and the type of the plasticizer additives on the thermal and electrochemical properties for this standard composition were investigated. The Al_2O_3 composition was varied between 1 and 5 wt%. The ionic conductivity of bare electrospun PEO:$LiBF_4$ SPE standard material has been improved by a factor ten to 1.9×10^{-6} S cm^{-1} at T = 293 K when 5 wt% of Al_2O_3 is added. For solution-casted PEO:$LiBF_4$ standard compositions 18:1 with an initial ionic conductivity of 6.7×10^{-8} S cm^{-1}, the addition of 2 wt% Al_2O_3 increased the performance to 1.4×10^{-7} S cm^{-1}, both at T = 293 K. If succinonitrile and Al_2O_3 was admixed to the solution casted standard material, the ionic conductivity was further increased to reach 5.5×10^{-5} S cm^{-1} at T = 293 K. This material with a composition of 18:3:1 + 2 wt% Al_2O_3, outperforms the standard material by three orders of magnitude.

Patrick Walke and Anna Kirchberger contributed equally to this study.

Dedicated to Prof. Dr. Richard Dronskowski on the occasion of his 60th birthday.

***Corresponding author: Tom Nilges,** Chemistry Department, Technische Universität München, Lichtenbergstraße 4, 85748 Garching bei München, Germany, E-mail: tom.nilges@tum.de
Patrick Walke, Anna Kirchberger and Felix Reiter, Chemistry Department, Technische Universität München, Lichtenbergstraße 4, 85748 Garching bei München, Germany,
E-mail: patrick.walke@tum.de (P. Walke), anna.koehlmeier@tum.de (A. Kirchberger), felix.reiter@tum.de (F. Reiter)
Daniel Esken, Evonik Operations GmbH, Rodenbacher Chaussee 4, 63457 Hanau-Wolfgang, Germany

Keywords: aluminum oxide; electrospinning; impedance spectroscopy; poly (ethylene oxide); solid polymer electrolytes.

1 Introduction

The importance of safe and environmentally friendly high-power solid polymer electrolytes (SPEs) is considered to be consistently growing, facing the ongoing changes in energy storage technology. The progress in solid lithium electrolyte technologies regarding environmental considerations, commercial applicability, and energy density with a large electrochemical window is aiming at a commercial product with high performance. The goal is to create an alternative to the widely used liquid lithium accumulators. Solid polymer electrolytes, when compared to liquid electrolytes show a drastically reduced danger of flammability, no significant tendency for short circuits as a result of depressed dendrite growth, and eliminated battery bloating upon the emerge of potentially hazardous vapors. A solid electrolyte construction also possesses advantages for the use in electromobility or in portable devices as the rigid casing for the liquid reservoir is unnecessary. This is the consequence of the reduced heat dissipation, which allows a light flexible battery construction in smallest spaces [1–3].

On the downside, solid state electrolytes have currently one major drawback compared to liquid counterparts: the low conductivity at room temperature [1, 4]. One common option to tackle this problem is the addition of ceramic additives like Li super ionic conductors (LISICON) [5], Na super ionic conductor (NASICON) [6–8], lithium phosphorus oxynitride (LIPON) [9–11], TiO_2 [10–12], SiO_2 [11–16], ZnO [17], $BaTiO_3$ [18, 19], lithium lanthanum titanate (LLTO) [20], lithium lanthanum zirconium tantalum oxide (LLZTO) [21–23] or Al_2O_3 [1, 7, 11, 12, 16, 24] to polymer electrolytes. Thereby, an increase of conductivity of SPEs of up to 1.5×10^{-4} S cm^{-1} was reported using combinations of Al_2O_3 fillers and plasticizers [21, 24–26]. The enhancement of conductivity of SPEs with fillers was observed and a further conductivity increase is expected which could enable widespread commercial application. Further, the stability of the

electrochemical window can be enlarged by the use of fillers [20, 27]. The interactions of the ceramics embedded in the polymer with the conductive salts are not yet fully understood and make a specific optimization of the electrolytes complicated. The addition of fillers and thereby the smaller volume fractions of polymers raise the hope to minimize the interfacial barrier of the Li^+ transport from the superionic particles of the ceramic fillers to the polymer [10].

In contrast to the conduction mechanism for polymers including ceramic fillers, the conductivity mechanism of lithium ions in polyethylene oxide (PEO) is well studied [28, 29]. PEO serves as an interesting polymer for SPEs due to its ability to provide solvation of the lithium ions and owing to its flexible backbone to accelerate ion motion. We therefore decided to investigate this polymer and commercially available, nanostructured filler material Al_2O_3 as a suitable combination for SPEs.

2 Results and discussion

Ceramic filler tends to improve the electrochemical performance of SPEs [30]. Figure 1 shows different possible Li^+ conduction pathways with a low A), moderate B) and high amount of filler C).

Taking this general mechanism into account we started a systematic investigation of PEO-based Li ion conducting SPEs with various amounts of polymer, conducting salt, and plasticizer in order to address the different situations arising from Al_2O_3 usage. Another aspect deals with the influence of the preparation method on the electrochemical performance.

2.1 Adjustment of the molar ratio of the components used for PEO:$LiBF_4$ membranes

In a first step, the molar ratio of PEO:$LiBF_4$ was varied to find the composition with the highest ionic conductivity, which was chosen for further experiments as standard. Membranes prepared *via* electrospinning were compared regarding the crystallinity, thermal properties and conductivities derived from PEIS. As seen before by Freitag et al., the Li ion conductivity in electrospun membranes rises with the $LiBF_4$ content in the membranes [2]. In addition to the two plasticizer-free compositions examined in previous work (PEO:$LiBF_4$ 36:1 and 18:1), a third molar ratio (PEO:$LiBF_4$ 27:1) was also tested in this study to prove the concept.

The ionic conductivity at T = 293 K raised from 1.5×10^{-7} S cm^{-1} for the PEO:$LiBF_4$ 36:1 membrane, to 5.0×10^{-7} S cm^{-1} for the PEO:$LiBF_4$ 18:1 one. As the ionic conductivity raised with temperature, the values 4.6×10^{-6} S cm^{-1} and 1.9×10^{-5} S cm^{-1} were achieved at 328 K, respectively. For the SPE with a molar composition of 27:1 the value lies in between for both temperatures (compare Figure 2a). X-ray powder diffraction (P-XRD) data of the prepared membranes illustrated the amorphous character of all samples. Samples with a molar composition of PEO:$LiBF_4$ 36:1 (compare Figure 2b) showed a few reflections at 19.2° in 2θ and between 22.8 and 23.8° in 2θ, which we assigned to a crystalline phase of PEO, as described in literature [31].

The thermal properties of the prepared membranes were investigated *via* Differential Scanning Calorimetry (DSC) in a temperature range from 173 to 523 K. It was found that the melting point (T_m) was not significantly influenced

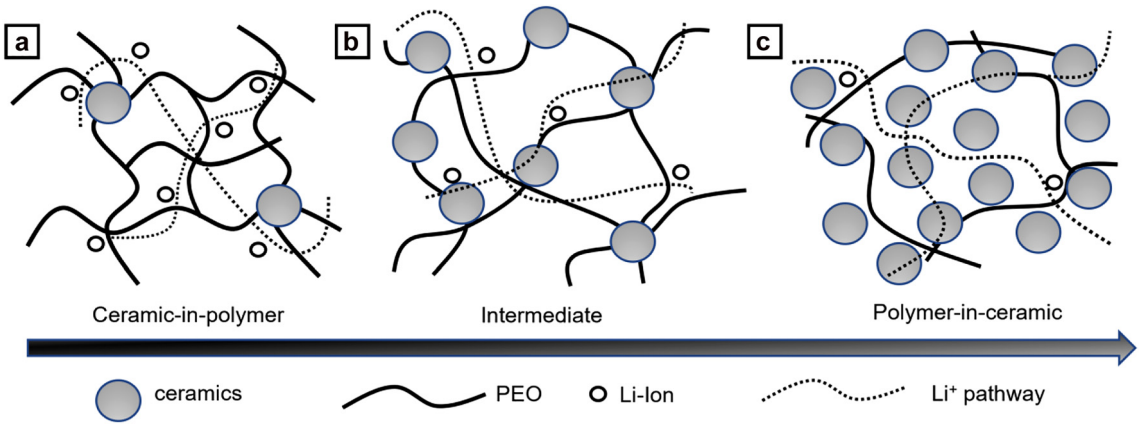

Figure 1: Illustration of the different conduction pathways in a SPEs based on PEO with a growing amount of ceramic fillers. Figure adapted from literature [30].

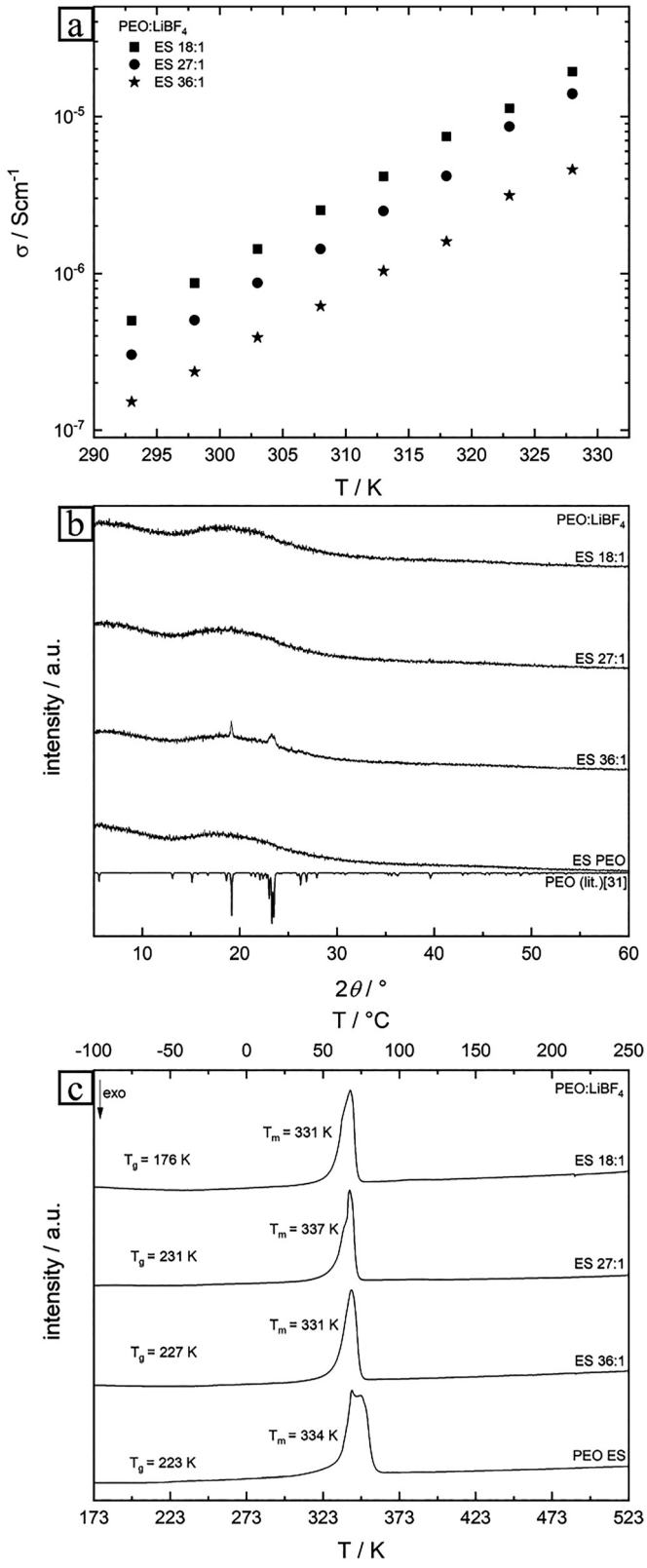

Figure 2: a) Ionic conductivities in a temperature range from 293 to 328 K, b) X-ray powder diffraction (P-XRD) from 5 to 60° in 2θ and c) DSC in the temperature range from 173 to 523 K of electrospun PEO:$LiBF_4$ SPEs with different molar compositions of 36:1, 27:1 and 18:1.

by the concentration of the conducting salt. In contrast, the glass transition temperature (T_g) was shifted to a significantly lower temperature for the PEO:$LiBF_4$ 18:1 sample (T_g = 176 K) compared to the one of pure PEO (T_g = 223 K) and was later found to show the highest ionic conductivity, as shown in Figure 2a.

2.2 Screening of the preparative methods for optimized PEO:$LiBF_4$ membranes

To validate the positive effect of the electrospinning in the preparation process of a SPE, the electrospun sample with the highest Li ion mobility (PEO:$LiBF_4$ 18:1) was compared to membranes of the same composition prepared by solution casting and hot pressing. Thereby, it can be seen that the SPEs prepared by electrospinning showed a higher ionic conductivity than those prepared by the other techniques in the measured temperature range. While hot pressed membranes with a molar composition of PEO:$LiBF_4$ 18:1 denoted an ionic conductivity from 2.5×10^{-8} S cm^{-1} at 293 K to 1.3×10^{-6} S cm^{-1} at 328 K, the solution casted membranes with the same molar ratio showed 6.7×10^{-8} S cm^{-1} and 3.0×10^{-6} S cm^{-1} at the same temperature. These conductivities were about one order of magnitude lower than those observed for the electrospun membrane PEO:$LiBF_4$ 18:1 (compare Figure 3a). The interested reader is referred to the literature regarding the reason for the conductivity improvement in the case of electrospun polymer electrolytes [2, 3]. For the products of all preparative methods, the crystallinity of the obtained membranes was investigated *via* P-XRD. While the electrospun sample was, as discussed before, amorphous, the SPEs obtained from hot pressing and solution casting showed significant amounts of crystalline PEO phase (compare Figure 3b). This agrees with the specific conductivities that were derived from impedance data. Electrospun membranes showed the highest conductivity, followed by solution casted and hot pressed ones. It is reported in the literature that crystallized PEO tends to shows lower ion mobility compared to amorphous PEO [32].

For the examination of the thermal properties of PEO:$LiBF_4$ 18:1 samples prepared by different methods *via* DSC, the first heating cycle with a scan rate of 10 K min^{-1} was used for comparison as the unique fiber structure of the electrospun SPE was destroyed after the sample is molten once. The difference in melting temperature for the tested compounds is negligible (compare Figure 3c), all values were found between 329 and 331 K. In contrast, T_g for the ES 18:1 (T_g = 176 K) sample was significantly lower compared to T_g of the SC 18:1 sample (T_g = 227 K), while the highest T_g of 248 K was found for HP 18:1. This illustrates that the PEO

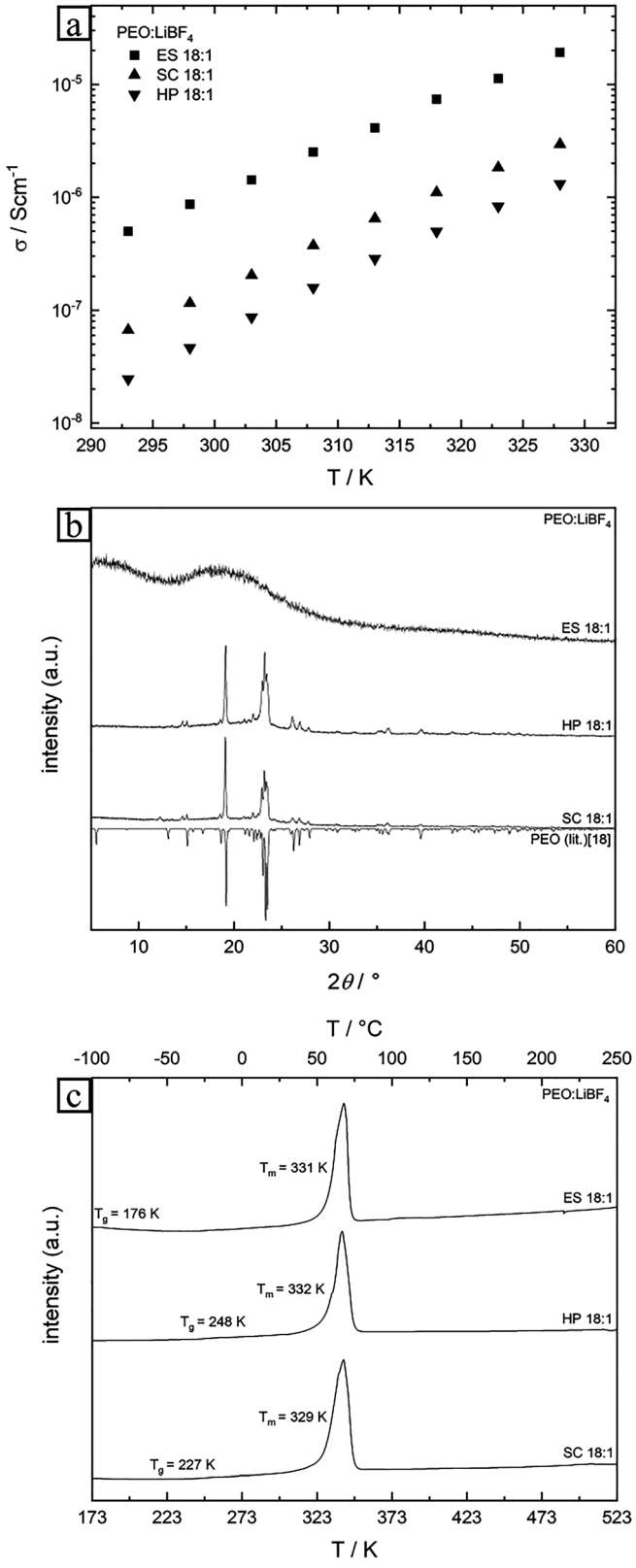

Figure 3: a) Ionic conductivities in a temperature range from 293 to 328 K, b) P-XRD from 5 to 60° in 2θ and c) DSC in the temperature range from 173 to 523 K of PEO:$LiBF_4$ 18:1 SPEs prepared by electrospinning (ES), solution casting (SC) and hot pressing (HP).

matrix of the SPEs offers the highest chain mobility when prepared by electrospinning, thus leading to the highest specific ionic conductivity of the ES 18:1 membrane compared to those prepared by other techniques.

As hot pressed samples in general show the poorest performance and the preparative method, as performed in our facilities, is not suitable for producing homogenous membranes with inorganic particles, hot pressing therefore was not used for further experiments in this study.

2.3 Plasticizer-free PEO:$LiBF_4$ membranes with nanostructured Al_2O_3 as an additive

Using the PEO:$LiBF_4$ 18:1 standard, Al_2O_3-nanostructured particles were added in different amounts to the electrospinning solutions. We used 1 to 5 wt% of Al_2O_3 in our experiments. All electrospun membranes were subjected to electrochemical characterization by impedance analyses. The results showed a positive effect on the conductivity in a temperature range from 293 to 328 K if 3 to 5 wt% of nanostructured Al_2O_3 particles were added. Amounts of more than 5 wt% Al_2O_3 were not applied because such materials are not electrospinnable anymore. The highest conductivities were found for an electrospun PEO:$LiBF_4$ 18:1 sample with 3 wt% Al_2O_3 ranging from 1.9×10^{-6} S cm^{-1} at 293 K to 2.4×10^{-4} S cm^{-1} at 328 K. In contrast, SPEs with 1 and 2 wt% of Al_2O_3 showed decreased ionic conductivities in comparison to the membranes free of inorganic additives (compare Figure 4a). The crystallinity of all membranes was checked *via* P-XRD. PEO tends to show at least some hints of ordering when Al_2O_3 is admixed. While a particle-free membrane with a molar composition of PEO:$LiBF_4$ 18:1 displays no sharp reflections between 5 and 60° in 2θ, all diffractograms of electrospun membranes containing 1 to 5 wt% of nanostructured Al_2O_3 particles showed at least the main reflections of partially ordered PEO between 18 and 24° 2θ. Nevertheless, the ES polymer fibers were dominated by amorphous phase fractions as compared with the SC and HP ones, and therefore conductivities were still higher than those from solution casted or hot pressed membranes (compare Figure 4c).

We performed similar sets of experiments for solution-casted (SC) membranes with the standard composition PEO: $LiBF_4$ 18:1 and nanostructured Al_2O_3 filler. For all tested amounts of nanostructured particles, ranging from 0 to 5 wt%, the ionic conductivities were significantly lower compared to the ones of electrospun membranes (compare Figure 4a and c). In this set of experiments, the membranes with an Al_2O_3 content of

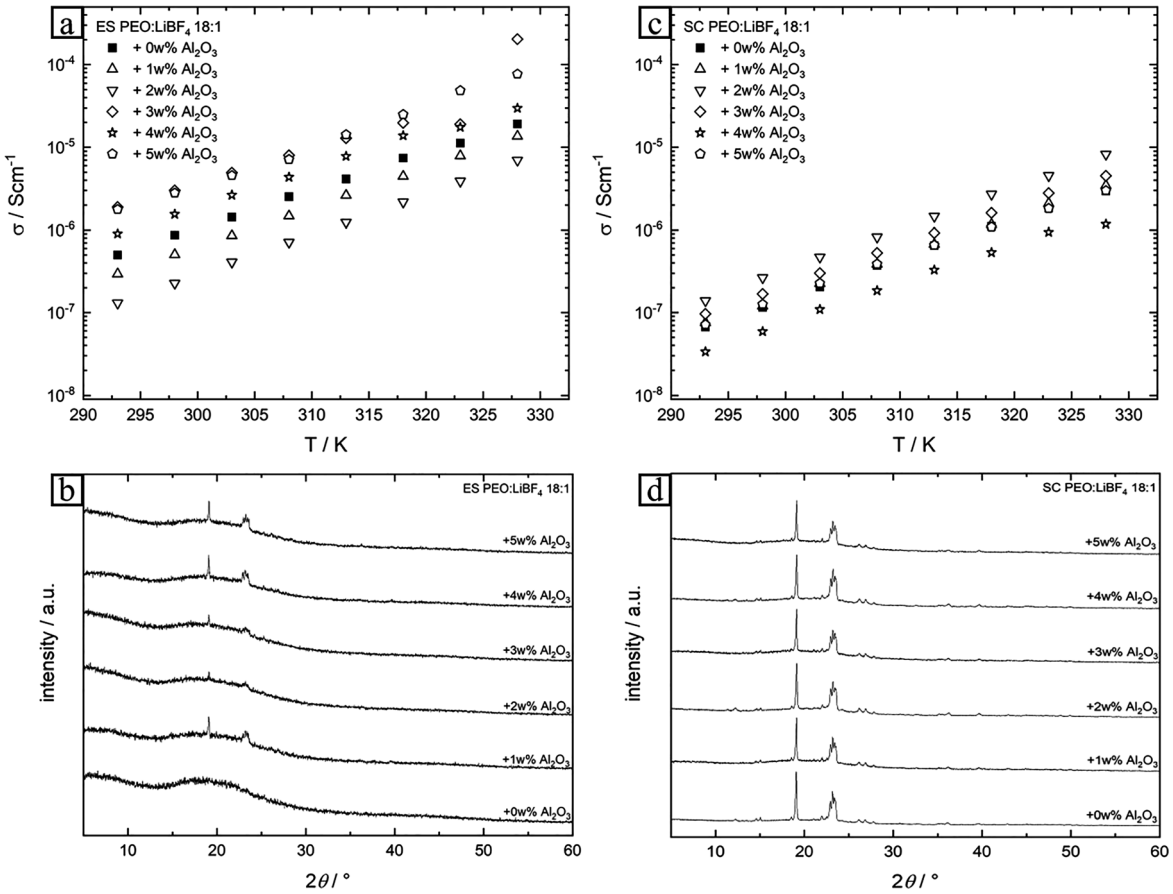

Figure 4: a) Ionic conductivity of electrospun PEO:$LiBF_4$ 18:1 membranes in a temperature range from 298 to 328 K. b) P-XRD from 5 to 60° in 2θ of electrospun (ES) PEO:$LiBF_4$ 18:1 membranes with different Al_2O_3 content, ranging from 0 to 5 wt%. c) Ionic conductivity of solution casted (SC) PEO:$LiBF_4$ 18:1 membranes in a temperature range from 298 to 328 K and d) P-XRD from 5 to 60° in 2θ of solution casted (SC) PEO:$LiBF_4$ 18:1 membranes with different Al_2O_3 content, ranging from 0 to 5 wt%.

2 wt% performed best with an ionic conductivity of 1.4×10^{-7} S cm^{-1} at 293 K, rising to 8.2×10^{-6} S cm^{-1} at 328 K.

Like for Al_2O_3 free samples, the P-XRD patterns collected of SC membranes (Figure 4d) indicated a higher amount of ordered polymer (compare Figure 4b). To check if the nanostructured Al_2O_3 particles were not agglomerated and equally distributed over the polymer membranes, the particle size distribution in the solutions was determined by dynamic light scattering (DLS) before, and Al distribution via energy dispersive X-ray spectroscopy (EDX) after membrane preparation. The influence of the Ultra Turrax mixing on the particle size distribution was investigated. The mean particle diameter of the aggregates was reduced from 1858 to 277.5 nm when using 0.035 g of agglomerated Al_2O_3 in 10 mL acetonitrile. The particle size distribution was also narrowed (compare Figure 5a). It is important to break Al_2O_3 agglomerates as effectively as possible prior to usage because we observed less reproducible results with agglomerated Al_2O_3 samples. The distribution across a solution casted membrane with the composition of PEO:SN:$LiBF_4$ 18:1 + 5 wt% Al_2O_3 is shown in Figure 5b and c. The EDX mapping of Al showed a homogenous distribution of Al across the whole membrane.

2.4 Plasticizer-containing PEO:SN:$LiBF_4$ membranes with nanostructured Al_2O_3 as an additive

Succinonitrile (SN) was added in a molar ratio of PEO:SN:$LiBF_4$ 18:3:1 as a supplement to the added nanostructured Al_2O_3 particles [2]. Adding 1 to 5 wt% Al_2O_3 to ES SPE membranes lead to, a reduction of the ionic conductivity in all cases compared with Al_2O_3-free samples. The membrane with 1 wt% nanostructured inorganic filler performed best. This material is characterized by the highest ionic conductivity of 2.5×10^{-6} S cm^{-1} at 293 K which raised to 5.8×10^{-4} S cm^{-1}

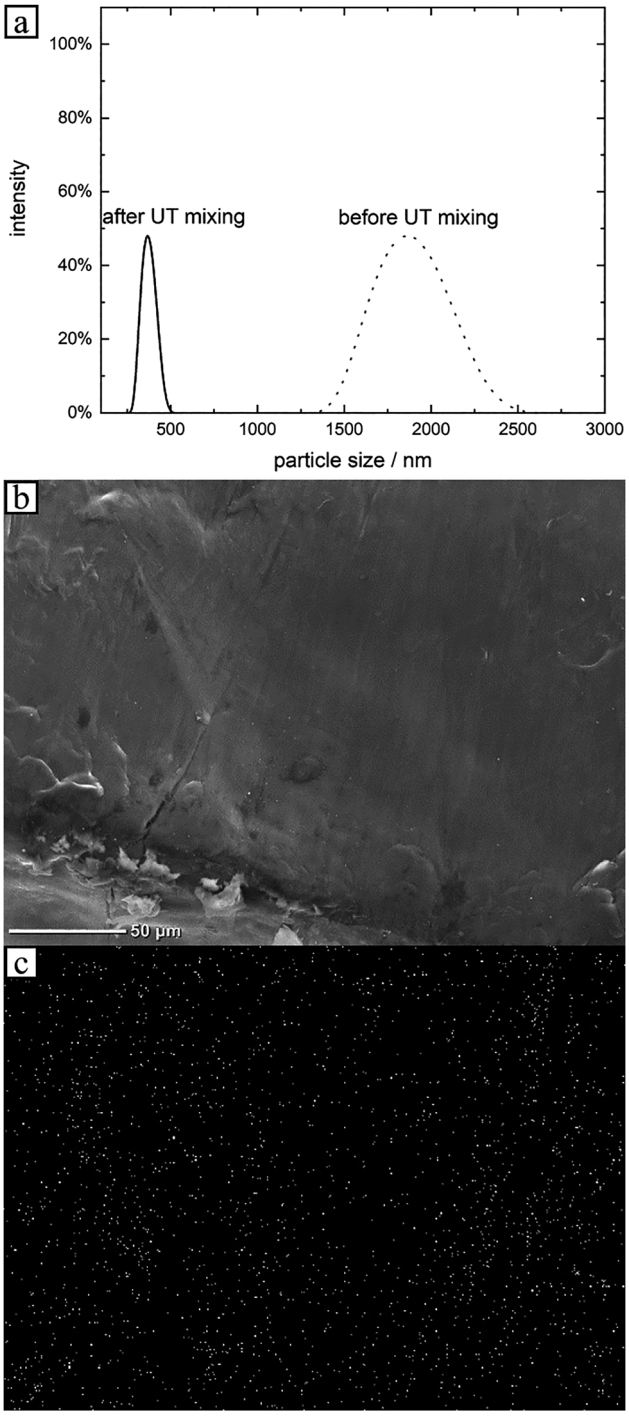

Figure 5: a) Dynamic light scattering (DLS) particle size distribution before and after Ultra Turrax (UT) mixing for 2 × 2 min at 10,000 rpm in acetonitrile. b) SEM at 440× magnification and c) EDX Al-mapping at 440× magnification showing the same area of a solution casted PEO:$LiBF_4$ 18:1 SPE with 5 wt% Al_2O_3.

at 328 K (compare Figure 6a). For all other compositions, the specific ionic conductivities were similar, ranging from 1.1×10^{-6} S cm^{-1} for ES PEO:SN:$LiBF_4$ 18:3:1 + 4 wt% Al_2O_3 to 2.5×10^{-6} S cm^{-1} for a ES PEO:SN:$LiBF_4$ 18:3:1 + 1 wt% Al_2O_3, both at 293 K. It appeared that for plasticizer-containing ES membranes the addition of Al_2O_3 showed no positive effect on the ionic conductivity. Pure ES PEO:SN:$LiBF_4$ 18:3:1 SPE showed an ionic conductivity of 2.5×10^{-5} S cm^{-1} at 293 K. This conductivity is comparable to a HP PEO:LiTFSI 16:1 sample (5,000,000 g mol^{-1} PEO, 298 K) for which a value of 1.0×10^{-5} S cm^{-1} was found [33].

For all SPEs, the X-ray diffraction patterns indicated a higher degree of ordering when SN was admixed. Besides the main reflections of a crystalline PEO phase, no hints for any other ordered system was found (compare Figure 6d).

If we took a look on the SC membranes, the same trend of reduced ionic conductivity upon Al_2O_3 intake was observed. With higher Al_2O_3 contents of 3–5 wt%, we saw an even stronger depression of the conductivity than for the ES membranes. Ionic conductivities were spread over a wide range, from 1.8×10^{-9} S cm^{-1} for SC PEO:SN:$LiBF_4$ 18:3:1 + 3 wt% Al_2O_3 to 4.2×10^{-7} S cm^{-1} for a SC PEO:SN:$LiBF_4$ 18:3:1 + 5 wt% Al_2O_3 membrane, both at 293 K (compare Figure 6). Only the 1 and 2 wt% SC samples outperformed a pure ES PEO:SN:$LiBF_4$ 18:3:1 membrane by almost half an order of magnitude. Conductivities were 5.5×10^{-5} S cm^{-1} for SC PEO:SN:$LiBF_4$ 18:3:1 + 2 wt% and 2.3×10^{-5} S cm^{-1} for ES PEO:SN:$LiBF_4$ 18:3:1.

The XRD patterns of the SC PEO:SN:$LiBF_4$ 18:3:1 + x wt% Al_2O_3 SPEs (x = 1–5) samples showed higher ordering of PEO chains for all tested compositions.

Obviously, the increasing amount of Al_2O_3 in plasticizer-containing ES membranes seemed not to affect the PEO chain mobility, and as a consequence the conductivity was almost identical. This situation changed drastically in the case of SC membranes. Here we saw a spread of conductivity over almost five orders of magnitude, dependent on the Al_2O_3 content. Low Al_2O_3 contents of 1–2 wt% were beneficial and pushed conductivities in the same region as observed for ES materials. Obviously, the underlying conduction mechanism according to Figure 1 seemed not to change significantly for ES materials while this supposed to be the case for SC materials. Which mechanism occurs in both cases is subject to further investigations.

In the light of scalability and larger scale industrial fabrication of polymer electrolytes such an observed behavior might be beneficial because SC is less costly and much easier scalable than ES. In general, the crystallinity of the final material must be reduced for both preparative methods to further optimize the materials. Also, Al_2O_3-dependent mechanical properties need to be determined to address further optimization potential.

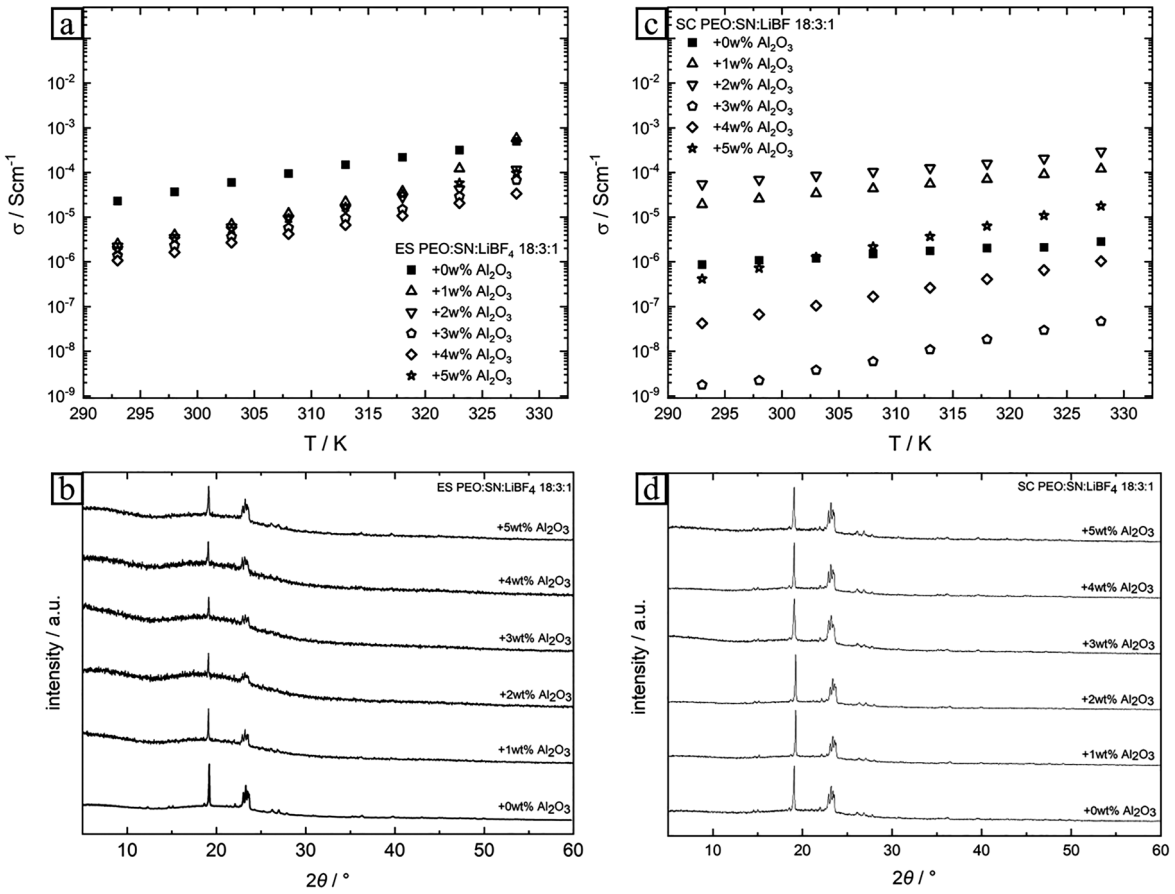

Figure 6: a) Ionic conductivity of electrospun (ES) PEO:SN:$LiBF_4$ 18:3:1 membranes in a temperature range from 298 to 328 K and b) P-XRD from 5 to 60° in 2θ of electrospun (ES) PEO:SN:$LiBF_4$ 18:3:1 membranes with different Al_2O_3 content, ranging from 0 to 5 wt%. c) Ionic conductivity of solution casted (SC) PEO:SN:$LiBF_4$ 18:3:1 membranes in a temperature range from 298 to 328 K. d) P-XRD from 5 to 60° in 2θ of solution casted (SC) PEO:SN:$LiBF_4$ 18:3:1 membranes with different Al_2O_3 content, ranging from 0 to 5 w%.

3 Conclusion

The application of commercially available, nanostructured Al_2O_3 as an inorganic additive to SPEs is found to be beneficial. Important positive issues are to break agglomerates of nanostructured particles prior to mixing with polymers and to realize homogenous distribution in the final product. For plasticizer- and filler-free membranes with a molar composition of PEO:$LiBF_4$ 18:1, the electrospun membranes performed with a ten times higher ionic conductivity compared to membranes prepared by solution casting or hot pressing over the temperature range from 293 to 328 K. Conductivities at 293 K were 5.0×10^{-7} S cm^{-1} for ES, 6.7×10^{-8} S cm^{-1} for SC, and 2.5×10^{-8} S cm^{-1} for HP, respectively. As hot pressed material showed the lowest ionic conductivity and this preparative method itself was not suitable to ensure homogenous distribution of inorganic filler particles in a polymer matrix, the effect of Al_2O_3 addition was not investigated.

For electrospun SPEs, the addition of 3–5 wt% nanostructured Al_2O_3 enhanced the ionic conductivity at 293 K to 1.9×10^{-6} S cm^{-1} for a composition of PEO:$LiBF_4$ 18:1 + 5 wt% Al_2O_3. A similar positive effect was observed for solution casted samples with a composition of PEO:$LiBF_4$ 18:1 + x wt% Al_2O_3 (x = 1–5), with conductivities reaching 1.4×10^{-7} S cm^{-1} at 293 K for the x = 2 sample. Thus, the addition of nanostructured Al_2O_3 can improve the ionic conductivities of SPEs independent of the solution-based preparative method of choice, but still electrospun SPEs outperform these materials with ten times higher conductivities. If succinonitrile (SN), a well-known plasticizer for PEO systems, was added to the system the ionic conductivity was increased to 2.5×10^{-5} S cm^{-1} at 293 K for a electrospun PEO:SN:$LiBF_4$ 18:3:1 Al_2O_3-free membrane. Adding SN to PEO:SN:$LiBF_4$ + x wt% Al_2O_3 systems, did not further increase the ionic conductivity for electrospun SPEs. The most effective optimization of the ionic conductivity was found for solution casted SPEs when SN and Al_2O_3 were added

simultaneously as plasticizer and inorganic filler, respectively. The highest ionic conductivity for solution casted PEO:SN:$LiBF_4$ + Al_2O_3 was observed at 2 wt% showing 5.5×10^{-5} S cm^{-1} at 293 K, which translates to a 1000 times conductivity improvement compared to the initial solution casted PEO:$LiBF_4$ membrane.

For all samples, the usage of nanostructured Al_2O_3 as filler had no significant effect on the temperature range of application, in which the SPEs could be used. We found no significant depression of the melting temperature which would limit the upper application range. The tendency to long range ordering of polymer chains within the membranes, as illustrated from P-XRD, was not increased with up to 5 wt% inorganic filler content, which renders a usage of Al_2O_3 as a filler material possible.

4 Experimental

4.1 Synthesis of membranes

4.1.1 Electrospinning (ES) and solution casting (SC)

To prepare a polymer solution suitable for electrospinning and solution casting, PEO (Sigma Aldrich, 300,000 g mol^{-1}) was stirred in acetonitrile (Sigma Aldrich, purified) until it was fully dissolved (ca. 1 h). Succinonitrile (Sigma Aldrich) was added to the solution. In a last step, the $LiBF_4$ was admixed. Subsequently, the solution was stirred for 12 h to ensure full homogenization. To examine the effect of different amounts of nanostructured Al_2O_3 (AEROXIDE® Alu 130, Evonik), the desired amount was suspended via Ultra-Turrax mixing (2 × 2 min, 10,000 rpm) in the solvent used. All steps were carried out under dry conditions in an inert atmosphere (O_2 < 10 ppm; H_2O < 0.1 ppm). For detailed quantities and molar ratios of all starting materials, see Table 1. Each sample composition is given in molar ratios, in the case of PEO based on the repetition unit.

The solution was casted on a glass (SC samples) or taken up by syringe and transferred to an electrospinning apparatus (ES samples) as described in the literature [2]. During the electrospinning, a voltage of 18–22 kV was applied, the distance between the tip of the cannular and the grounded collector averaged 20 cm, while the solution was pumped with a feedrate of 1.5–3 mL.

4.1.2 Hot pressing (HP)

As a solvent-free preparation method hot pressing was used. Starting materials were homogenized in a mortar und placed in a self-made pressing tool under inert atmosphere.

Table 1: Synthesis parameters for membrane preparation.

Sample composition	PEO (g)	SN (g)	$LiBF_4$ (g)	Al_2O_3 (g)	MeCN (mL)
PEO:$LiBF_4$					
ES 36:1	0.700	–	0.041	–	10
ES 27:1	0.700	–	0.055	–	10
ES/SC 18:1	0.700	–	0.083	–	10
HP 18:1	0.700	–	0.083	–	–
ES/SC 18:1 + 1 wt% Al_2O_3	0.700	–	0.083	0.007	10
ES/SC 18:1 + 2 wt% Al_2O_3	0.700	–	0.083	0.014	10
ES/SC 18:1 + 3 wt% Al_2O_3	0.700	–	0.083	0.021	10
ES/SC 18:1 + 4 wt% Al_2O_3	0.700	–	0.083	0.028	10
ES/SC 18:1 + 5 wt% Al_2O_3	0.700	–	0.083	0.035	10
PEO:SN:$LiBF_4$					
ES 18:3:1	0.700	0.212	0.083	–	10
ES/SC 18:3:1 + 1 wt% Al_2O_3	0.700	0.212	0.083	0.007	10
ES/SC 18:3:1 + 2 wt% Al_2O_3	0.700	0.212	0.083	0.014	10
ES/SC 18:3:1 + 3 wt% Al_2O_3	0.700	0.212	0.083	0.021	10
ES/SC 18:3:1 + 4 wt% Al_2O_3	0.700	0.212	0.083	0.028	10
ES/SC 18:3:1 + 5 wt% Al_2O_3	0.700	0.212	0.083	0.035	10

The pressing tool was placed in a hydraulic press at 5 t and 363 K for 2 h. The obtained membranes were dried for 24 h under vacuum at r.t.

4.2 Powder X-ray diffraction

All samples were checked for crystallinity by powder X-ray diffraction performed by a STOE STADIP diffractometer using Cu$K\alpha_1$ radiation (λ = 1.54051 Å), fitted with a germanium monochromator and a DECTRIS Mythen 1K solid state detector system. Data was collected between 5 and 80° in 2θ. A disk of 10 mm diameter was punched out of the membranes, placed between Scotch Magic Tape and mounted in a flat-bed sample holder. All experiments were carried out at r.t.

4.3 Thermal analysis

The thermal behavior of the solid polymer electrolytes was investigated by differential scanning calorimetry (DSC) in

aluminum crucibles with a Netzsch Maia DSC 200 F3 calorimeter, in a temperature range of 123–523 K, with a heating rate of 10 K min^{-1} under continuous nitrogen flow.

4.4 Scanning electron microscopy (SEM) and energy dispersive X-ray spectroscopy (EDX)

For SEM imaging and EDX analysis, samples were fixed on a graphite sample holder and brought into the vacuum chamber of a JOEL JCM-6000 NeoScop™ with an internal JOEL JED-2200 EDS unit. An acceleration voltage of 15 kV was applied.

4.5 Electrochemical analysis

Ionic conductivity values of PEO:SN:$LiBF_4$ + x wt% Al_2O_3 membranes were calculated from potentiostatic electrochemical impedance spectroscopy data (PEIS) obtained with a Metrohm Autolab B.V. PGSTAT204 potentiostat including a FRA 32 M module. Samples were placed between two stainless steel electrodes in rhd TSC standard battery cells. PEIS data were recoded applying an amplitude of 20 mV, in the frequency range of 1 MHz to 0.1 Hz, at temperatures from 293–328 K in steps of 5 K. The resulting Nyquist plots were fitted using the software Nova 2.0 [34]. The thickness of the samples was determined after the measurements with a micrometer screw (Holex, 0–25 mm, 0.001 mm accuracy).

4.6 Dynamic light scattering

Dynamic light scattering (DLS) was performed on a Malvem Zetasizer Nano ZS instrument in disposable poly(styrene) cuvettes at a wavelength of 633 nm. Particle sizes between 0.4 and 10,000 nm were measured. The Al_2O_3 particles were dispersed and measured in acetonitrile at T = 25 °C.

Acknowledgment: This project was part of a collaboration with Evonik Operations GmbH. We thank Evonik for providing nanostructured Al_2O_3 (AEROXIDE® Alu 130), extruded polymer samples and helpful discussions.

Author contributions: All the authors have accepted responsibility for the entire content of this submitted manuscript and approved submission.

Research funding: None declared.

Conflict of interest statement: The authors declare no conflicts of interest regarding this article.

References

1. Fullerton-Shirey S. K., Maranas J. K. *J. Phys. Chem. C* 2010, *114*, 9196–9206.
2. Freitag K. M., Kirchhain H., van Wuellen L., Nilges T. *Inorg. Chem.* 2017, *56*, 2100–2107.
3. Walke P., Freitag K., Kirchhain H., Kaiser M., van Wuellen L., Nilges T. Z. *Anorg. Allg. Chem.* 2018, *644*; https://doi.org/10.1002/zaac.201800370.
4. Arinicheva Y., Wolff M., Lobe S., Dellen C., Fattakhova-Rohlfing D., Guillon O., Böhm D., Zoller F., Schmuch R., Li J., Winter M., Adamczyk E., Pralong V. Ceramics for electrochemical storage. In *Advanced Ceramics for Energy Conversion and Storage*; Elsevier: Amsterdam, 2020; pp. 549–709; https://doi.org/10.1016/b978-0-08-102726-4.00010-7.
5. Bonizzoni S., Ferrara C., Berbenni V., Anselmi-Tamburini U., Mustarelli P., Tealdi C. *Phys. Chem. Chem. Phys.* 2019, *21*, 6142–6149.
6. Zhang Z., Xu K., Rong X., Hu Y.-S., Li H., Huang Chen L. *J. Power Sources* 2017, *372*, 270–275.
7. Hou W., Guo X., Shen X., Amine K., Yu H., Lu J. *Nano Energy* 2018, *52*, 279–291.
8. Yu X., Xue L., Goodenough J. B., Manthiram A. *Adv. Funct. Mater.* 2021, *31*, 2002144.
9. LaCoste J., He Z., Li Z., Zakutayev A., Fei L. *ECS Meeting Abstracts* 2020, *MA2020-01*, 311–311.
10. Croce F., Appetecchi G. B., Persi L., Scrosati B. *Nature* 1998, *394*, 456–458.
11. Ahn J. H., Wang G. X., Liu H. K., Dou S. X. *J. Power Sources* 2003, *119–121*, 422–426.
12. Appetecchi G. B., Croce F., Persi L., Ronci F., Scrosati B. *Electrochim. Acta* 2000, *45*, 1481–1490.
13. Navarra M. A., Lombardo L., Bruni P., Morelli L., Tsurumaki A., Panero S., Croce F. *Membranes* 2018, *8*, 126.
14. Capiglia C., Mustarelli P., Quartarone E., Tomasi C., Magistris A. *Solid State Ionics* 1999, *118*, 73–79.
15. Mustarelli P., Quartarone E., Tomasi C., Magistris A. *Solid State Ionics* 2000, *135*, 81–86.
16. Commarieu B., Paolella A., Daigle J.-C., Zaghib K. *Curr. Opin. Electrochem.* 2018, *9*, 56–63.
17. Xiong H.-M., Zhao X., Chen J.-S. *J. Phys. Chem. B* 2001, *105*, 10169–10174.
18. Sun H. Y., Sohn H. J., Yamamoto O., Takeda Y., Imanishi N. *J. Electrochem. Soc.* 1999, *146*, 1672–1676.
19. Itoh T., Ichikawa Y., Uno T., Kubo M., Yamamoto O. *Solid State Ionics* 2003, *156*, 393–399.
20. Liu W., Liu N., Sun J., Hsu P.-C., Li Y., Lee H.-W., Cui Y. *Nano Lett.* 2015, *15*, 2740–2745.
21. Xie Z., Wu Z., An X., Yue X., Xiaokaiti P., Yoshida A., Abudula A., Guan G. *J. Membr. Sci.* 2020, *596*, 117739.
22. Gao L., Li J., Ju J., Cheng B., Kang W., Deng N. *Compos. Sci. Technol.* 2020, *200*, 108408.
23. Li W., Sun C., Jin J., Li Y., Chen C., Wen Z. *J. Mater. Chem. A* 2019, *7*, 27304–27312.
24. Vishwakarma V., Jain A. *J. Power Sources* 2017, *362*, 219–227.
25. Pitawala H. M. J. C., Dissanayake M. A. K. L., Seneviratne V. A. *Solid State Ionics* 2007, *178*, 885–888.
26. Shin J.-H., Passerini S. *Electrochim. Acta* 2004, *49*, 1605–1612.

27. Wetjen M., Navarra M. A., Panero S., Passerini S., Scrosati B., Hassoun J. *ChemSusChem* 2013, *6*, 1037–1043.
28. Gadjourova Z., Andreev Y. G., Tunstall D. P., Bruce P. G. *Nature* 2001, *412*, 520–523.
29. Bruce P. G. *Electrochim. Acta* 1995, *40*, 2077–2085.
30. Chen L., Li Y., Li S.-P., Fan L.-Z., Nan C.-W., Goodenough J. B. *Nano Energy* 2018, *46*, 176–184.
31. Takahashi Y., Sumita I., Tadokoro H. J. *Polymer Sci: Polymer Phys. Ed.* 1973, *11*, 2113–2122.
32. Stephan A. M. *Eur. Polym. J.* 2006, *42*, 21–42.
33. Hahn M., Rosenbach D., Krimalowski A., Nazarenus T., Moos R., Thelakkat M., Danzer M. A. *Electrochim. Acta* 2020, *344*, 136060.
34. Nova (version 2.0); Metrohm Autolab B.V.: Utrecht, The Netherlands, 2015.

3.3 Fast Magnesium Conducting Electrospun Solid Polymer Electrolyte

Patrick Walke[a,b], Janio Venturini[a], Robert Spranger[b], Leo van Wüllen[b], Tom Nilges[a]

[a] Technical University Munich, Department for Chemistry, Lichtenbergstraße 4, 85748 Garching bei München

[b] TUMint.Energy Research GmbH, Lichtenbergstraße 4, 85748 Garching bei München

[c] Augsburg University, Institute of Physics, Universitätsstraße 1, 86159 Augsburg

Submitted Manuscript

The switch to multivalent ions is one part of the search for safe and more powerful battery systems.[108] One example for the use of divalent ions is magnesium ion batteries (MIBs). In contrast to lithium, magnesium metal is less reactive and supposed to be dendrite-free during cycling, what makes it a possible anode material.[69] Here the advantages of electrospun polymer electrolytes, as demonstrated for lithium before[60, 104, 105, 106], are combined with a magnesium conducting salt. The electrospun polymer electrolytes are compared to solution casted membranes with the same molar compositions. The highest ionic conductivity of 10^{-5} S/cm at 293 K is achieved with an electrospun PEO:$Mg(TFSI)_2$ 36:1 membrane. The respective solution casted membrane showed low ionic conductivity of 10^{-9} S/cm at 293 K. Succinonitrile (SN) is tested as solid lubricant to enhance the PEO chain mobility and thus the ionic conductivity of the system. Sn is not increasing the ionic conductivity in the case of PEO:$Mg(TFSI)_2$ solid polymer electrolytes. As a result the conductivity of an electrospun PEO:SN:$Mg(TFSI)_2$ membrane is near to 10^{-7} S/cm at 293 K. Magnesium ion transport through the electrospun membranes is proven *via* cyclic voltammerty of the SPEs between magnesium metal electrodes. The low current seems to be due to a passivating interface, observed by impedance spectroscopy, build up by the polymer and the electrodes being in contact.
The amorphous character of the electrospun membranes is investigated *via* powder X-ray diffraction. To show the homogeneous distribution of the conducting salt across the membranes energy dispersive X-ray spectroscopy is conducted. With solid-state NMR experiments the mobility of PEO chains and the TFSI-anion is detected and the absences of impurities from the used solvents or water is shown. The latter is confirmed by *Karl-Fischer*-titration. The fibrous structure of the electrospun polymer

membranes is illustrated by SEM imaging.
Our electrospun PEO:$Mg(TFSI)_2$ solid polymer electrolyte shows high ionic conductivity at low magnesium ion concentration compared to the magnesium ion conducting solid polymer electrolytes reported in literature (compare section 1.3 Magnesium Ion Batteries).

Author Contributions: P.W. prepared the polymer membranes and conducted P-XRD, DSC, SEM, EDX, *Karl Fischer*-titration, impedance spectroscopy and cyclic voltammetry experiments. R.S. did solid-state NMR experiments. P.W., J.V., R.S., L.v.W. and T.N. discussed the data and wrote the manuscript.

Fast Magnesium Conducting Electrospun Solid Polymer Electrolyte

Patrick Walke,[a,b] Janio Venturini,[a] Robert Spranger,[c] Leo van Wüllen[c] and Tom Nilges*[a]

[a] Patrick Walke, Dr. Janio Venturini, Prof. Dr. Tom Nilges
Synthesis and Characterization of Innovative Materials
Chemistry Department
Technical University of Munich
Lichtenbergstraße 4, 85748 Garching bei München, Germany
E-mail: tom.nilges@tum,de

[b] Patrick Walke
TUMint.Energy Research GmbH
Lichtenbergstraße 4, 85748 Garching bei München, Germany

[c] Robert Spranger, Prof. Dr. Leo von Wüllen
Institute of Physics
University of Augsburg
Universitätsstraße 1, 86159 Augsburg, Germany

Supporting information for this article is given via a link at the end of the document.

Abstract: Magnesium Ion based Solid Sate Batteries (MIBs) are subject of intensive studies due to abundance of magnesium, its advantages in volumetric capacity and the reduced dendrite growth. Here we report on a true solid polymer electrolyte system without liquid additives or plasticizers that reaches conductivities above 10^{-5} Scm^{-1} at room temperature and above 10^{-4} Scm^{-1} at 50°C. An electrospun polymer electrolyte membrane fabricated from a polymer electrolyte featuring a composition of PEO:$Mg(TFSI)_2$ 36:1 was identified as the best performing system. Magnesium transport was substantiated by different methods and the electrochemical properties including SEI formation were investigated. Electrospinning as a preparation method has been identified as a powerful tool to enhance the electrochemical properties beside conventional polymer membrane fabrication techniques.

Introduction

Since the introduction of Lithium-Ion Batteries (LIB) in 1981 by *J. Goodenough* and their commercialization through Sony, the need to store electrical energy keeps growing.[1] High capacity batteries are indispensable not only for portable devices, but also to store energy produced from sustainable methods. Despite the current advances in lithium-air, lithium-sulfur or sodium-ion devices, the switch to multivalent ions constitutes an integral part of the post lithium ion research.[2] One of the most abundant and lightest divalent ions is Mg^{2+}, which is homogenously distributed all over the globe.[3] Although the gravimetric specific capacity of metallic Mg (2300 mAh/g) is lower compared to Li metal (3862 mAh/g), the volumetric capacity is relatively high, 3997 mAh/cm^3 (compare Li metal, 2062 mAh/cm^3).[1b, 4] Other important advantages of magnesium ion batteries (MIB) are the lower reducing character and the less-pronounced tendency to form dendrites of Mg metal in contrast to pure Li. These features

make Mg metal anodes more applicable with a variety of solvents and polymers.[5] Early electrolyte solutions with enhanced Mg dissolution und depleting abilities were based on *Grignard* reactions, before magnesium aluminate chloride complex solutions were intensively studied by the group of D. Aurbach.[1b, 6] Electrolyte solutions more similar to those used in LIBs, are reported to show reasonable ionic conductivities and electrochemical behavior.[7] A full cell with Mg metal anode and $MgMn_2O_4$ cathode can be operated in a solution of 0.5 M $Mg(ClO_4)_2$ in acetonitrile acting as electrolyte.[8] Although it is reported that $Mg(TFSI)_2$ dissolved in ethers tends to form an insulating film on Mg metal anodes,[3b] a 1.0 M solution of $Mg(TFSI)_2$ in diglyme shows an ionic conductivity of 5×10^{-3} Scm^{-1} at r.t. with good Mg dissolution and deposition ability.[9] Besides liquid electrolytes, a variety of gel polymer electrolytes (GPEs) showed reasonably high conductivities.[10] A PVDF-HFP:$Mg(O_3SCF_3)_2$ with a molar ratio of 27:1, conducting- salt-containing polymer host enhanced by 40w% 1-ethyl- 3-methylimidazolium trifluoromethanesulfonate ionic liquid (EMITf) operating at r.t. reaches 4.63×10^{-3} Scm^{-1}.[11] To calculate the molarity of the statistical co-polymer the average of the molar mass of the repeating units is used. By using 50w% of EMITf on a poly(ethylene oxide) (PEO) based host with a molar composition of PEO:$Mg(O_3SCF_3)_2$ 25:1, an ionic conductivity of 5.6×10^{-4} Scm^{-1} is achieved at r.t., as compared to the same polymer:conducting salt host showing significantly lower ionic conductivity of 4×10^{-6} Scm^{-1} if no ionic liquid (IL) is added.[12] In addition to ILs, inorganic fillers can be added to enhance the electrochemical properties of SPEs. An ionic conductivity of 1.6×10^{-4} Scm^{-1} at 30 °C is reported when 75w% of 1-butyl-1-methylpyrrolidinium bis(trifluoromethyl)sulfonyl imide (Pyr_{14}-TFSI) ionic liquid and 10w% TiO_2 are added to a PVDF-HFP:$Mg(ClO_4)_2$ host with a molar ratio of 5:8.[13] ILs are not the only compounds used as a liquid ingredient in GPEs. A ratio of 500w% of an ethylene carbonate/propylene carbonate (EC+PC) mixture is admixed to a polyacrylnitrile:$Mg(O_3SCF_3)_2$ 19:1 membrane to reach 1.7×10^{-4} Scm^{-1}.[14] The same carbonate combination is used to mobilize Mg ions in a poly(methyl methacrylate):$Mg(O_3SCF_3)_2$ host with a molar composition of 8:1. The resulting maximum ionic conductivity is reached at 3×10^{-4} Scm^{-1} with 300w% EC+PC (liquid).[15] Instead of mixing short ether molecules, adding poly(ethylene glycol) dimethyl ether (PEGDE) was tried on an oligo(ethylene oxide)-crafted polymethacrylate (PEO-PMA) matrix. If an overall ratio of EO:MgX_2 of 128:1 is prepared the ionic conductivity ranges from 1×10^{-5} Scm^{-1} (X= O_3SCF_3), through 2×10^{-5} Scm^{-1} (X= ClO_4), to 1×10^{-4} Scm^{-1} (X= TFSI).[16] Because of the low molar mass of the used PEGDE (400-800 $gmol^{-1}$), this electrolyte is more related to GPEs than to SPEs as stated by the authors. Although liquid electrolyte components are less of a safety issue in MIBs compared to LIBs due to the less reactive nature of the metal, the use of solid polymer electrolytes (SPEs) would introduce additional benefits such as reduced weight, toxicity, and risk of leaking. For a brief summary on inorganic MIB electrolytes, the interested reader is referred to a summary of *Zhan et al*.[17] A solvent-free example of SPEs

is PVDF:$Mg(NO_3)_2$ 27:5, showing a poor ionic conductivity of 6×10^{-8} Scm^{-1}, which can be increased to 1.6×10^{-6} Scm^{-1} by adding 3w% MgO, both at r.t.[18] As PEO is a well-known polymer to conduct alkali metals, several PEO:MgX_2 combinations without further additives have been tested. Most of these show low ionic conductivities ranging from 10^{-9} Scm^{-1} (X= ClO_4) to 10^{-7} Scm^{-1} (X= TFSI) at r.t.[10], the latter at a molar composition of PEO:$Mg(TFSI)_2$ of 40:1.[19] This composition is close to the composition of choice in our study, as we use PEO:$Mg(TFSI)_2$ 36:1 as the highest Mg salt concentration for electrospun SPE membranes. Such conductivities are not competitive with state-of the art solid electrolytes and need to be improved prior to application. Target conductivities are in the range of 10^{-4} Scm^{-1}.[20] As compared to standard procedures for polymer electrolyte fabrication, such as solution casting and hot pressing, the electrospinning process drastically changes the morphology of the self-standing samples. The first two methods form bulk membranes, as used in all polymer electrolyte studies reported earlier on, while the latter leads to membranes consisting of thin polymer fibers. The positive effect of the electrospinning technique to PEO-based membranes has already been investigated by our group for Li and Na ion conducting SPEs with different *A*X (*A*= Li, Na; X= BF_4, TFSI).[21] As it is reported in literature that crystallinity in polymers hinders the ionic conductivity, we aimed for an amorphous phase as product. We additionally checked the influence of succinonitrile (SN) as a plasticizer for PEO.[22] The outstanding properties of the products combined with the high grade of adaptability and the possibility of upscaling the electrospinning process to a roll-to-roll process make our electrospun polymer membrane a promising candidate to aim for lighter, safer and more efficient battery systems in the future.[23]

Results and Discussion

Electrospinning is a powerful method to achieve large area fibrous membranes with various additives and compositions. By electrospinning solutions of PEO:SN:$Mg(TFSI)_2$ with different molar compositions, highly amorphous membranes of submicrometric fibers are obtained. The fibers form homogenous membranes with up to 80 µm thickness. Figure 1 summarizes P-XRD experiments for various membranes where only few reflections were found. Reflections at 19.2° and 23.2° 2θ can be assigned to short range ordering of PEO chains.[24] No reflections indicating the presence of ordered succinonitrile or $Mg(TFSI)_2$ are detected. Plasticizer and conductive salt do not influence the thickness or geometry of the fibers if the viscosity is controlled by the amount of solvent used. This is also true for the crystallinity as one cannot see any significant difference in number and intensity of reflections for the different samples.

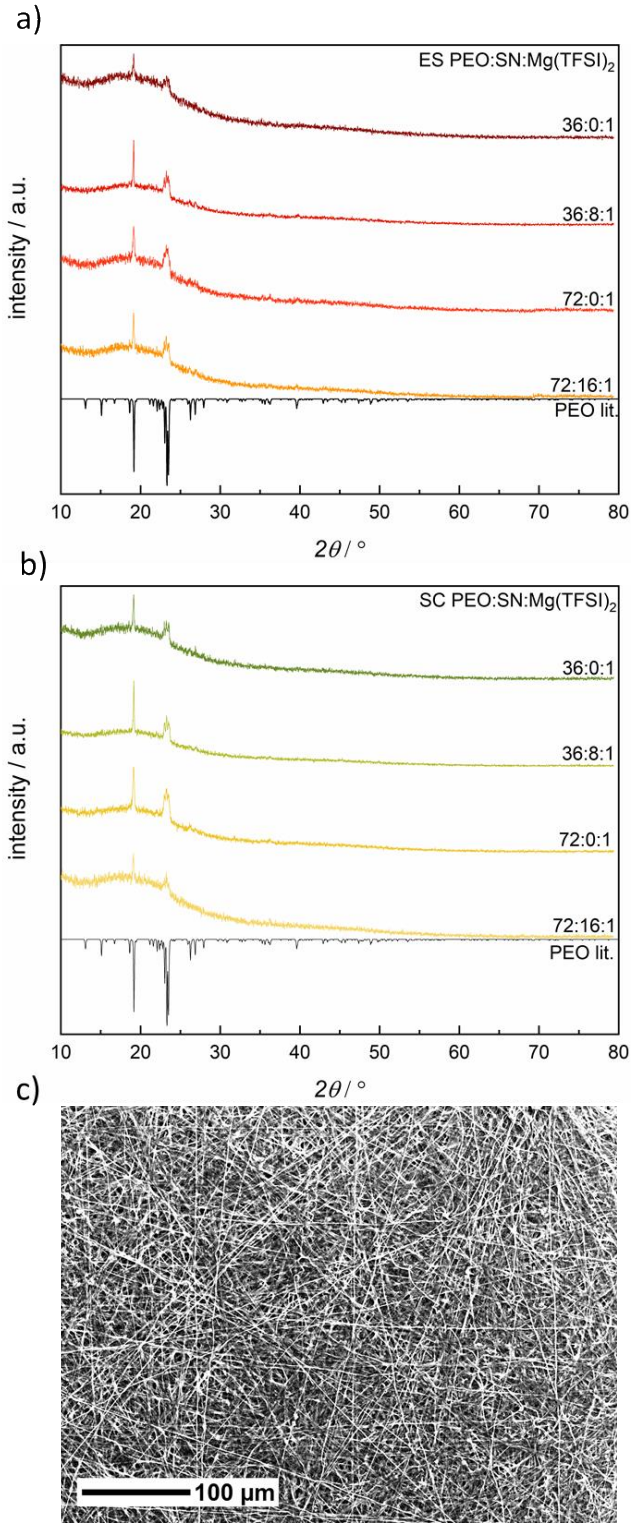

Figure 1. P-XRD of a) electrospun (ES) and b) solution casted (SC) PEO:SN:$Mg(TFSI)_2$ SPEs with different molar compositions compared to a crystalline phase of PEO from literature, [24] c) SEM image of an electrospun PEO:SN:$Mg(TFSI)_2$ 36:0:1 SPE with 250-fold magnification.

The thermal properties of the membranes were studied by differential scanning calorimetry (DSC). Melting points decrease from 332 K and 333 K, for PEO:SN:$Mg(TFSI)_2$ 72:16:1 and 72:0:1 respectively, to 322 K when the conducting salt concentration is increased to 36:0:1. This trend is even more pronounced if the glass transition temperature is considered (257 K at 72:0:1, 234 K at 36:0:1), see Figure 2.

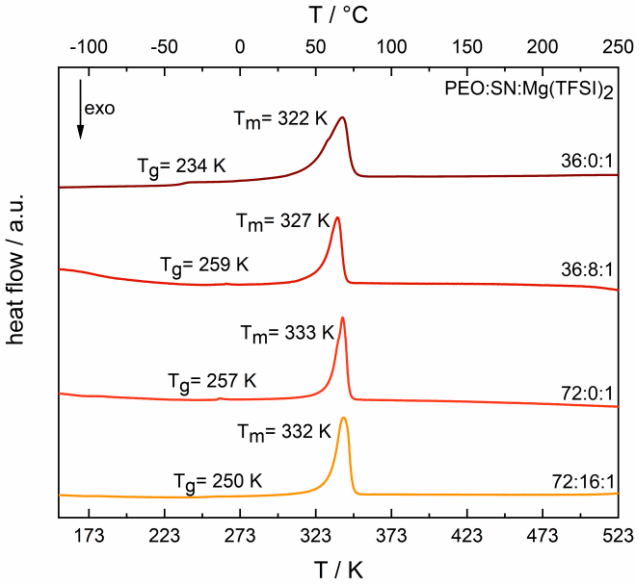

Figure 2. DSC curve of electrospun PEO:SN:$Mg(TFSI)_2$ SPEs at different molar compositions and their fitted melting points T_m and glass transition temperatures T_g.

Ionic conductivities were determined by impedance spectroscopy. The ionic conductivity is dependent on the conducting salt concentration and the temperature. The electrospun sample with a molar composition of PEO:SN:$Mg(TFSI)_2$ of 72:0:1 showed a conductivity of 6.0×10^{-8} Scm^{-1} at 273 K and 1.0×10^{-5} Scm^{-1} at 323 K. The highest ionic conductivity is achieved with a PEO:SN:$Mg(TFSI)_2$ 36:0:1 SPE showing 1.8×10^{-6} Scm^{-1} at 273 K, which increases to 1.6×10^{-4} Scm^{-1} at 323 K, while a solution-casted sample of the same composition showed a drastically lower ionic conductivity, from 1.6×10^{-9} Scm^{-1} to 1.8×10^{-7} Scm^{-1} in the same temperature range (see Figure 3a).This again corroborates the superior performance of electrospun SPEs as compared to solution casted SPEs, as already observed by us for related systems[21b] Consistently, the electrospun sample also showed the lowest glass transition temperature, which is directly linked to the mobility of PEO chains. All displayed ionic conductivities are calculated from the 4th cycle of temperature dependent impedance spectroscopy to ensure a stable system during the measurement. The influence of the electrode material on the impedance spectroscopy results was checked by using stainless steel and Mg metal electrodes. While measuring with stainless steel blocking electrodes, the impedance showed the typical polarization at low frequencies; using Mg-metal, a second semi-circle was detected at low frequencies in the Nyquist plot. This second semi-circle is assigned to the charge transfer from the Mg metal electrode to the SPE membrane (see S1, Supporting Information). With 20 consecutive impedance measurements at constant temperature (293 K) and voltage

(0 V vs. OCV), the behavior of detected resistances was investigated. While the resistance at high frequencies – which is assigned to the grain boundaries of the SPE – goes down by 13% due to compression of the sample, the charge transfer resistance goes up by 80% due to the formation of an electrolyte-electrode-interface (see S2, Supporting Information).

At this stage, a question of whether succinonitrile (SN), a commonly used plasticizer in Li-containing SPEs, is beneficial for Mg-based PEO-SPEs – as observed for other PEO:SN systems containing salts like $LiBF_4$, $NaBF_4$ or LiTFSI [21a, 21b, 21c] - was raised. The use of succinonitrile during the electrospinning of $Mg(TFSI)_2$-containing SPEs decreased the ionic conductivity to 5.3×10^{-8} Scm^{-1} at 273 K for a PEO:SN:$Mg(TFSI)_2$ 36:8:1 composition, and it seems therefore not applicable for electrospun PEO based SPEs with $Mg(TFSI)_2$ conductive salt. We realized in brief drying experiments followed by solid state NMR spectroscopy that the SN content drops during the synthesis process of the membranes, and SN vanishes upon drying. Therefore, the 36:8:1 composition represents the starting conditions and the actual SN content after the workup procedure is reduced.

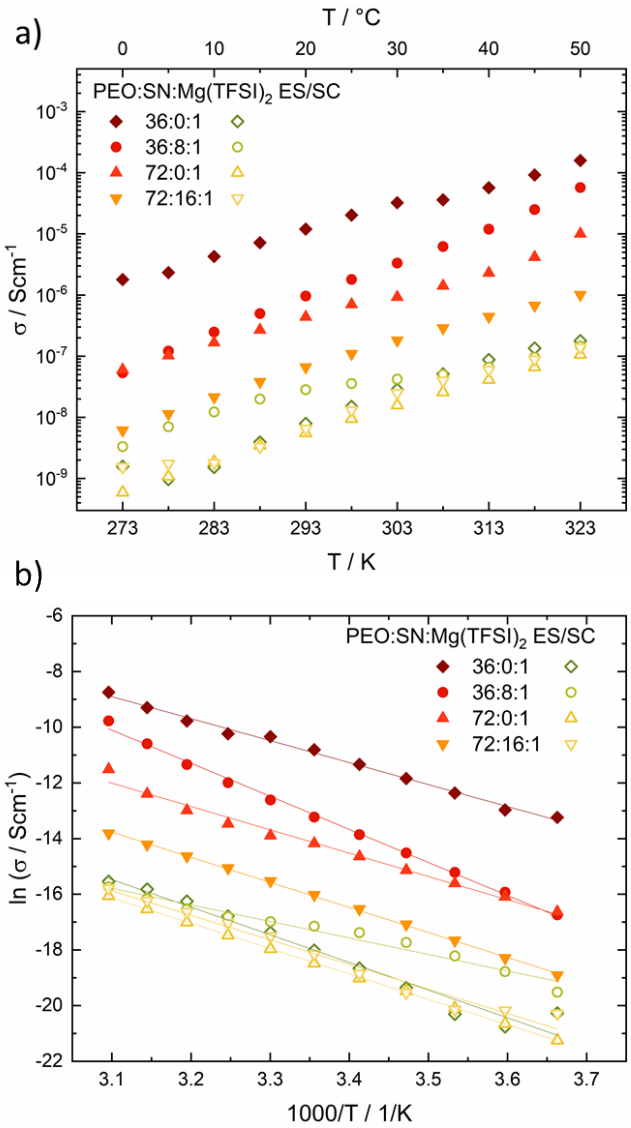

Figure 3. a) Ionic conductivity and b) Arrhenius type plots of electrospun (filled symbols) and solution casted (empty symbols) SPEs with different compositions in a temperature range from 273 K to 323 K.

The activation energy derived from the ionic conductivity is 66 $kJmol^{-1}$ for the sample with the highest specific ionic conductivity, rising to 99 $kJmol^{-1}$ for a sample with lower conducting salt concentration (72:0:1). If the same solutions used for electrospinning are processed via solution casting, the ionic conductivities of the non-porous casted membranes drop at least two orders of magnitude, to 1.5×10^{-9} Scm^{-1} at 273 K for an PEO:SN:$Mg(TFSI)_2$ 36:0:1 composition. Activation energies calculated for those membranes differ from 49 $kJmol^{-1}$ to 82 $kJmol^{-1}$, see Figure 3b. This contrast in ionic conductivity clearly shows the beneficial influence of the electrospinning process on the electrochemical properties of the membranes. For the sample with the highest ionic conductivity – an electrospun, plasticizer-free PEO:SN:$Mg(TFSI)_2$ 36:0:1 membrane – neither NMR spectroscopy (see S6, Supporting Information) nor Karl-Fischer-titration give rise to water contamination in the sample

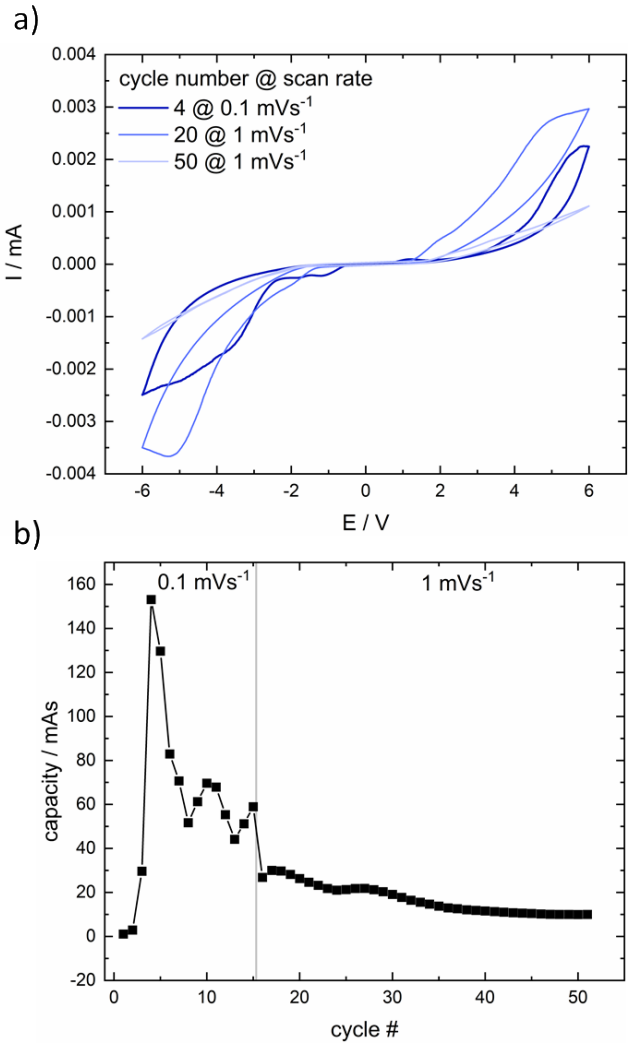

Figure 4. a) Single cycles of cyclic voltammetry at different scan rates of a PEO:SN:$Mg(TFSI)_2$ 36:0:1 membrane between Mg metal electrodes in a coin cell. b) Capacity over cycle number calculated from CV cycling, scan rates given in the graph.

EDX spectroscopy was performed on a piece of the same membrane. The areal scan shows a homogenous distribution of Mg and F across the membrane. Besides Si coming from the

used glassware, only C, O, F, Mg and S are detected. All these elements can be assigned to the polymer or the $Mg(TFSI)_2$ conducting salt (see S3, Supporting Information).

The ability of PEO:SN:$Mg(TFSI)_2$ SPEs to transport Mg ions through the membrane was proven by cyclic voltammetry of plasticizer-free membranes with the highest ionic conductivity (36:0:1) between two Mg metal electrodes. The capacity dropped within the first 10-15 cycles, before reaching a plateau for at least 35 more cycles, as shown in Figure 4. Obviously, a passivation process at the SPE-electrode interface is initiated after the first cycles, causing a significant capacity loss during cycling. This is a widely known fact for Mg electrodes [25] and needs to be optimized in the future. However, the set of experiments at least substantiates the transport of Mg ions through the SPE.

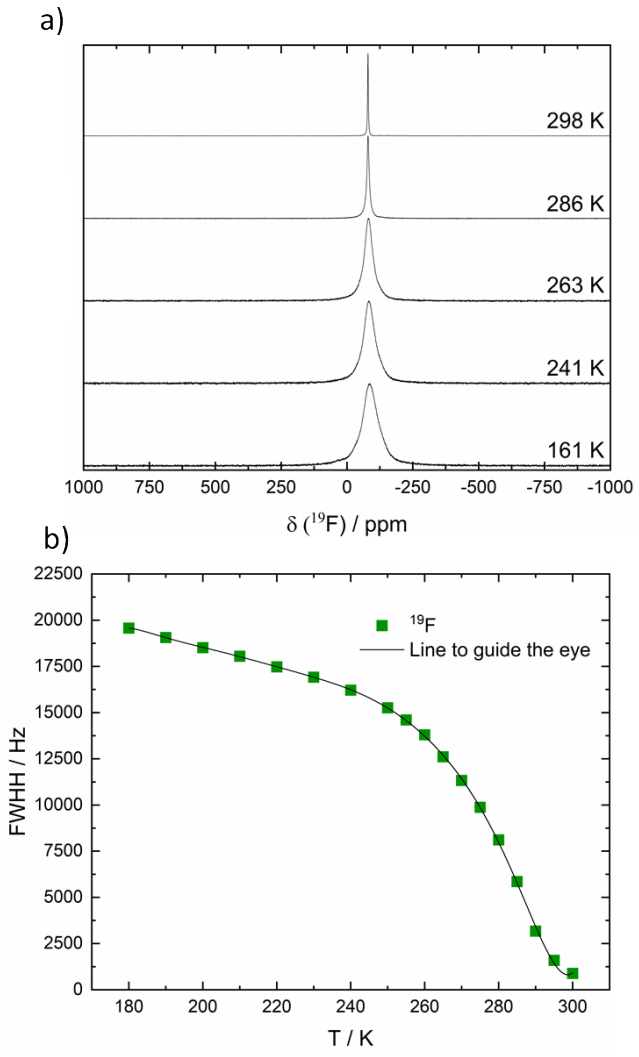

Figure 5. a) Temperature-dependent static ^{19}F spectra and b) the evolution of the ^{19}F line width as a function of temperature for the PEO:SN:$Mg(TFSI)_2$ 36:0:1 membrane. The line is merely a visual aid.

To further investigate the Mg-based membranes, the promising electrospun PEO:SN:$Mg(TFSI)_2$ 36:0:1 plasticizer-free membrane was chosen. To obtain direct information about the dynamics in the membranes, ^{25}Mg NMR would be ideally suited. However, the very

low gyromagnetic ratio (-1.639×10^7 $rads^{-1}T^{-1}$) necessitates specialized probes not available in our laboratory. Therefore, we had to restrict the analysis of the dynamics to the TFSI anion and the PEO chains employing ^{19}F, ^{13}C and ^{1}H NMR spectroscopy. To analyze the ion dynamic of $Mg(TFSI)_2$, static temperature-dependent ^{19}F spectra were recorded, as shown in Figure 5a. The ^{19}F signal is mainly dominated by the chemical shift and by dipole interactions, leading to the broadening of the

signal. These internal interactions scale with the second Legendrian polynomial $3cos^2(\beta) - 1$, with β representing the angle between the direction of the external magnetic field B_0 and directions of the principal axis of the respective interaction. Any motional process will lead to an averaging or partial averaging of these interactions, entailing a narrowing of the NMR line width (motional narrowing). As obvious from inspection of Figure 5b, in which the observed ^{19}F static line width is plotted as a function of temperature, a drastic line narrowing of the ^{19}F static line width is observed starting at around 260 K, indicating the onset of dynamics at this temperature.

This temperature-dependent narrowing of the NMR line allows an estimation of the activation energy of the dynamic process of the TFSI-anion. According to the empirical Waugh-Fedin relation $E_A = 0.156 \times T_{onset}$, the activation energy can be estimated.[26] The onset temperature here is calculated as the temperature when the line width reduces to

$$(\upsilon_{rigid\ lattice} - \upsilon_{motional\ narrowing})/2 + \upsilon_{motional\ narrowing}.$$

From this an activation energy of 43 kJ/mol ($T_{onset} = 277\ K$) was determined. The calculated activation energy of the $Mg(TFSI)_2$-based plasticizer-free sample is comparable to the LiTFSI plasticizer-free sample with an activation energy of 41 kJ/mol for a PEO:LiTFSI 18:1 membrane,[21a] showing a minor increase in the activation energy when changing from a single charged cation, lithium, to a double charged one, magnesium.

To further investigate the PEO-based membranes and analyze the behavior of the host material PEO, its properties as well as its dynamics, ^{13}C-NMR measurements were performed. To analyze the temperature dependent behavior, ^{13}C-MAS single pulse and ^{13}C-{^{1}H}-CP-MAS experiments, both functioning as dipolar filters, were performed. Whereas the single pulse excitation ^{13}C-MAS NMR experiment filters out ^{13}C nuclei in mobile environments, since the resonances of ^{13}C in immobile PEO are broadened beyond detectability, the efficiency of the cross-polarization process in the ^{13}C-{^{1}H}-CP-MAS experiment relies on the heteronuclear dipolar coupling between ^{13}C and ^{1}H, thus highlighting ^{13}C nuclei embedded in immobile environments.

The temperature-dependent ^{13}C-MAS single pulse experiments, Figure 6a, do not provide a signal at low temperatures. This shows the immobility of the PEO-host material as well as the frozen dynamic of the TFSI-anion in this temperature range, which is consistent with the temperature-dependent ^{19}F measurements. Only at higher temperatures a signal at 70 ppm grows in, evolving into a triplet (J(C-H) coupling with the methylene protons) at temperatures of 316 K and above.

This splitting indicates a rather vivid segmental dynamic of the PEO chains which removes the enormous line broadening due to strong ^{1}H-^{13}C-dipolar couplings and therefore enables the resolution of the J-multiplet.

Such an enormous chain mobility has also been observed in other PEO:salt and PEO:SN:salt (salt: $LiBF_4$, $NaBF_4$ or LiTFSI) samples, in[21a, 21c, 27] The ^{13}C signal of the TFSI-anion at around 120 ppm is also observable at high temperatures correlating with the PEO- signal, suggesting that the dynamic processes of the TFSI-anion and the PEO-host structure are correlated.

In addition, the enormous chain mobility manifests itself in the fact that no significant ^{13}C-{^{1}H}-CP-MAS signal was detected at room temperature (Figure 6b). Lowering the temperature (and thereby decreasing the chain mobility), a ^{13}C CPMAS signal gradually grows in, which splits into several individual contributions, a group of peaks ranging from 70 to 74 ppm and a broad component at 68.9 ppm. The narrow peaks can be assigned to the different crystal positions of the PEO, noting that not all 14 different peaks can be resolved[28] and the broad resonance can be assigned to the amorphous PEO phase. This assignment is supported by the evolution of the CP signal intensity with contact time (see S4, Supporting Information).[29]

The appearance of the ^{13}C CPMAS signal at 175 K closely resembles that of an electrospun PEO:SN:$LiBF_4$ sample. For this sample, Kirchhain showed[30] employing ^{13}C-{^{1}H}-CP-^{7}Li REDOR (rotational echo double resonance) NMR (see S5. Supporting Information), that the broad resonance experienced local proximity to lithium cations and was assigned to an amorphous Li-containing PEO phase. The carbon atoms contributing to the narrow signals on the other hand did not show any dipolar coupling to ^{7}Li and were therefore assigned to a pure Li-free crystalline PEO phase.

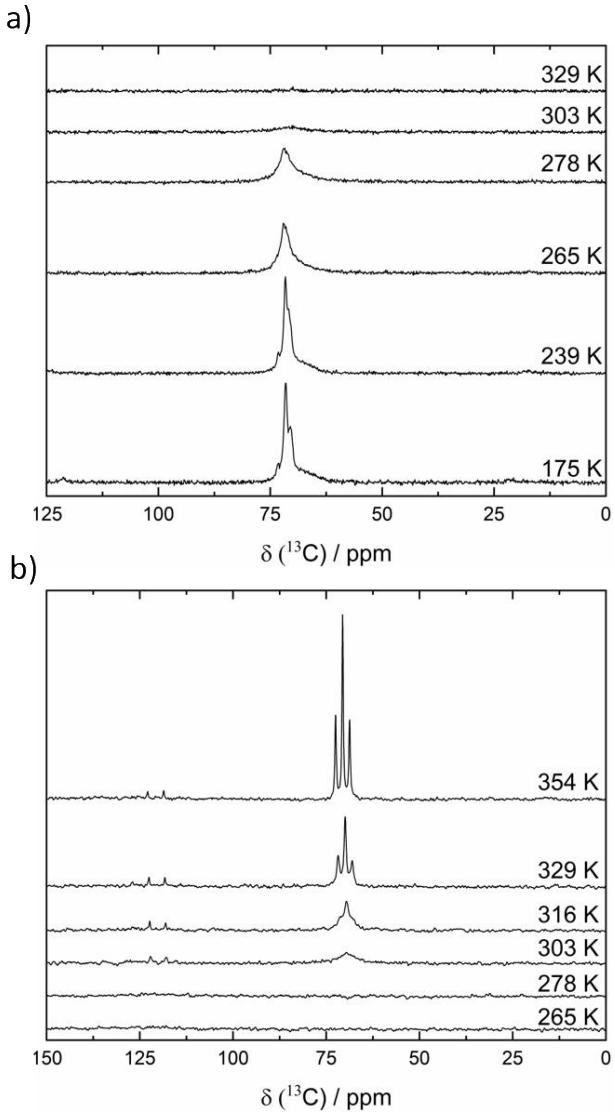

Figure 6. a) Temperature-dependent ^{13}C-MAS spectra and b) ^{13}C-{^{1}H}-CP-MAS spectra for the PEO:SN:Mg(TFSI)$_2$ 36:0:1 membrane.

Conclusions

Our electrospun PEO-based solid polymer electrolyte PEO:Mg(TFSI)$_2$ 36:1 shows an ionic conductivity of 2.0×10^{-5} Scm^{-1} at r.t. without the use of any liquid, organic, or inorganic additive. The ionic conductivity is at least one order of magnitude higher as compared to those SPEs reported in literature while the concentration of the Mg^{2+} ions is lower than in most of them, compare Figure 7. By using electrochemical and analytical methods, we showed that PEO:SN:Mg(TFSI)$_2$ SPEs with different molar compositions can successfully be prepared by electrospinning and solution casting. The electrospun PEO:Mg(TFSI)$_2$ 36:1 membrane shows the highest ionic conductivity over the complete measured temperature range from 273 K to 323 K, the melting temperature of the system. The analysis of the thermal behavior led to the conclusion that a membrane at a molar composition of PEO:Mg(TFSI)$_2$ 36:1 has a lowered

glass transition temperature. Solid State NMR attests the absence of any impurities or side phases other than the PEO/$Mg(TFSI)_2$ electrolyte. In accordance with the results from powder X-ray diffraction a crystalline and an amorphous phase are reported. As the membranes are free of water and other solvents, the determined conductivity has to be ascribed to the Mg^{2+} and $TFSI^-$ ions in the SPE. The mobility of the latter is also confirmed by ^{19}F NMR. In previous studies, the beneficial effect of SN as an additive on the ionic conductivity on PEO electrolytes has been demonstrated[21], acting as a solid lubricant to promote the PEO chain mobility. For the $Mg(TFSI)_2$ containing electrolytes, SN seems to be extracted from the SPE during the drying process. The conducted cyclic voltammetry and impedance spectroscopy in symmetrical Mg metal cells also clarify that the Mg^{2+} ions contribute to the ionic conductivity, as Mg metal electrodes function as blocking electrodes to every species other than Mg^{2+} ions. The current in the cyclic voltammetry is low due to the known problem of an electrode-SPE-interface resistance formation due to passivation processes. This charge transfer resistance is determined via impedance spectroscopy. It rises with time to a plateau, illustrating that a passivation process occurs on the Mg-electrode. Although metallic Mg is known to be less reactive compared to lithium or sodium, this indicates that the reactivity is still high enough to build up an interface layer when in contact with the SPE, albeit not affecting the high ion mobility in the electrolyte. All these results lead to the conclusion that the electrospun PEO:$Mg(TFSI)_2$ 36:1 SPE is an Mg ion conductor with 1000x higher conductivity compared to the PEO:$Mg(TFSI)_2$ SPEs with similar molar composition reported in literature. Together with the demonstrated increase in conductivity when switching from solution casting to electrospinning, this work emphasizes potential of Mg ion electrolytes and the positive effect of electrospinning to the field.

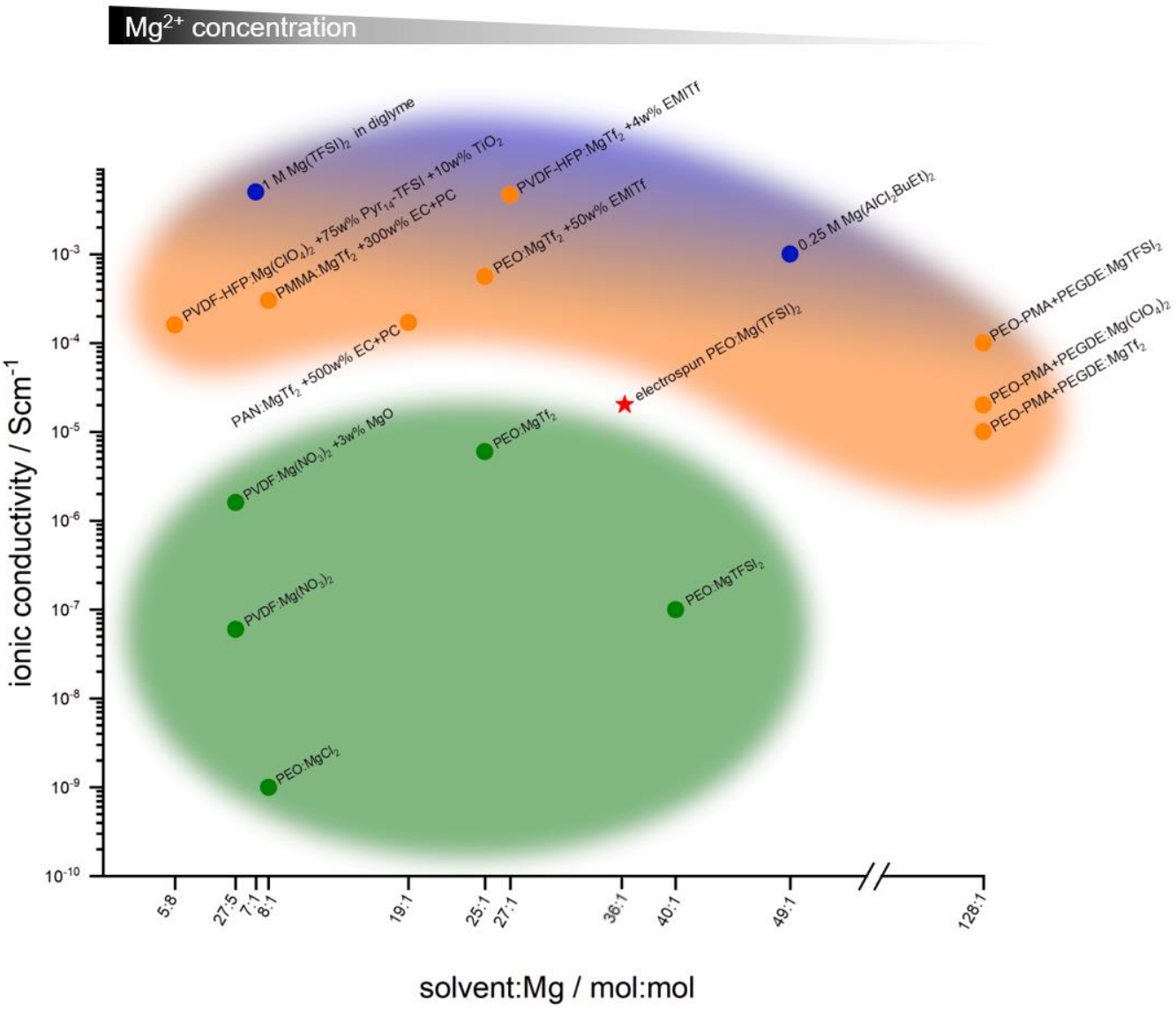

Figure 7. Room temperature ionic conductivity of solid polymer electrolytes (green), gel polymer electrolytes (orange) and two examples of liquid electrolytes (blue) sorted by their Mg^{2+} concentration. Red star marks the electrospun PEO:$Mg(TFSI)_2$ 36:1 membrane, which is the best performing pure, (ionic) liquid-free, solid electrolyte in this work. [6, 9-16, 18-19]

Acknowledgements

This work was founded by the DFG under grants Ni1095/9-1 and WU237/9-1 and is part of the project “Industrialisierbarkeit von Festkörperelektrolytzellen” funded by the Bavarian Ministry of Economic Affairs, Regional Development and Energy.

Keywords: solid polymer electrolyte • magnesium battery • electrospinning • impedance spectroscopy • ionic conductivity

Literature

[1] a) K. Mizushima, P. C. Jones, P. J. Wiseman, J. B. Goodenough, *Solid State Ionics* **1981**, 3-4, 171; b) R. Attias, M. Salama, B. Hirsch, Y. Goffer, D. Aurbach, *Joule* **2019**, 3, 27.

[2] a) A. Ponrouch, J. Bitenc, R. Dominko, N. Lindahl, P. Johansson, M. R. Palacin, *Energy Storage Materials* **2019**, 20, 253; b) R. C. Massé, E. Uchaker, G. Cao, *Science China Materials* **2015**, 58, 715.

[3] a) C. Xu, Y. Chen, S. Shi, J. Li, F. Kang, D. Su, *Scientific Reports* **2015**, 5, 14120; b) L. P. Lossius, F. Emmenegger, *Electrochimica Acta* **1996**, 41, 445.

[4] J. Song, E. Sahadeo, M. Noked, S. B. Lee, *The Journal of Physical Chemistry Letters* **2016**, 7, 1736.

[5] a) M. Jäckle, A. Groß, *The Journal of Chemical Physics* **2014**, 141, 174710; b) R. Davidson, A. Verma, D. Santos, F. Hao, C. Fincher, S. Xiang, J. Van Buskirk, K. Xie, M. Pharr, P. P. Mukherjee, S. Banerjee, *ACS Energy Letters* **2019**, 4, 375.

[6] a) D. Aurbach, Z. Lu, A. Schechter, Y. Gofer, H. Gizbar, R. Turgeman, Y. Cohen, M. Moshkovich, E. Levi, *Nature* **2000**, 407, 724; b) Y. Gofer, O. Chusid, H. Gizbar, Y. Viestfrid, H. E. Gottlieb, V. Marks, D. Aurbach, *Electrochemical and Solid-State Letters* **2006**, 9, A257.

[7] Z. Ma, D. R. MacFarlane, M. Kar, *Batteries & Supercaps* **2019**, 2, 115.

[8] Q. D. Truong, M. Kempaiah Devaraju, P. D. Tran, Y. Gambe, K. Nayuki, Y. Sasaki, I. Honma, *Chemistry of Materials* **2017**, 29, 6245.

[9] N. Sa, N. N. Rajput, H. Wang, B. Key, M. Ferrandon, V. Srinivasan, K. A. Persson, A. K. Burrell, J. T. Vaughey, *RSC Advances* **2016**, 6, 113663.

[10] B. Park, J. L. Schaefer, *Journal of The Electrochemical Society* **2020**, 167, 070545.

[11] X. Tang, R. Muchakayala, S. Song, Z. Zhang, A. R. Polu, *Journal of Industrial and Engineering Chemistry* **2016**, 37, 67.

[12] Y. Kumar, S. A. Hashmi, G. P. Pandey, *Electrochimica Acta* **2011**, 56, 3864.

[13] R. Deivanayagam, M. Cheng, M. Wang, V. Vasudevan, T. Foroozan, N. V. Medhekar, R. Shahbazian-Yassar, *ACS Applied Energy Materials* **2019**, 2, 7980.

[14] G. G. Kumar, N. Munichandraiah, *Solid State Ionics* **2000**, 128, 203.

[15] G. Girish Kumar, N. Munichandraiah, *Electrochimica Acta* **2002**, 47, 1013.

[16] M. Morita, N. Yoshimoto, S. Yakushiji, M. Ishikawa, *Electrochemical and Solid-State Letters* **2001**, 4, A177.

[17] Y. Zhan, W. Zhang, B. Lei, H. Liu, W. Li, *Frontiers in Chemistry* **2020**, 8, 125.

[18] Nidhi, S. Patel, R. Kumar, *Journal of Alloys and Compounds* **2019**, 789, 6.

[19] A. Bakker, S. Gejji, J. Lindgren, K. Hermansson, M. M. Probst, *Polymer* **1995**, 36, 4371.

[20] J. C. Bachman, S. Muy, A. Grimaud, H.-H. Chang, N. Pour, S. F. Lux, O. Paschos, F. Maglia, S. Lupart, P. Lamp, L. Giordano, Y. Shao-Horn, *Chemical Reviews* **2016**, 116, 140.

[21] a) P. Walke, K. M. Freitag, H. Kirchhain, M. Kaiser, L. van Wüllen, T. Nilges, *Zeitschrift für anorganische und allgemeine Chemie* **2018**, 644, 1863; b) K. M. Freitag, H. Kirchhain, L. v. Wüllen, T. Nilges, *Inorganic Chemistry* **2017**, 56, 2100; c) K. M. Freitag, P. Walke, T. Nilges, H. Kirchhain, R. J. Spranger, L. van Wüllen, *Journal of Power Sources* **2018**, 378, 610.

[22] A. Manuel Stephan, *European Polymer Journal* **2006**, 42, 21.

[23] a) L. Persano, A. Camposeo, C. Tekmen, D. Pisignano, *Macromolecular Materials and Engineering* **2013**, 298, 504; b) W. E. Teo, S. Ramakrishna, *Nanotechnology* **2006**, 17, R89.

[24] Y. Takahashi, I. Sumita, H. Tadokoro, *Journal of Polymer Science: Polymer Physics Edition* **1973**, 11, 2113.

[25] B. Li, R. Masse, C. Liu, Y. Hu, W. Li, G. Zhang, G. Cao, *Energy Storage Materials* **2019**, 22, 96.

[26] J. Waugh, E. I. Fedin, *Soviet Physics-Solid State* **1963**, 4, 1633.

[27] N. Voigt, L. van Wüllen, *Solid State Ionics* **2014**, 260, 65.

[28] D. Harris, T. Bonagamba, M. Hong, K. Schmidt-Rohr, *Polymer* **2005**, 46, 11737.

[29] T. K.-J. Köster, L. van Wüllen, *Solid State Ionics* **2008**, 178, 1879.
[30] H. Kirchhain, Festkörper-NMR-Spektroskopie an Batterie-materialien: Charakterisierung innovativer Feststoffelektrolyte und Hochtemperatur-MAS-NMR, *Dissertation*, Augsburg, **2020**.

Supporting Information:

Fast Magnesium Conducting Electrospun Solid Polymer Electrolyte

Patrick Walke,[a,b] Janio Venturini,[a] Robert Spranger,[c] Leo van Wüllen[c] and Tom Nilges*[a]

[a] Patrick Walke, Dr. Janio Venturini, Prof. Dr. Tom Nilges
Synthesis and Characterization of Innovative Materials
Chemistry Department
Technical University Munich
Lichtenbergstraße 4, 85748 Garching bei München, Germany
E-mail: tom.nilges@tum,de
[b] Patrick Walke
TUMint.Energy Research GmbH
Lichtenbergstraße 4, 85748 Garching bei München, Germany
[c] Robert Spranger, Prof. Dr. Leo von Wüllen
Institute of Physics
Augsburg University
Universitätsstraße 1, 86159 Augsburg, Germany

Table of Contents

Experimental Procedures

Synthesis of Membranes

The electrospinning solution was prepared by dissolving PEO (M_W = 300000 g/mol, Sigma Aldrich) in acetonitrile (> 99%, Sigma Aldrich). After the polymer was fully dissolved, $Mg(TFSI)_2$ (> 99%, Sigma Aldrich) were added in a specific molar ratio (see Table 1). After one hour of homogenization, succinonitrile (SN) (> 99 %, Sigma Aldrich, dried at 340 K and 0.1 mbar) was added if necessary (see Table S1).

Table S1. Molar composition of polymer membranes and the used amount of educts.

PEO:SN:$Mg(TFSI)_2$	PEO	SN	$Mg(TFSI)_2$	acetonitrile
36:0:1	0.3500 g	-	0.1291 g	5.5 mL
36:8:1	0.3500 g	0.1415 g	0.1291 g	7.5 mL
72:0:1	0.3500 g	-	0.0645 g	6 mL
72:16:1	0.3500 g	0.1415 g	0.0645 g	6.5 mL

Fibrous membranes were manufactured in a homemade electrospinning apparatus, as described elsewhere.[1] All PEO:SN:$Mg(TFSI)_2$ solid polymer electrolytes were obtained by passing the prepared solution through a capillary (0.9 mm inner diameter) with a flow rate of 2-3 mL/h. A voltage of 17-20 kV was applied at the capillary. The fibers were collected on a grounded ring collector (10 cm diameter). The obtained dense fiber network was dried for 24 h at 10^{-3} mbar at r.t. and stored under inert atmosphere in a glovebox (mBraun, H_2O < 0.1 ppm, O_2 < 0.1 ppm) before being submitted to characterization methods. Additionally, solution casted samples were prepared by casting the prepared solutions on glass and drying them at 10^{-2} mbar at r.t. for 24 h.

X-ray powder diffraction phases analysis

Powder XRD measurements of selected membranes were executed on a *STOE STADI-P* diffractometer (Cu-Kα_1 radiation, λ= 1.54051 Å, Ge monochromator) with a flat-bed sample holder. α-Si (a = 5.43096 Å) was used as internal standard. The sample membranes were

punched out from the already-prepared and dried membranes and measured directly in transmission geometry.

Differential Scanning Calorimetry

Thermal properties of selected membranes were examined by Differential Scanning Calorimetry (DSC) in Al-crucibles using a DSC 200 calorimeter F3 Maia by *Netzsch*. The crucibles were closed inside a Glovebox (H_2O < 0.1 ppm, O_2 < 0.1 ppm). The measurements are conducted in a temperature range from 123 K to 523 K with a heating rate of 10 K/min. Only the first heating cycle is used for comparison.

Potentiostatic Electrochemical Impedance Spectroscopy

To evaluate the ionic conductivity, disks of 10 mm diameter were placed between two stainless steel electrodes (8 mm diameter) in a *TSC battery* cell (*rhd instruments*). During the measurement a pressure of 3.4 bar was applied to the sample. The cell was placed in a temperature-controlled cell stand (*Microcell HC, rhd instruments*) and connected to a potentiostat (*Metrohm Autolab* B.V. Typ PGSTAT204). Impedance spectroscopy was performed in a frequency range from 10 MHz to 10 Hz with an amplitude of 20 mV. The temperature was varied for four cycles from 273 K to 323 K in 5 K steps. Each temperature was held constant for 20 min before the electrochemical measurement was started, to ensure a uniform temperature across the sample. The thickness of the membranes was measured using a micrometer screw (Holex, 0-25 mm) with 0.001 mm accuracy.

Cyclic Voltammetry

Electrochemical cycling was performed in symmetric cells using 2032-type coin cells. Therefore, 17 mm disks of the samples were placed between Mg metal electrodes (0.5 mm thickness,14 mm diameter, 99%, *Sigma Aldrich*). Cycling voltammetry was carried out from -6 V to 6 V with a scan rate of 0.1 mV/s at 298 K using a *Biologic VMP3* potentiostat.

Karl Fischer titration

To conduct conventional Karl-Fischer-Titration, a piece (30 mg) of the electrospun membrane is dissolved in pre-dried (0.0 ppm H_2O) acetonitrile (1 mL).

NMR spectroscopy

For the solid state nuclear magnetic resonance experiments a BRUKER Avance III spectrometer in combination with a 7 T magnet was used. The experiments were performed at resonance frequencies of 18.4 MHz, 75.5 MHz, 282.5 MHz and 300.2 MHz for ^{25}Mg, ^{13}C, ^{19}F and ^{1}H respectively. To reference the NMR-spectra MgCl(aq), $CFCl_3$(aq), and Adamantane were used for ^{25}Mg, ^{19}F, and ^{13}C and ^{1}H, respectively. For the measurements a 4mm triple resonance and a 4mm double resonance probe were used. To obtain information about the dynamic processes of the $Mg(TFSI)_2$ salt, static temperature dependent ^{19}F measurements were performed.

For the temperature calibration, static ^{207}Pb NMR measurements of $Pb(NO_3)_2$ were performed, using the temperature dependence of the chemical shift of ^{207}Pb as a chemical shift thermometer.[2] In addition ^{13}C-MAS experiments were performed to investigate the PEO host structure of the membrane.

The relaxation delays for the ^{19}F single pulse experiments were 5 s; for the ^{13}C single pulse experiments relaxations delays between 10 s and 30 s were used. For the ^{13}C-{^{1}H}-CP-MAS relation delays of 10 s were used.

Scanning Electron Microscopy and Energy-Dispersive X-Ray Spectroscopy

To observe the fibrous structure of the prepared membranes, small samples of the dried SPEs are fixed to a conductive carbon tape and attached to the sample holder of the scanning electron microscope (SEM). As energy-dispersive X-ray spectroscopy (EDX) is required, the sample holder is transferred to the vacuum chamber of a JOEL JCM-6000 NeoScop™, which is operated with a JEOL JED-2200 EDS. For SEM imaging an acceleration of 15 kV is applied.

Results and Discussion

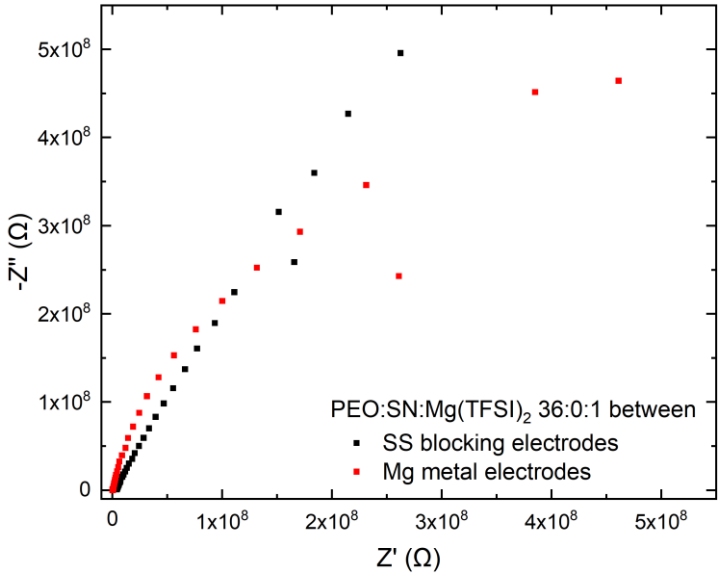

Figure S1. Nyquist plot to display the influence of using stainless steel (SS) blocking electrodes or Mg metal electrodes on the low frequency behavior of a PEO:SN:$Mg(TFSI)_2$ 36:0:1 SPE.

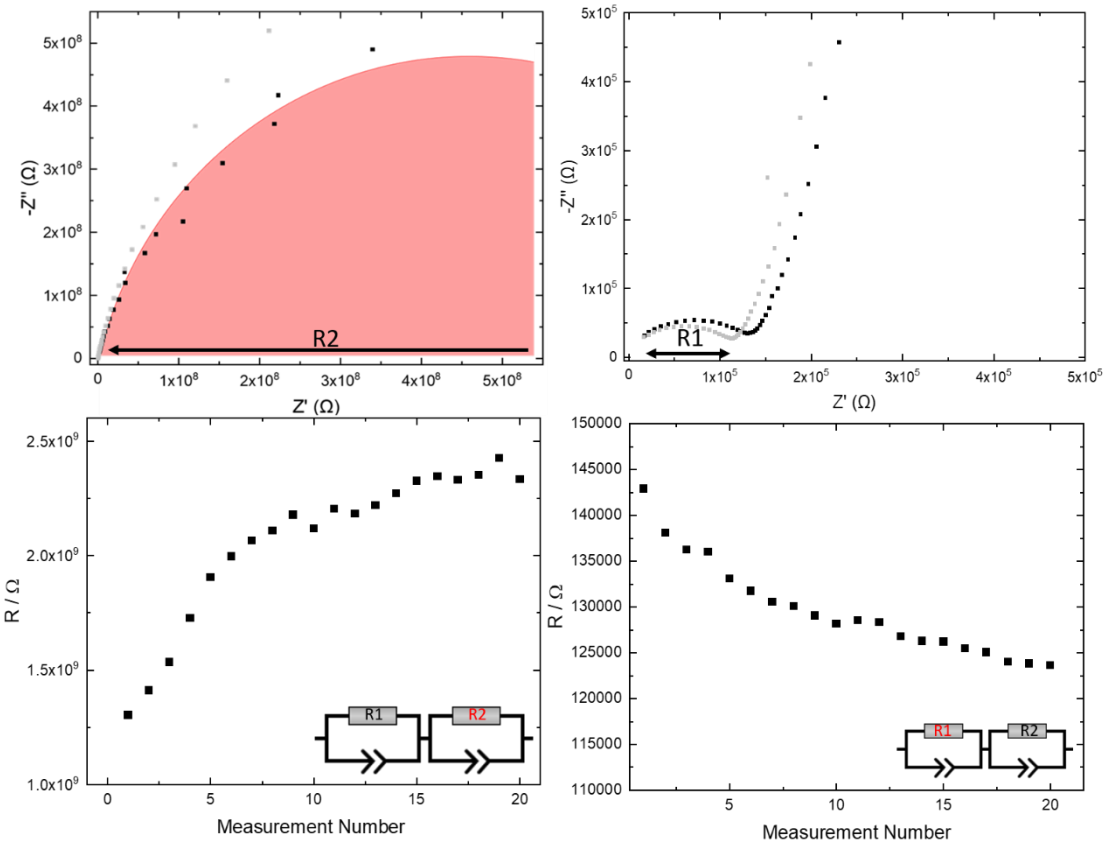

Figure S2. Nyquist plot of an electrospun PEO:$Mg(TFSI)_2$ 36:1 membrane measured between two Mg metal electrodes. Evolution of R1 and R2 over time (rising number of measurement).

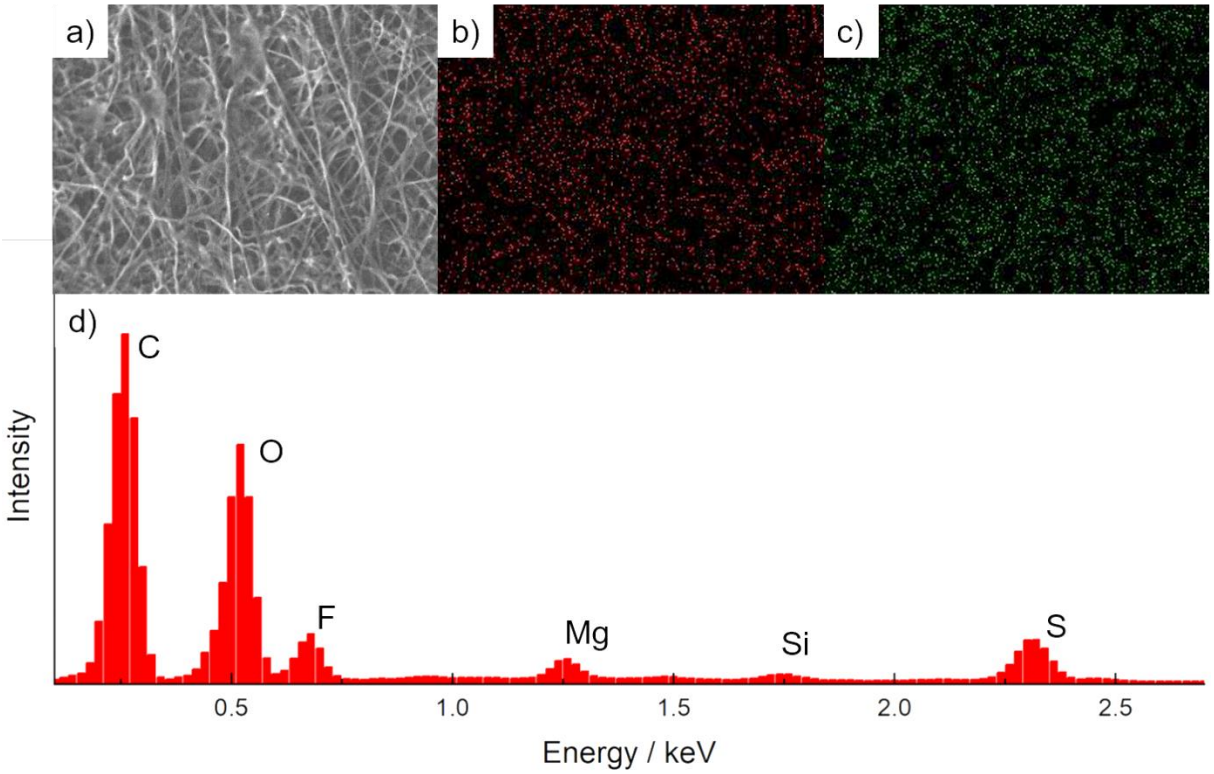

Figure S3. a) SEM picture, b) Mg mapping, and c) F mapping of the same area of an electrospun PEO:Mg(TFSI)$_2$ 36:1 membrane. d) Elements and their intensity found via EDX of the same sample.

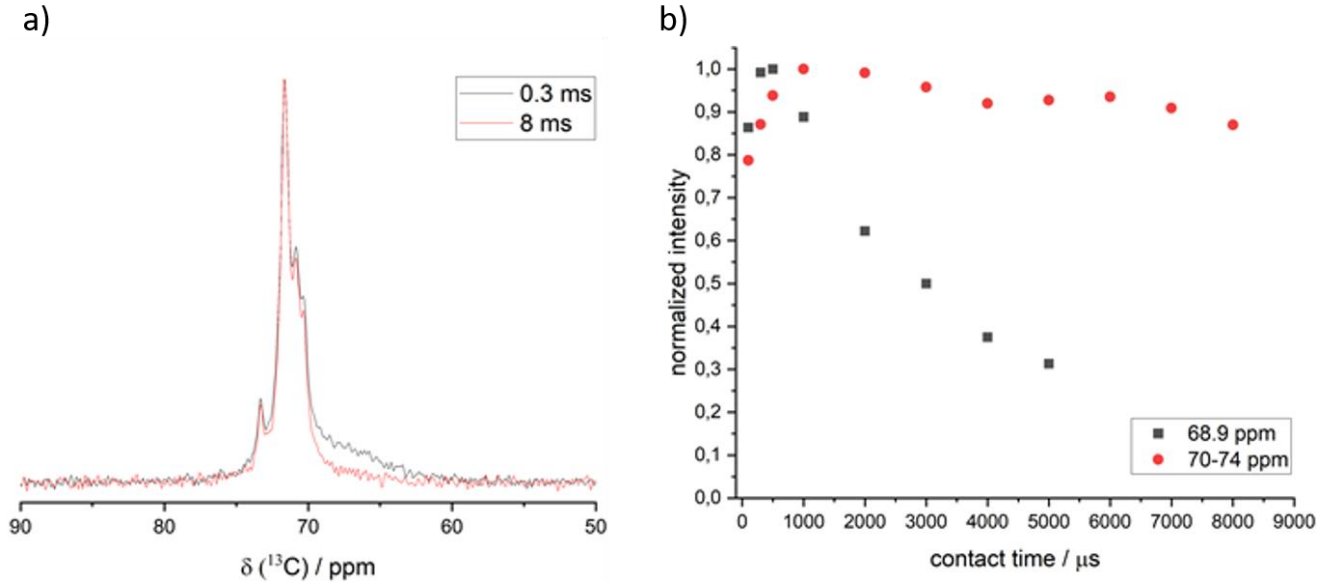

Figure S4. a) ^{13}C-{^{1}H}-CP-MAS NMR spectra of the PEO:SN:Mg(TFSI)$_2$ 36:0:1 membrane for contact times of 0.3 and 8 ms and b) the corresponding CP evolution curves of the normalized intensity of the broad resonance and the sum of the peak assemble as a function of the contact time.

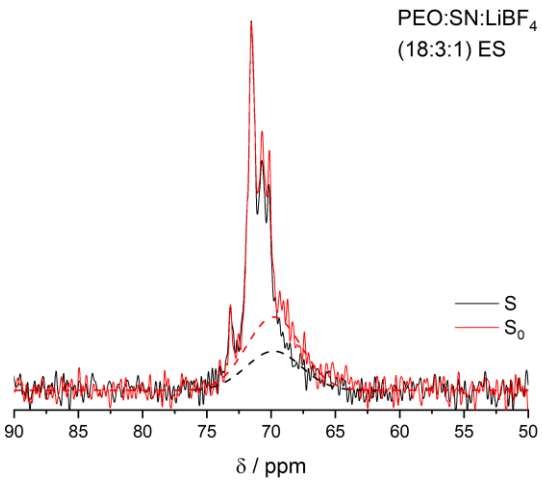

Figure S5. ^{13}C-{^{1}H}-CP-^{7}Li-REDOR of PEO:SN:$LiBF_4$ (18:3:1) electrospun membrane at 212 K. The reference experiment S_0 is shown in red, the REDOR-experiment S in black with 10 rotor periods. The deference of broad amorphous phases is shown with the plot(dotted line) of both experiments, while the narrow peaks don't show a REDOR-effect.[3]

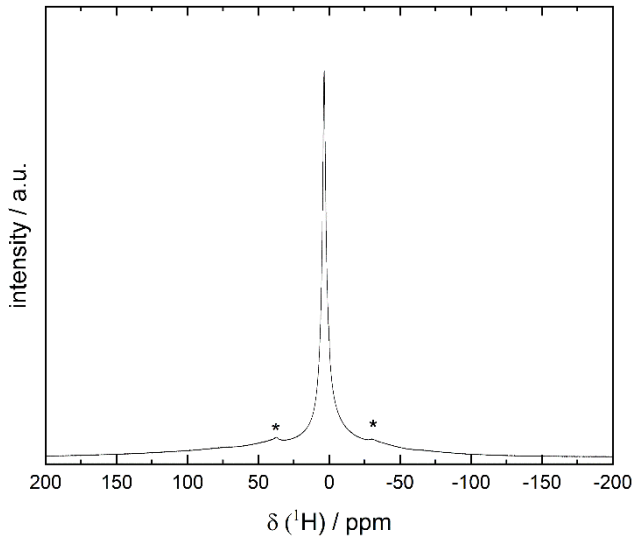

Figure S6. ^{1}H-MAS spectra of electrospun PEO:SN:$Mg(TFSI)_2$ 36:0:1 membrane at room temperature, which shows the proton signal of PEO and no other signs of measurable amounts of water or solvents. The spinning side bands of the main signal is marked with asterisk.

References

[1] K. M. Freitag, H. Kirchhain, L. v. Wüllen, T. Nilges, *Inorganic Chemistry* **2017**, *56*, 2100-2107
[2] A. Bielecki, D. P. Burum, *Journal of Magnetic Resonance, Series A* **1995**, *116*, 215-220.
[3] H. Kirchhain, Festkörper-NMR-Spektroskopie an Batterie-materialien: Charakterisierung innovativer Feststoffelektrolyte und Hochtemperatur-MAS-NMR, Dissertation, Augsburg, **2020**.

Author Contributions

Patrick Walke prepared the solid polymer electrolytes and conducted impedance, cyclic voltammetry, P-XRD and DSC measurements. Robert Spranger performed the solid-state NMR spectroscopy. Patrick Walke, Janio Venturini, Robert Spranger, Leo van Wüllen and Tom Nilges discussed the data and wrote the manuscript.

4 Summary

In this work polymer electrolytes are prepared *via* electrospinning. Homogeneous polymer membranes consisting of equally distributed sub-micrometer fibers can be manufactured with this technique.[95] The method is also suitable for up-scaling to industrial scale.[109] In combination with poly(ethylene oxide) different LiX (X = BF_4^-, $TFSI^-$), $Mg(TFSI)_2$, succinonitrile (SN) as an inorganic additive and nanostructured Al_2O_3 are used. For the system PEO:$LiBF_4$, a solid polymer electrolyte without any additives, the ionic conductivity is increased by electrospinng by over one order of magnitude compared to hotpressed samples of the same composition (PEO:$LiBF_4$ 18:1). Conductivities of solution casted membranes are between those of electrospun and hot pressed SPEs. The main reasons for this behavior are the reduced crystallinity of electrospun polymer fibers accompanied by a reduce glass transition temperature and the unique fiber structure (Figure 7).[60]

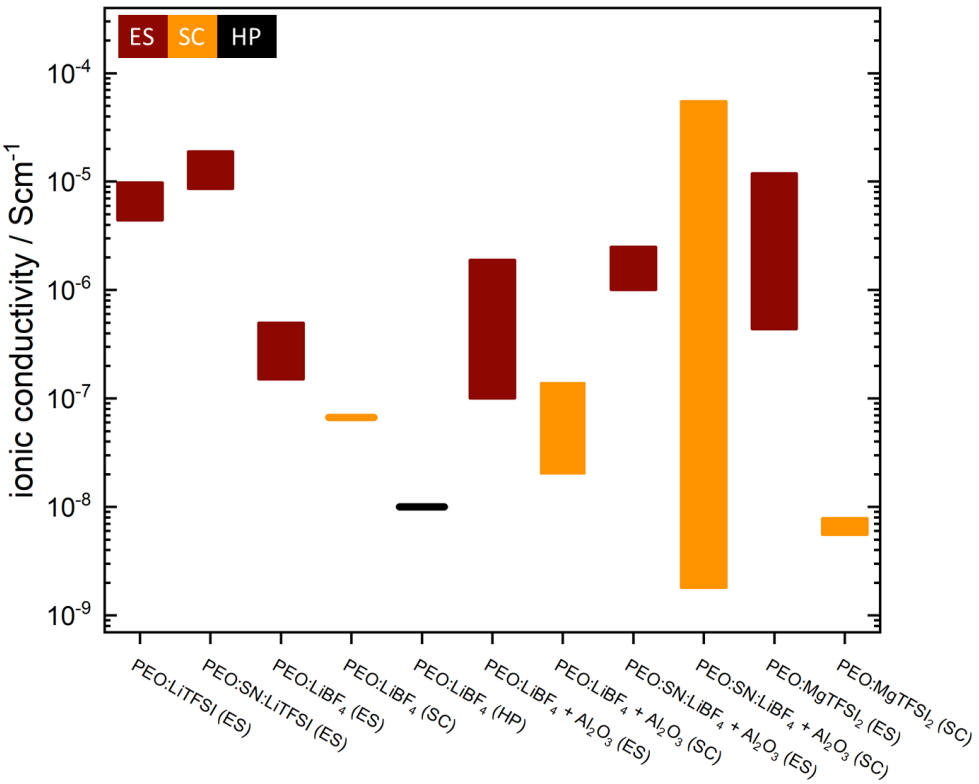

Figure 7: *Ionic conductivities [Scm^{-1}] of different polymer electrolyte systems prepared via electrospinning (ES), solution casting (SC) or hot pressing (HP).*[60, 106]

The same trend but even more pronounced can be observed for the system $MgTFSI_2$. The ionic conductivity of solution casted SPEs with a molar composition of PEO:$MgTFSI_2$ 36:1 is determined to be 7.9×10^{-9} S/cm at 293 K, while the same SPE manufactured by electrospinning shows a ionic conductivity of 1.2×10^{-5} S/cm at 293 K.

If SN as an inorganic additive is used, like in the system PEO:SN:LiTFSI, the ionic conductivity is increased. A SN free PEO:LiTFSI 36:1 membrane has a from impedance spectroscopy calculated ionic conductivity of 4.4×10^{-6} S/cm at 293 K. This is increased to 1.9×10^{-5} S/cm at 293 K if SN is added to obtain a molar composition of PEO:SN:LiTFSi 36:8:1. Due to partial crystallization of the polymer, the effect of SN on the inonic conductivity is less pronounced compared to earlier studies of our group.[106, 104, 105] In the case of nanostructured Al_2O_3 being used as inorganic additive the positive influence of electrospinning as preparation method is still noticeable. When 3wt% of Al_2O_3 are added to a PEO:$LiBF_4$ 18:1 SPE during electrospinning, an ionic conductivity of 1.9×10^{-6} S/cm at 293 K is achieved. The maximum ionic conductivity of 1.4×10^{-7} S/cm for solution casted membranes with addition of Al_2O_3 is reached at 2wt%. Here, the electrospun electrolyte outperforms the solution casted electrolyte by one order of magnitude.[60] Solution casted membranes only show higher ionic conductivities than the comparable electrospun systems if inorganic and organic additives are used together. A composition of PEO:SN:$LiBF_4$ with 2wt% Al_2O_3 showed with 5.5×10^{-5} S/cm a slightly higher ionic conductivity than an electrospun PEO:SN:$LiBF_4$ 18:3:1 with 2.3×10^{-5} S/cm.[60] For all other studied systems electrospinning is the method of choice if high ionic conductivities are desired.

List of Publications

Electrospun Li(TFSI)@Polyethylene Oxide Membranes as Solid Electrolytes
P. Walke, K.M. Freitag, H. Kirchhain, M. Kaiser, L. Van Wüllen, T. Nilges, *Zeitschrift für anorganische und allgemeine Chemie*, **2018**, *644*, 1863-1874.

Effect of nanostructured Al_2O_3 on poly(ethylene oxide)-based solid polymer electrolytes
P. Walke, A. Kirchberger, F. Reiter, D. Esken, T. Nilges, *Zeitschrift für Naturforschung B*, **2021**, *76*, 615-624.

Fast Magnesium Conducting Electrospun Solid Polymer Electrolyte
P. Walke, J. Venturini, R. Spranger, L. van Wüllen, T. Nilges
Submitted Manuscript

Electrospun-sodiumtetrafluoroborate-polyethylene oxide membranes for solvent-free sodium ion transport in solid state sodium ion batteries
K.M. Freitag, **P. Walke**, T. Nilges, H. Kirchhain, R.J. Spranger, L. van Wüllen, *Journal of Power Sources*, **2018**, *378*, 610-617.

Influence of copper on the capacity of phosphorus-anodes in sodium-ion-batteries
C. Ott, A. Degg, **P. Walke**, F. Reiter, T. Nilges, *Journal of Solid State Chemistry*, **2019**, *270*, 636-641.

Flexible and ultrasoft inorganic 1D semiconductor and heterostructure systems based on SnIP
C. Ott, F. Reiter, M. Baumgartner, M. Pielmeier, A. Vogel, **P. Walke**, S. Burger, M. Ehrenreich, G. Kieslich, D. Daisenberger, J. Armstrong, U.K. Thakur, P. Kumar, S. Chen, D. Donadio, L.S. Walter, R.T. Weitz, K. Shankar, T. Nilges, *Advanced Functional Materials*, **2019**, *29*, 1900233.

Evaluating the high-voltage stability of conductive carbon and ethylene carbonate with various lithium salts
M. Metzger, **P. Walke**, S. Solchenbach, G. Salitra, D. Aurbach, H.A. Gasteiger, *Journal of the Electrochemical Society*, **2020**, *167*, 160522.

Conference Appearances

Conferences with Poster Contribution:

19th International Symposium on the Reactivity of Solids, Bayreuth, Germany, 2018
"Eletrospun Alkali Metal Salt@PEO-Membranes for Lithium Ion Batteries"

8th Energy Colloquium of the Munich School of Engineering: "Advances in Energy Transition", Garching-Hochbrück, Germany, 2018
"Mixed Alkali Effect in Electrospun Solid Polymer Electrolytes"

20. Vortragstagung für Anorganische Chemie - Wöhler-Vereinigung und Fachgruppe Festkörperchemie und MateriafForschung, online, 2020
"Electrospun LiTFSI@"PEO Membrane as Solid Polymer Electrolyte"

Batterieforum Deutschland, online, 2022
"Electrospun LiTFSI@"Poly(etylene oxide) Membranes as Solid Polymer Electrolyte"

List of Figures

List of Tables

References

[1] A. Manthiram, X. Yu, and S. Wang. *Nat. Rev. Mater.*, 2(4):16103, **2017**.

[2] J. Wen, Y. Yu, and C. Chen. *Materials Express*, 2(3):197–212, **2012**.

[3] T. Famprikis, P. Canepa, J.A. Dawson, M.S. Islam, and C. Masquelier. *Nat. Mater.*, 18(12):1278–1291, **2019**.

[4] T. Bartsch, F. Strauss, T. Hatsukade, A. Schiele, A.-Y. Kim, P. Hartmann, J. Janek, and T. Brezesinski. *ACS Energy Letters*, 3(10):2539–2543, **2018**.

[5] W. Xu, J. Wang, F. Ding, X. Chen, E. Nasybulin, Y. Zhang, and J.-G. Zhang. *Energy Environ. Sci.*, 7:513–537, **2014**.

[6] J. Janek and W. G. Zeier. *Nat. Energy*, 1(9):16141, **2016**.

[7] D. Karabelli, K. P. Birke, and M. Weeber. *Batteries*, 7(1), **2021**.

[8] M. Walter, M. V. Kovalenko, and K. V. Kravchyk. *New J. Chem.*, 44:1677–1683, **2020**.

[9] N. Kamaya, K. Homma, Y. Yamakawa, M. Hirayama, R. Kanno, M. Yonemura, T. Kamiyama, Y. Kato, S. Hama, K. Kawamoto, and A. Mitsui. *Nat. Mater.*, 10(9):682–686, **2011**.

[10] F. Hao, F. Han, Y. Liang, C. Wang, and Y. Yao. *MRS Bulletin*, 43(10):775–781.

[11] A. Mauger, M. Armand, C.M. Julien, and K. Zaghib. *J. Power Sources*, 353:333–342, **2017**.

[12] J.W. Fergus. *J. Power Sources*, 195(15):4554–4569, **2010**.

[13] F. Zheng, M. Kotobuki, S. Song, M.O. Lai, and L. Lu. *J. Power Sources*, 389:198–213, **2018**.

[14] D. Rettenwander and M. Wilkening. *Nachrichten aus der Chemie*, 66(5):499–504, **2018**.

[15] X. Yao, B. Huang, J. Yin, G. Peng, Z. Huang, C. Gao, D. Liu, and X. Xu. *Chin, Phys. B*, 25(1):018802, **2016**.

[16] J.C. Bachman, S. Muy, A. Grimaud, H.-H. Chang, N. Pour, S.F. Lux, O. Paschos, F. Maglia, S. Lupart, P. Lamp, L. Giordano, and Y. Shao-Horn. *Chem. Rev.*, 116(1):140–162, **2016**.

[17] I. Abrahams, P.G. Bruce, W.I.F. David, and A.R. West. *Acta Cryst.*, B45(5):457–462, **1989**.

[18] A.R. Rodger, J. Kuwano, and A.R. West. *Solid State Ionics*, 15(3):185–198, **1985**.

[19] J. Hassoun, R. Verrelli, P. Reale, S. Panero, G. Mariotto, S. Greenbaum, and B. Scrosati. *J. Power Sources*, 229:117–122, **2013**,.

[20] B. Krebs and J. Mandt. *Z. Naturforsch. B*, 32(4):373–379, **1977**.

[21] H.-J. Deiseroth, S.-T. Kong, H. Eckert, J. Vannahme, C. Reiner, T. ZaiÃŸ, and M. Schlosser. *Angew. Chem.*, 47(4):755–758, **2008**.

[22] V. Epp, Ö. Gün, H.-J. Deiseroth, and M. Wilkening. *J. Phys. Chem. Lett.*, 4(13):2118–2123, **2013**.

[23] V. Thangadurai, H. Kaack, and W.J.F. Weppner. *J. Am. Ceram. Soc.*, 86(3):437–440, **2003**.

[24] R. Murugan, V. Thangadurai, and W. Weppner. *Angew. Chem. Int. Ed.*, 46(41):7778–7781, **2007**.

[25] A. Aatiq, M. Ménétrier, L. Croguennec, E. Suard, and C. Delmas. *J. Mater. Chem.*, 12:2971–2978, **2002**.

[26] H. Aono, N. Imanaka, and G. Adachi. *Acc. Chem. Res.*, 27(9):265–270, **1994**.

[27] A. Rabenau. *Solid State Ion.*, 6(4):277–293, **1982**.

[28] W. Schnick and J. Luecke. *Solid State Ion.*, 38(3):271–273, **1990**.

[29] M. Matsuo, Y. Nakamori, S.-I. Orimo, H. Maekawa, and H. Takamura. *Appl. Phys. Lett.*, 91(22):224103, **2007**.

[30] K. Takahashi, K. Hattori, T. Yamazaki, K. Takada, M. Matsuo, S. Orimo, H. Maekawa, and H. Takamura. *J. Power Sources*, 226:61–64, **2013**.

[31] A.S. Bhalla, R. Guo, and R. Roy. *Mat. Res. Innovat*, 4(1):3–26, **2000**.

[32] Y. Inaguma, C. Liquan, M. Itoh, T. Nakamura, T. Uchida, H. Ikuta, and M. Wakihara. *Solid State Commun.*, 86(10):689–693, **1993**.

[33] H.D. Lutz, W. Schmidt, and H. Haeuseler. *J. Phys. Chem. Solids*, 42(4):287–289, **1981**.

[34] H.D. Lutz, P. Kuske, and K. Wussow. *Solid State Ionics*, 28-30:1282–1286, **1988**.

[35] D.E. Fenton, J.M. Parker, and P.V. Wright. *Polymer*, 14(11):589, **1973**.

[36] P. V. Wright. *Brit. Poly. J.*, 7(5):319–327, **1975**.

[37] W. H. Meyer. *Adv. Mater.*, 10(6):439–448, **1998**.

[38] Y. Jiang, X. Yan, Z. Ma, P. Mei, W. Xiao, Q. You, and Y. Zhang. *Polymers*, 10(11), **2018**.

[39] D. Fauteux, A. Massucco, M. McLin, M. Van Buren, and J. Shi. *Electrochim. Acta*, 40(13):2185–2190, **1995**.

[40] D. Zhou, D. Shanmukaraj, A. Tkacheva, M. Armand, and G. Wang. *Chem*, 5(9):2326–2352, **2019**.

[41] M.B. Armand, P.G. Bruce, M. Forsyth, B. Scrosati, and W. Wieczorek. *Energy Materials*, pages 1–31, **2011**.

[42] Q. Zhang, K. Liu, F. Ding, and X. Liu. *Nano Res.*, 10(12):4139–4174, **[**2017.

[43] E. Strauss, S. Menkin, and D. Golodnitsky. *J. Solid State Electrochem.*, 21(7):1879–1905, **2017**.

[44] K. Karuppasamy, R. Antony, S. Alwin, S. Balakumar, and X. Sahaya Shajan. *Materials Science Forum*, 807:41–63, 2 **2015**.

[45] S.N.M. Johari, N.A. Tajuddin, H. Hanibah, and S.K. Deraman. *Int. J. Electrochem. Sci*, 16(211049):2, **2021**.

[46] S. Ibrahim, S.M.M. Yasin, R. Ahmad, and M.R. Johan. *Solid State Sci.*, 14(8):1111–1116, **2012**.

[47] G. Chiodelli, P. Ferloni, A. Magistris, and M. Sanesi. *Solid State Ion.*, 28:1009–1013, **1988**.

[48] F.M. Gray, J.R. MacCallum, and C.A. Vincent. *Solid State Ion.*, 18-19:282–286, **1986**.

[49] T. Shodai, B.B. Owens, H. Ohtsuka, and J.-I. Yamaki. *J. Electrochem. Soc.*, 141(11):2978–2981, **1994**.

[50] A. Vallée, S. Besner, and J. Prud'Homme. *Electrochim. Acta*, 37(9):1579–1583, **1992**.

[51] L.-Z. Fan, Y.-S. Hu, A.J. Bhattacharyya, and J. Maier. *Adv. Funct. Mater.*, 17(15):2800–2807, **2007**.

[52] N. Voigt and L. van Wüllen. *Solid State Ion.*, 260:65–75, **2014**.

[53] J. R. Nair, L. Imholt, G. Brunklaus, and M. Winter. *Electrochem. Soc. Interface*, 28(2):55–61, **2019**.

[54] J. Mindemark, M.J. Lacey, T. Bowden, and D. Brandell. *Prog. Polym. Sci.*, 81:114–143, **2018**.

[55] J. Zhu, Z. Zhang, S. Zhao, A.S. Westover, I. Belharouak, and P.-F. Cao. *Adv. Energy Mater.*, 11(14):2003836, **2021**.

[56] Y. Ito, K. Kanehori, K. Miyauchi, and T. Kudo. *J. Mater. Sci.*, 22(5):1845–1849, **1987**.

[57] F. Groce, F. Gerace, G. Dautzemberg, S. Passerini, G.B. Appetecchi, and B. Scrosati. *Electrochim. Acta*, 39(14):2187–2194, **1994**.

[58] K.S. Ngai, S. Ramesh, K. Ramesh, and J.C. Juan. *Ionics*, 22(8):1259–1279, **2016**.

[59] C.-W. Liew, S. Ramesh, and R. Durairaj. *J. Mater. Res.*, 27(23):2996â€“3004, **2012**.

[60] P. Walke, A. Kirchberger, F. Reiter, D. Esken, and T. Nilges. *Z. Naturforsch*, 76(10-12):615–624, **2021**.

[61] F. Croce, G. B. Appetecchi, L. Persi, and B. Scrosati. *Nature*, 394(6692):456–458, **1998**.

[62] H.-Y. Sun, H.-J. Sohn, O. Yamamoto, Y. Takeda, and N. Imanishi. *J. Electrochem. Soc.*, 146(5):1672–1676, **1999**.

[63] H.-M. Xiong, X. Zhao, and J.-S. Chen. *J. Phys. Chem.*, 105(42):10169–10174, **2001**.

[64] X. Qian, N. Gu, Z. Cheng, X. Yang, E. Wang, and S. Dong. *Electrochim. Acta*, 46(12):1829–1836, **2001**.

[65] P.A.R.D. Jayathilaka, M.A.K.L. Dissanayake, I. Albinsson, and B.-E. Mellander. *Electrochim. Acta*, 47(20):3257–3268, **2002**.

[66] Y. Horowitz, M. Lifshitz, A. Greenbaum, Y. Feldman, S. Greenbaum, A.P. Sokolov, and D. Golodnitsky. *J. Electrochem. Soc.*, 167(16):160514, **2020**.

[67] F. Baskoro, H.Q. Wong, and H.-J. Yen. *ACS Appl. Energy Mater.*, 2(6):3937–3971, **2019**.

[68] J. Muldoon, C. B. Bucur, and T. Gregory. *Chem. Rev.*, 114(23):11683–11720, **2014**.

[69] Q. Liu, H. Wang, C. Jiang, and Y. Tang. *Energy Storage Materials*, 23:566–586, **2019**.

[70] D. Aurbach, Z. Lu, A. Schechter, Y. Gofer, H. Gizbar, R. Turgeman, Y. Cohen, M. Moshkovich, and E. Levi. *Nature*, 407(6805):724–727, **2000**.

[71] D. Aurbach, G.S. Suresh, E. Levi, A. Mitelman, O. Mizrahi, O. Chusid, and M. Brunelli. *Adv. Mater.*, 19(23):4260–4267, **2007**.

[72] R. Mohtadi and F. Mizuno. *Beilstein J. Nanotechnol.*, 5:1291–1311, **2014**.

[73] Q.D. Truong, M. Kempaiah Devaraju, P.D. Tran, Y. Gambe, K. Nayuki, Y. Sasaki, and I. Honma. *Chem. Mater.*, 29(15):6245–6251, **2017**.

[74] Z. Ma, D.R. MacFarlane, and M. Kar. *Batteries & Supercaps*, 2(2):115–127, **2019**.

[75] J.H. Ha, B. Adams, J.-H. Cho, V. Duffort, J.H. Kim, K.Y. Chung, B. W. Cho, L.F. Nazar, and S.H. Oh. *J. Mater. Chem. A*, 4:7160–7164, **2016**.

[76] J.H. Connor, W.E. Reid, and G.B. Wood. *J. Electrochem. Soc.*, 104(1):38, **1957**.

[77] T.D. Gregory, R.J. Hoffman, and R.C. Winterton. *J. Electrochem. Soc.*, 137(3):775–780, **1990**.

[78] R. Attias, M. Salama, B. Hirsch, Y. Goffer, and D. Aurbach. *Joule*, 3(1):27–52, **2019**.

[79] L.P. Lossius and F. Emmenegger. *Electrochim. Acta*, 41(3):445–447, **1996**.

[80] I. Shterenberg, M. Salama, H.D. Yoo, Y. Gofer, J.-B. Park, Y.-K. Sun, and D. Aurbach. *J. Electrochem. Soc.*, 162(13):A7118, 2015.

[81] S.-Y. Ha, Y.-W. Lee, S.W. Woo, B. Koo, J.-S. Kim, J. Cho, K.T. Lee, and N.-S. Choi. *ACS Appl. Mater. Interfaces*, 6(6):4063–4073, **2014**.

[82] N. Sa, N.N. Rajput, H. Wang, B. Key, M. Ferrandon, V. Srinivasan, K.A. Persson, A.K. Burrell, and J.T. Vaughey. *RSC Adv.*, 6:113663–113670, **2016**.

[83] M. Morita, N. Yoshimoto, S. Yakushiji, and M. Ishikawa. *Electrochem. Solid-State Lett.*, 4(11):A177, **2001**.

[84] Y. Zhan, W. Zhang, B. Lei, H. Liu, and W. Li. *Frontiers in Chemistry*, 8, **2020**.

[85] R.C. Agrawal and G.P. Pandey. *J. Phys. D: Appl. Phys.*, 41(22):223001, **2008**.

[86] Y. Wang, S. Song, C. Xu, N. Hu, J. Molenda, and L. Lu. *Nano Materials Science*, 1(2):91–100, **2019**.

[87] B. Park and J.L. Schaefer. *J. Electrochem. Soc.*, 167(7):070545, **2020**.

[88] A. Bakker, S. Gejji, J. Lindgren, K. Hermansson, and M.M. Probst. *Polymer*, 36(23):4371–4378, **1995**.

[89] Nidhi, S. Patel, and R. Kumar. *Journal of Alloys and Compounds*, 789:6–14, **2019**.

[90] A. Formhals, October 2 **1934**. US Patent 1,975,504.

[91] L.S.J.M. Larrondo and R. St. John Manley. *J. Polym. Sci., Polym. Phys. Ed.*, 19(6):909–920, **1981**.

[92] P.K. Baumgarten. *J. Colloid Interface Sci.*, 36(1):71–79, **1971**.

[93] S. Ramakrishna. *An introduction to electrospinning and nanofibers*. World scientific, **2005**.

[94] G.I. Taylor. *Proc. R. Soc. A. Math. Phys. Eng. Sci.*, 280(1382):383–397, **1964**.

[95] J. Xue, T. Wu, Y. Dai, and Y. Xia. *Chem. Rev.*, 119(8):5298–5415, **2019**.

[96] D.H. Reneker and I. Chun. *Nanotechnology*, 7(3):216–223, sep **1996**.

[97] S-H. Tan, R. Inai, M. Kotaki, and S. Ramakrishna. *Polymer*, 46(16):6128–6134, **2005**.

[98] M.S. Islam, B.C. Ang, A. Andriyana, and A.M. Afifi. *SN Applied Sciences*, 1(10):1–16, **2019**.

[99] J.-W. Jung, C.-L. Lee, S. Yu, and I.-D. Kim. *J. Mater. Chem. A*, 4:703–750, **2016**.

[100] S.N. Banitaba and A. Ehrmann. *Polymers*, 13(11), **2021**.

[101] S.N. Banitaba, D. Semnani, B. Rezaei, and A.A. Ensafi. *Polymer Int.*, 68(4):746–754, **2019**.

[102] S.N. Banitaba, D. Semnani, E. Heydari-Soureshjani, B. Rezaei, and A.A. Ensafi. *JOM*, 71(12):4537–4546, **2019**.

[103] S.N. Banitaba, D. Semnani, A. Fakhrali, S.V. Ebadi, E. Heydari-Soureshjani, B. Rezaei, and A.A. Ensafi. *Ionics*, 26(7):3249–3260, **2020**.

[104] K.M. Freitag, H. Kirchhain, L. van Wüllen, and T. Nilges. *Inorg. Chem.*, 56(4):2100–2107, **2017**.

[105] K.M. Freitag, P. Walke, T. Nilges, H. Kirchhain, R.J. Spranger, and L. van Wüllen. *J. Power Sources*, 378:610–617, **2018**.

[106] P. Walke, K.M. Freitag, H. Kirchhain, M. Kaiser, L. van Wüllen, and T. Nilges. *Z. Anorg. Allg. Chem.*, 644:1863–1874, **2018**.

[107] E. Strauss, S. Menkin, and D. Golodnitsky. *J. Solid State Electrochem.*, 21(7):1879–1905, **2017**.

[108] A. Ponrouch, J. Bitenc, R. Dominko, N. Lindahl, P. Johansson, and M. R. Palacin. *Energy Storage Materials*, 20:253–262, **2019**.

[109] L. Persano, A. Camposeo, C. Tekmen, and D. Pisignano. *Macromol. Mater. Eng.*, 298(5):504–520, **2013**.